Instituto Tecnológico y de Estudios Superiores de Monterrey

Campus Monterrey

School of Engineering and Sciences

URBAN RADIO PROPAGATION FOR VEHICULAR ENVIRONMENTS, A SPATIAL
VEHICULAR TRAFFIC DENSITY CHANNEL CHARACTERIZATION.

A dissertation presented by

Fausto Lenin Granda Gutiérrez

Submitted to the
School of Engineering and Sciences
in partial fulfillment of the requirements for the degree of

Doctor of Philosophy

in

Information Technologies and Communications

Major in Telecommunications

Monterrey Nuevo León, December 4th, 2018

Instituto Tecnológico y de Estudios Superiores de Monterrey

Campus Monterrey

School of Engineering and Sciences

The committee members, hereby, certify that have read the dissertation presented by Fausto Lenin Granda Gutiérrez and that it is fully adequate in scope and quality as a partial requirement for the degree of Doctor of Philosophy in Information Technologies and Communications, with a major in Telecommunications.

Dra. Leyre Azpilicueta
Tecnológico de Monterrey
School of Engineering and Sciences
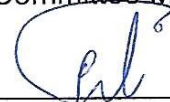Principal Advisor

Dr. Cesar Vargas Rosales
Tecnológico de Monterrey
Co-advisor

Dr. José Ramón Rodríguez Cruz
Universidad Autónoma de Nuevo León
Committee Member

Dra. Rafaela Villalpando Hernández
Tecnológico de Monterrey
Committee Member

Dr. Mahdi Zareei
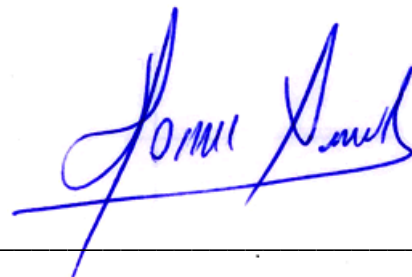Tecnológico de Monterrey
Committee Member

Dr. Rubén Morales Menéndez
Dean of Graduate Studies
School of Engineering and Sciences

Monterrey Nuevo León, December 4th, 2018

Declaration of Authorship

I, Fausto Lenin Granda Gutiérrez, declare that this dissertation titled, Urban Radio Propagation for Vehicular Environments, a Spatial VTD Channel Characterization, and the work presented in it are my own. I confirm that:

- This work was done wholly or mainly while in candidature for a research degree at this University.
- Where any part of this dissertation has previously been submitted for a degree or any other qualification at this University or any other institution, this has been clearly stated.
- Where I have consulted the published work of others, this is always clearly attributed.
- Where I have quoted from the work of others, the source is always given. Except for such quotations, this dissertation is entirely my own work.
- I have acknowledged all main sources of help.
- Where the dissertation is based on work done by myself jointly with others, I have made clear exactly what was done by others and what I have contributed myself.

_____

Fausto Lenin Granda Gutiérrez

Monterrey, Nuevo León, December 4th, 2018

Dedication

To my beloved and tireless team: Elizabeth, Melissa, Isaac.

To my strength and support: my parents and relatives.

To my earthly angels: my sincere and loyal friends.

To my torch and academic compass: my teachers and advisors.

To my alpha and omega: my new God who beats endlessly into my hearth.

Acknowledgements

I would like to express my sincere gratitude to my advisors, Dr. Leyre Azpilicueta and Dr. Cesar Vargas, for your patience, support and continuous motivation, to purse the highest objectives in my PhD formation. You were my torch and compass in this amazing journey.

Besides my advisors, I would like to thank my thesis committee: Dr. Mahdi Zareei, Dr. José Ramon Rodriguez, Dr. Rafaela Villalpando, for your insightful comments, and fruitful suggestions.

I thank my friends and classmates: Diego, Jaime, Mikel, Juan Manuel, Elsa, Alberto, for the enjoyable discussions and celebrations we have had in the DTC. Thanks to Luz María for your friendship and encouragement to participate in sports.

Thanks to Ecuador and Mexico, for let me enjoy this magnificent opportunity.

Urban Radio Propagation for Vehicular Environments, a Spatial VTD Channel Characterization

By

Fausto Lenin Granda Gutiérrez

Abstract

Vehicular Ad Hoc Networks (VANETs) are envisaged to be a critical building block of Smart Cities and Intelligent Transportation System (ITS). Although there is a significant research effort in V2X (Vehicle-to-Infrastructure or Vehicle-to-Vehicle) radio channel characterization, the use of a deterministic approach as a complement of theoretical and empirical models is required to understand more accurately the propagation phenomena in urban environments.

In this work, three computational tools were integrated to simulate the effects of the Vehicular Traffic Density (VTD) in the Urban Radio Propagation Channel (URPC) at 5.9Ghz: a 3D Ray-Launching (3D-RL), a detailed geographic database and a microscopic traffic simulator. Considerations as distance segmentation and spatial position from the transmitter were taken into account for accuracy and consistency in the subsequent analysis. Large-scale, small-scale, multipath metrics and coverage analysis is complemented with statistical characterization to explain the influence of different VTD levels in the URPC. Large-scale and small-scale results show the impact that factors such as relative Transmitter-Receiver (TX-RX) position, distance, link frequency, obstacles geometry, obstacles dielectric properties, and vehicle speed, have in the V2X propagation channel where parameters such as path loss exponent, amplitude of fading, and distribution shape factor cannot be assumed constant given the non-stationary nature of the vehicular communications channel. Otherwise, statistical characterization shows that Lognormal, and Weibull distributions can describe the fading RSS behavior for the VTD tested levels. The influence of the VTD in more significant in V2V and I2V links where. higher RSS values are related with the high VDT level, mainly in the vicinity of the TX, while there are not clear tendency or significant change in the RSS for V2X in remote areas from TX. These results are useful for radio-planning Wireless Sensor Networks (WSNs) designers and deployment of urban Road Side Units (RSUs).

List of Figures

List of Tables

Contents

1. Introduction

According to the World Health Organization, about 1.25 million people die each year as a result of road traffic crashes and without action, these have been predicted to rise to become the 7th leading cause of death by 2030, [1]. In 2014, motor-vehicle traffic-related injuries accounted for 16.9% of all injury deaths in United States, [2]. In Mexico, during 2015 the traffic accidents in urban and suburban zones caused approximately 111.000 victims between drivers, passengers, pedestrians, cyclists and others, [3]. The potential to improve different aspects on the roads (security, travel time, real-time information of traffic and road conditions, etc.) has attracted the commercial, governmental and research interest in Vehicular Ad-hoc networks (VANET's), where connectivity has three major approaches to bi-directional wireless communication: vehicle-to-vehicle (V2V), vehicle-to-infrastructure (V2I) and vehicle-to-pedestrian (V2P).

The V2I and I2V communication is the bi-directional wireless exchange of data (control and information) between vehicles and Road Side Units (RSUs) while V2V is related with the wireless communication between vehicles. The IEEE 802.11p standard, [4], was developed for V2V and V2I operation at 5.9GHz in the United States, while in Europe and Japan, the government has licensed the 5.8GHz spectrum band for vehicular communications. The deployment of the V2I and V2V applications as intersection collision warning systems (ICWS), [5], vehicle collision prediction, [6], and others aimed at the convergence of sensing, infrastructure and information technologies into intelligent traffic management systems (ITMS), rely on the understanding of the propagation phenomena and the accurate channel characterization.

The term channel characterization is used to describe the models, theory, and experimental data that constitute the understanding of a wireless channel, [7]. The characterization must be quantitative as thorough as possible, but not excessively

1

complex as to limit its usefulness, and the complete characterization concludes with a mathematical (statistical) model for the time-varying Channel Impulse Response (CIR) and its components. Wireless communications channels at urban environments have two remarkable characteristics:

- They are time dispersive, due to the multipath effect where different path lengths cause multiple replicas of the transmitted signal. Some propagation impairments are: reflection and scattering, diffraction and transmission loss, which give rise to issues such as temporal and spatial variation of path loss and multipath effects.

    - They present rapid changes between Line-of-sight (LoS), Quasi-line-of-sight (QLoS) and Non-line-of-sight (NLoS) due to the obstacle's geometry and scenario configuration. In a V2V environment, some research findings show a 12-13 dB on average reduction in the received signal when the LoS is obstructed by large cars (truck), [8]. The importance that VANET simulators should use geometry-based models that distinguish the instantaneous propagation into LoS, QLos and NLoS conditions is emphasized in [9].

The propagation phenomena can be characterized by empirical approach (measurement campaign) which requires technological, economical and human resources not always available, or modeled either statistically or deterministically. Ray-tracing modeling has been recognized as an accurate geometry-based-deterministic (GBD) tool to model propagation phenomena, [6], [7], yielding an excellent approximation of the real-world propagation with reasonable computational complexity. According to [12], if the complete geographic information is available and processing speed is not an issue, then ray-tracing-based GBD models could be used for maximum accuracy; even with limited details and material characterization, it can still result in accurate levels of prediction, [13].

With respect to vehicular mobility, a realistic representation of vehicle mobility requires using real-world road topology, accurate microscopic mobility modeling, and real

database traffic demand modeling, whereas a realistic representation of the signal propagation requires reproducing the actual physical radio propagation process, [14]. Simulation of Urban Mobility (SUMO) is a free and open traffic simulation suite allowing modelling of intermodal traffic systems including road vehicles, public transport and pedestrians. Simulation is performed on discrete time steps, and user can specify vehicle movement and vehicle flow. On the other hand, parameters as vehicle density, average vehicle speed and relative speed among vehicles significantly impact information propagation in V2V environments, [15]. Higher vehicular densities are related with shorter and more reliable wireless links, [16], which ease the message propagation better than in scenarios with a low vehicle density (where messages cannot exploit the inherent multi-hop capabilities of vehicular networks), [17]. A matching mechanism to tune the parameters of the lognormal model according to of the VANET topology characteristics over time and space for low and high vehicle density is presented in [14].

Based on the aforementioned issues, the main motivation of this proposal is to generate alternative techniques and methods for the understanding of the Urban Radio Propagation Channel (URPC) phenomenon, taking into account the vehicular density impact, which can lead us to a broader understanding of vehicular propagation phenomena and further development of more accurate propagation channel models.

1.1 Context and problem statement

Accurate channel models for vehicular communications are needed in scenarios where the high speed of the vehicles results in very short contact durations between transmitters (TX) and receivers (RX), generating limited or unfeasible communications. Vehicular communications in urban areas is highly variable, with both static and mobile objects creating a considerably changing channel over both space and time, where channel models for cellular systems cannot be used to describe the fading behavior of V2I channels because of the high mobility combined with the differences in antenna height, coverage range, density and location of mobile obstacles.

Previous research work in [11], and [18], evaluates some important parameters of a V2I wireless channel link for different frequencies (868MHz, 2.4Ghz, 5.9GHz), different

location of the TX and RX, different LoS, QLoS and NLoS conditions. Results show a detailed spatial path loss characterization and analyze the impact that the spatial distance, link frequency, placement of RSUs, and factors such as roundabout, geometry and relative position of the obstacles have in V2I propagation channel.

Some radio propagation studies and models have been reported in the literature [19], [20], [21], [22], [23], however, the implications of the VTD in the URPC are yet an underexplored area. As in the traffic mobility models, where a gap in the literature lies in the lack of accurate models that mimic the behavior of High Vehicular Traffic (HVT), [24], an open research in the URPC is the need of characterization research works related to the effects of vehicle density, average vehicle speed, relative speed among vehicles, etc. Authors in [17] recommend the use of different vehicle densities and city scenarios, to analyze the most representative factors that affect Warning Message Dissemination in VANETs. [16] states that higher vehicular density allows having shorter and more reliable wireless links, however, [15] concludes that the information propagation in V2V environments is significantly impacted by factors as vehicle density, average vehicle speed and relative speed among vehicles.

The results of this research could have some implications as:

- It could lead to the setup of a more accurate mathematical channel model whose performance evaluation would be more informative for research work on fields of: VANET's, Cognitive Radio (CR), TV- White Space (TVWS), Vehicular Dynamic Spectrum Access (VDSA).
- Indirectly, it would impact different areas related to VANET's as,[25] :
  o *Accident prevention:* connected vehicle technologies are aimed to give all drivers the tools they need to anticipate potential crashes and significantly reduce the number of lives lost each year.
  o *Mobility:* Connected vehicle mobility applications could enable system users and system operators to make smart choices that improve the overall mobility.

o *Environment:* Connected vehicle environmental applications can give motorists the real time information they need to make "green" transportation choices.

o *Socioeconomic benefits:* A study (2015) of the Intelligent Transportation Society of America concluded that four connected vehicle safety applications (intersection movement assist, left turn assist, forward collision warning, and lane change warning/ blind spot warning) can result in societal benefits annually if deployed across the entire U.S. vehicle fleet.

Research questions that could be posed for the problem statement are: Could the V2X Received Signal Strength (RSS) be affected by different levels of VTD? How significant is the VTD effect in the large-scale metrics? What are the implications of the VTD in the small-scale metrics? How different is the impact of the VTD when are compared V2I, I2V and V2V environments? What is the statistical behavior of the URPC under low, medium and high VTD conditions? What strategies for data selection can be posed for statistical analysis of this highly variable environments?

1.2 Hypothesis
Based on the problem statement and context, the following hypothesis is proposed:
- The VTD is a vehicular factor that generates URPC large-scale and small-scale variations for V2X communications at urban environments.

1.3 Objectives
The main objective of this research is to propose a methodology to characterize the VTD effects in the spatial URPC for V2I and V2V environments.

Specific objectives are:
- To characterize the V2V and V2I large-scale and small-scale statistical differences under LoS, QLoS and NLoS conditions for URPC, identifying those characteristics, approaches, differences and similarities between deterministic models in the literature.

5

- To develop more accurate V2V and V2I URPC characterization models, based on 3D-RL simulated results and statistical analysis.
- To characterize the VTD effects in the large-scale/small-scale radio propagation phenomena for low, medium and high levels of VTD.

1.4 Solution overview

The purpose of this research project is the characterization of the effects of the VTD in the URPC for V2I and V2V environments, which implies the spatial analysis of the large-scale/small-scale and statistical behavior of the wireless communication channel. The solution methodology considers three main stages: a) scenario representation, b) propagation simulation and, c) data analysis. The characteristics of each stage are explained as follows:

a) Scenario representation: the urban scenario geographical information is edited and parametrized into the 2D-traffic simulator and 3D-RL software. The geometry and geographic information of the streets, avenues, roundabouts, buildings, etc., result of the 2D-traffic simulator is accurately parametrized into the 3D-RL software.

b) Propagation simulation: the vehicular mobility and density behavior is simulated into the 2D-traffic simulator. User-predefined/aleatory routes and three different VTD vehicular occupation levels are considered. The V2I and V2V temporal and spatial variation of path loss and multipath effects are simulated into the 3D-RL software (PHY layer of the standard IEEE 802.11p).

c) Data analysis: the large-scale/small-scale, propagation and statistical behavior phenomena for V2V/V2I is analyzed. Time-dispersion parameters (mean excess delay, rms-delay spread, and excess delay spread) are obtained from the PDP generated by the 3D-RL simulator. The time varying nature of the channel are described by the Doppler spread and coherence time.

1.5 Research Scope

The scope and some limitations of this research proposal are described as follows:

- Simulation: Simulations play a vital role in implementing, testing and validating proposed algorithms and protocols in VANET[26]. The results of this research are based on computational simulations and statistical analysis. The vehicular mobility model is simulated in SUMO, an open source software while the characterization and propagation phenomena are simulated in a Matlab-based in-house Ray Launching software (3D-RL). Communication, statistical and neural network MATLAB toolboxes are needed for statistical analysis

- Mobility model: This research uses SUMO as microscopic traffic simulator with its defined mobility model for urban environment; no additional mobility models was assessed. The SUMO step time simulation (e.g. 1[s]) is defined by the "granularity" (cuboid size) used in the 3D-RL simulator, which in turn was defined by the specific scenario characteristics; there are not specific recommendation about this issue in the literature. Highway Mobility Models are not considered.

- Scenario characterization: The resulting URPC characterization took as reference an urban scenario which contains the typical elements of this type of environments: avenues, streets, central park, cars, buildings, foliage, pedestrians, lamppost, etc.; no additional environments (e.g., suburban, rural, etc.) were analyzed. Nonetheless, scenarios with sensitive different configuration, mainly respect with the location, geometry and dielectric characteristics of the obstacles, could lead to some important variations in the proposed characterization.

1.6 Dissertation Organization

Chapter 1: The Introduction and formal items of this research are covered in a coherent and sequential fashion: Motivation, Problem Statement and Context, Hypothesis, Objectives, Solution Overview and Research scope.

Chapter 2: An overview of the V2X communication, concepts and characteristics of the 3D Ray Launching technique (3D-RL), vehicular mobility (SUMO) and solution overview are tackled in this chapter.

Chapter 3: The channel characterization concept, the 3D-RL technique and the SUMO configuration are presented. The 3D-RL and SUMO integration is described in detail.

Chapter 4: The main results of the small-scale, large scale, coverage and measurement validation are presented and discussed. Also, a detailed description of scenario configuration and simulation parameters are laid out.

Chapter 5: A detailed statistical characterization of the VTD impact into the URPC is presented for V2I, I2V and V2V. Statistical measures as, Goodness-of-fit, divergence, Probability Plot, Squared Coefficient of Variation, among others are used to identify the statistical behavior of the Received Signal in the proposed urban scenario.

Chapter 6: Conclusions, new research strands and future work, are presented.

2. State of The Art and Solution Approach.

Some research projects at academic organizations are being conducted on Intelligent Transportation System (ITS), [27], [28]. The private sector is developing full autonomous vehicles, [29],[30]. The U.S. Department of Transportation (U.S.DOT) announced new Federal Highway Administration (FHWA) Vehicle-to-Infrastructure (V2I) that will boost the ongoing private [30], academic [28], and governmental [31] research efforts and projects in the area of ITS including applications ranging from safety critical [32], [6], [33] and traffic management [5], [34] up to gaming and in-car multimedia streaming, [35].

Applications reported in the Transit Vehicle-to-Infrastructure Assessment Study [36] are: Transit Vehicle-Pedestrian/ Cyclist Crossing Warning, Transit Stop/Station Pedestrian Safety, Transit Vehicle and Center Data Exchange Application, Transit Traveler Information Infrastructure Application, Red Light Violation Warning (RLVW), Left Turn Assist (LTA), Stop Sign Violation Warning (SSVW), Reduced Speed Zone Warning (RSZW), Pedestrian in Signalized Crosswalk Warning (PCW) etc. A proposed application aimed at assisting transit vehicle maneuvers and detours to handle special events at strategic locations to perform dynamic information collection/dissemination, is the V2I Portable Infrastructure which features the concept of portable infrastructure such as portable RSUs and signage. The design of accurate propagation models for realistic V2I enabling must take into account some unique characteristics in terms of antenna heights, placement of the RSUs, environment type (e.g., urban, suburban, highway) and specific considerations for small-scale fading due to particular location of antennas [37].

Countries such as Canada, the United States of America (USA), European nations, the Middle East and Japan are pioneers and adopters of ITS research and applications into vehicles, infrastructure and traffic management where governmental agencies are strongly involved and play a key role in delivering safe and efficient transportation. As an overview, in Canada, Transport Canada (http://www.tg.gc.ca) is focused on the development of relevant transportation policies and legislation, while in USA, the U.S

DOT aims to ensure a fast, safe, efficient, accessible and convenient transportation system that meets U.S. vital national interests and enhances the quality of life of the public. In Mexico, the Mexican Institute of Transport (http://www.imt.mx) conducts research projects around public and private transport and implements programs aimed at developing adequate human capital for the transportation sector.

Smart Cities must be able to take advantage of ITS, its applications and benefits on transportation operations according to main areas of research goals identified by the U.S. DOT (https://www.its.dot.gov): safety, mobility, efficiency, productivity, energy and environmental impacts, and customer satisfaction, offering to travelers more mobility options and access opportunities. To meet these goals, ITS technologies would be integrated into other operational areas of the Smart Cities as is proposed in the Smart Columbus program [38], where the advancements in connected vehicles (CV), automated vehicles (AV), and electric vehicles are integrated with the data from various sectors and sources to simultaneously power these technologies while leveraging the new information they provide. These ITS technologies can be seen as a part of a holistic or wider mobility approach where some sustainable transportation strategies such as strengthening urban road construction, improving operational efficiency and private traffic restriction have been proposed as sustainable strategies for transportation development, [39].

In 1999, the U.S. Federal Communication Commission (FCC) allocated 75 MHz of licensed spectrum at 5.9 GHz to be used as V2V and V2I communications known as Dedicated Short Range Communications (DSRC), and the IEEE 802.11p standard [4], part of the Wireless Access in Vehicular Environments (WAVE) initiative [40], was developed to operate at this 5.9 GHz band, with 75 MHz bandwidth and seven 10 MHz channels. This dedicated bandwidth provides a low-latency, short-to-medium-range wireless communications medium that permits fast and reliable data transmissions at high transmission rates, critical for safety applications specially in urban environments are characterized by the combination of different object types such as buildings, vehicles, pedestrians, vegetation etc., as well as their number, size, and density, that have a profound impact on radio propagation, [12].

Some propagation impairments such as reflection from, diffraction around and transmission loss through objects (influence of vegetation, building entry loss, cars, trees,

pedestrians, etc.), and external environment, give rise to issues such as Quasi-Line-of-Sight (QLoS), Non-Line-of-Sight (NLoS), temporal and spatial variation of path loss and multipath effects from reflected and diffracted components of the wave. In [8], the authors conclude that the received power is reduced by 12-13 dB on average, when the LoS is obstructed by large cars (trucks). The deployment of the V2I and V2V applications aimed at the convergence of sensing, infrastructure and information technologies into intelligent traffic management systems (ITMS), rely on the understanding of the propagation phenomena and the accurate channel characterization. The term channel characterization is used to describe the models, theory, and experimental data that constitute the understanding of a wireless channel in a specific environment, typically a function of channel bandwidth and center frequency, [7].The characterization must be quantitative as thorough as possible but not excessively complex as to limit its usefulness. Moreover, it must also be widely available for use in analysis, computer simulations, and experiments. The complete characterization concludes with a mathematical (statistical) model for the time-varying Channel Impulse Response (CIR) and its components.

The rapid changes in radio propagation conditions are one of the main challenges for channel modelling in vehicular communications and analytical models, stochastics models and ray tracing approaches are used to capture these propagation impairments. A measurement campaign is the ideal method to quantify the effect of this phenomena, however, not always the technological, economical and human resources are available. Analytical models that assume exponential path loss are not appropriate if scenarios with buildings are investigated [41], while stochastic models which describe the channel characteristics from a macroscopic point of view might lead to severe deviations from realistic behavior and application as safety cannot be modeled accurately.

Channel modeling approaches can be roughly classified into four categories [42]: (1) empirical (they require calibration but offer rapid results); (2) stochastic (characterize the channel from a frequency selection perspective); (3) geometry-based stochastic (commonly used for propagation prediction in mobile communication); and (4) deterministic (used in propagation prediction of specific environments). While stochastic and geometry-based stochastic could fail to characterize significant surrounding obstacles (foliage, lamppost, pedestrians, etc.) and V2I empirical tests provide useful

insight for specific in situ scenarios [43], the deterministic ray launching simulators are suited for vehicular propagation analysis of large-size scenarios yielding a reasonable tradeoff between accuracy and computational cost [10], [11], [44]. The principle of ray launching approaches is that a consistent number of path rays follows from the transmitter to the receiver over the direct, reflected and diffracted rays.

Ray-tracing modeling has been recognized as an accurate geometry-based-deterministic (GBD) tool to model propagation phenomena [6], [7] yielding an excellent approximation of the real-world propagation with a reasonable computational complexity; even with limited details and material characterization, it can still result in accurate levels of prediction, [13]. When the complete geographic information (e.g., location, dimensions, density, material properties of vehicles, buildings, and foliage) is available and processing speed is not an issue, then ray-tracing-based GBD models could be used for maximum accuracy, [12].
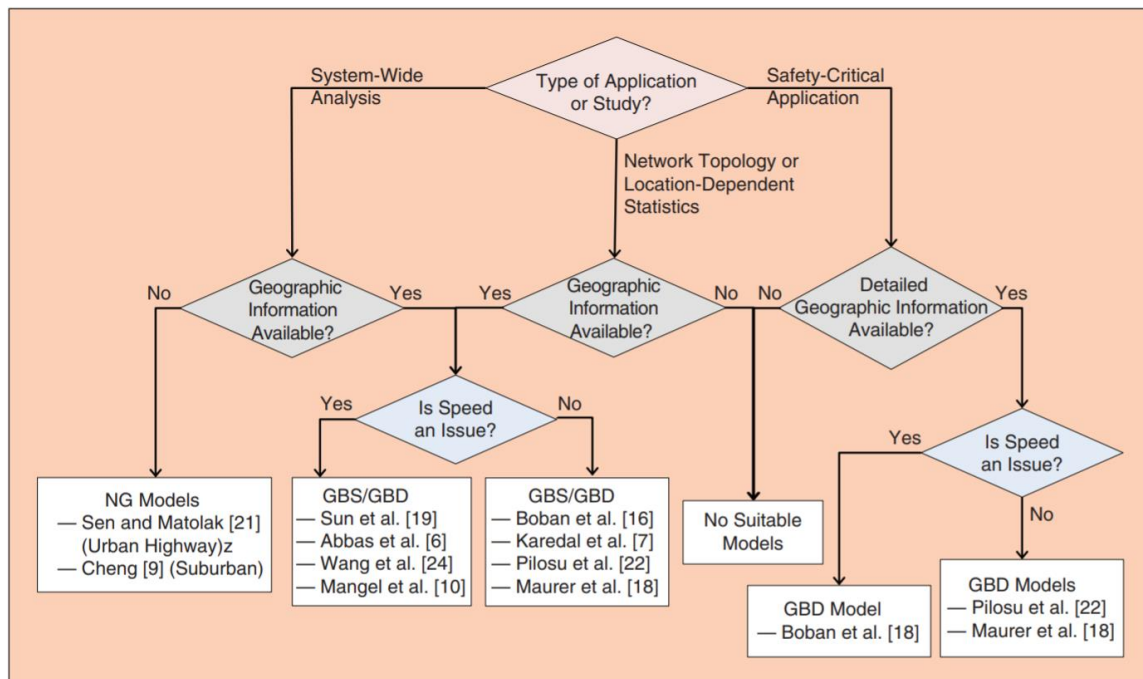
Figure 1. Guidelines for choosing a suitable channel model [12].

Figure 1 shows a guideline for choosing a suitable channel model, where the selection of the suitable model must consider three factors: the type of application (system-wide analysis or critical-safety application), the availability of geographical information, and the

12

influence of the velocity. Nongeometry-based (NG) models measure the channel characteristics in a specific environment and adjust the parameters of the path loss, shadowing, and the small-scale fading accordingly, while geometry-based-stochastic (GBS) models, which describe macroscopically the channel characteristics might lead to sensitive deviations from realistic behavior.

Some current state-of-the art simulators focus mainly on V2V or V2I communications operating in a cellular sense and, although the literature includes many propagation models and channel simulators for V2V systems [45], [46] there is a need for further studies to investigate V2I propagation using 3D deterministic tools in complex environments such as urban ones. Ray-tracing models yield an excellent approximation of the real-world propagation with a reasonable computational complexity, and even with limited details and materials characterization can still result in accurate levels of prediction of both geometry and shadow levels [13], and can serve as a tool to simulate radio shadowing environments. An empirical study of propagation in urban areas for V2I is presented [47]. The use of an in-house 3D ray-tracing software to analyze a statistical peer-to-peer channel model for outdoor urban environments is presented in [48]. The use of deterministic in-house or commercial 3D ray-tracing software to predict power as well as time, frequency and spatial dispersion in the radio channel in urban or V2X scenario is reported by [13], [49].

With respect to vehicular mobility, a realistic representation of vehicle mobility requires using real-world road topology, accurate microscopic mobility modeling, and real database traffic demand modeling, whereas a realistic representation of the signal propagation requires reproducing the actual physical radio propagation process, [14].

Vehicular mobility models are usually classified as either macroscopic or microscopic. The macroscopic description models interest is in vehicular density or mean velocity, and treating vehicular traffic according to fluid dynamics, while in the microscopic description each vehicle is a distinct entity, modeling its behavior in a more precise, but computationally more expensive way, [50]. Simulation of Urban Mobility (SUMO) is a free and open traffic simulation suite based on microscopic movement model developed by Stefan Krauß, [51], allowing modeling of intermodal traffic systems including road

vehicles, public transport and pedestrians. Simulation is performed on discrete time steps, and user can specify vehicle movement and vehicle flow. The human driving patterns block in SUMO is a car following model, and the path motion block includes a stochastic traffic assignment modeled by a probabilistic route choice.

With respect to the vehicular density, the authors in [16] state that higher vehicular density allows having shorter and more reliable wireless links in an infrastructure less approach of urban environments. Messages are propagated much more easily in high density scenarios than in scenarios with a low vehicle density (where messages cannot exploit the inherent multi-hop capabilities of vehicular networks) according to [17]. An analysis of the VANET topology characteristics over time and space for low and high vehicle density in a highway scenario (under LoS conditions) presented in [14], concludes that both lognormal and unit disk models fail to provide realistic VANET topology characteristics; they propose a matching mechanism to tune the parameters of the lognormal model according to the vehicle density.

Parameters such as vehicle density, average vehicle speed and relative speed among vehicles significantly impact information propagation in V2V environments, [15], while vehicular traffic flow has significant influence on the wireless signal propagation, [52]. Factors such as the number and size of the vehicles, the average vehicle arriving rate, and the average vehicle velocity determine the additional loss and signal fluctuation caused by the vehicular traffic flow. In this sense, it is important that VANET simulators should use geometry-based models that distinguish the instantaneous propagation into LoS, QLoS and NLoS conditions, and then apply an appropriate large-scale analysis for each case.

2.1 Solution Approach.

The effect of different VTD levels in the V2I, I2V and V2V propagation is simulated in a three-dimensional (3D) urban scenario where the vehicle mobility was simulated in SUMO, a microscopic vehicular mobility software widely used in this research field. The solution methodology is depicted in Figure 2, where are considered three stages:

14

a) Scenario representation: in this stage, the urban scenario is parametrized. The geographical information obtained from open platform is edited and parametrized into 2D-traffic simulator and 3D-RL software. The 2D-traffic simulator step-time must be carefully balanced with the 3D-RL cuboid size to get accurate results.
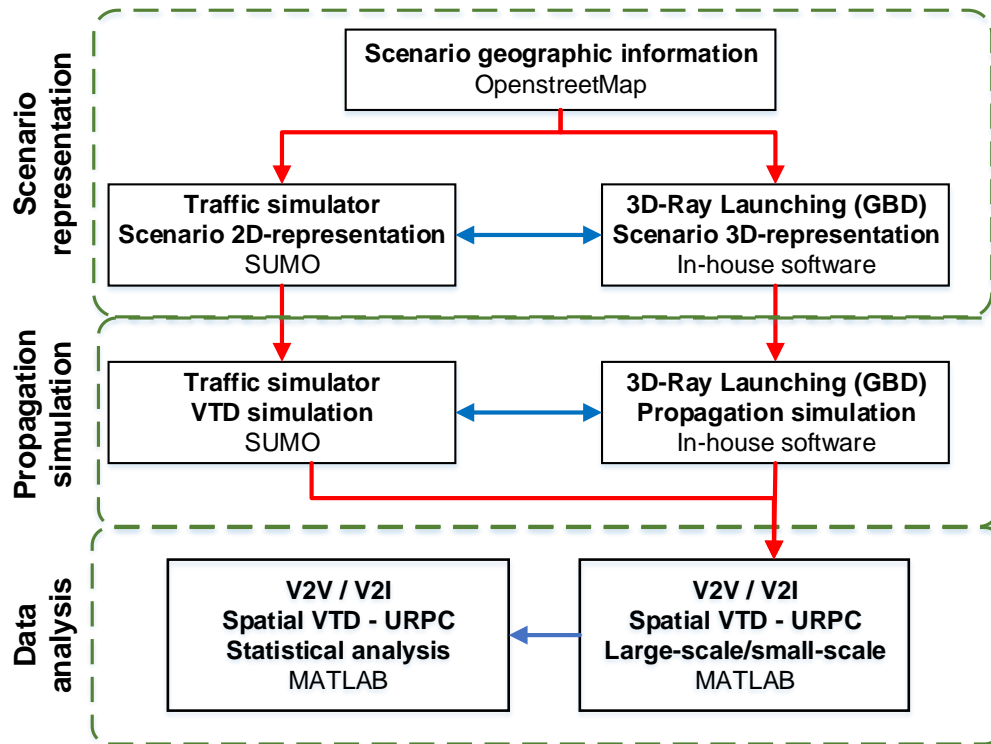
Figure 2. URPC- VTD solution overview

b) Propagation simulation and vehicular dynamics are simulation. The vehicular mobility and density are simulated in the 2D-traffic simulator and, information as quantity, position, velocity, acceleration, drive angle is generated. User-predefined/aleatory routes and three different VTD vehicular occupation levels are considered: low, medium and high with estimates values of 25%, 50% and 75% of vehicular scenario occupancy respectively. The IEEE 802.11p (PHY layer) standard is used to simulate the V2I and V2V propagation phenomenon into the 3D-RL software. Information as Received Signal Strength (RSS), Power Delay Profile (PDP) and Doppler profile (DP) is obtained as a result of temporal and spatial variation of path loss and multipath effects.

c) Data analysis: the large-scale/small-scale, propagation and statistical behavior of the RPC for V2V/V2I is analyzed. The spatial propagation loss is represented from the values of received signal strength as a function of TX-RX distance. Time-dispersion parameters are obtained from the PDP and DP generated by the 3D-RL simulator. The time varying nature of the channel is described by the Doppler spread and coherence time, [53].

A detailed exploratory analysis that considers the transmitter-receiver distance, the LoS, QLoS, NLoS conditions, large-scale path loss, multipath metrics, the comparison of measurements versus the 3D-RL simulation and analytical models, the impact of different VTD levels is presented in a holistic form as important contribution. Volumetric power estimations enable to obtain coverage/capacity ratios which aid in network deployment, whereas time domain estimation, such as volumetric power delay profile and delay spread values provide insight in equalization requirements as well as on the use and parameterization of adaptive modulation and coding schemes. Coverage/Capacity relations are introduced, providing node density values which aid in network deployment phases.

As summary of this section, the methodology to characterize the URPC for V2X under different VTD levels, considers three stages: the accurate scenario representation, the channel propagation and vehicular simulation, and, the V2I and V2V Large Scale, Small scale metrics and statistical characterization. The results are based on simulation and make use of computational tools as a deterministic 3D Ray-Launching algorithm, a detailed geographic database and a microscopic vehicular movement simulator, which integration is an important contribution for V2X URPC research and is explained in detail in the next section.

3. Ray-Launching and Vehicular Mobility Integration

This chapter introduces the description of the computational tools used and their integration. The background presents a brief explanation of the 3D-RL algorithm as the basis for the propagation analysis, the OSM and JOSM as geographic information source and map edition software respectively, and SUMO as microscopic vehicular mobility simulator. The integration of these tools is an important contribution. Figure 3 summarizes the approach of this chapter.
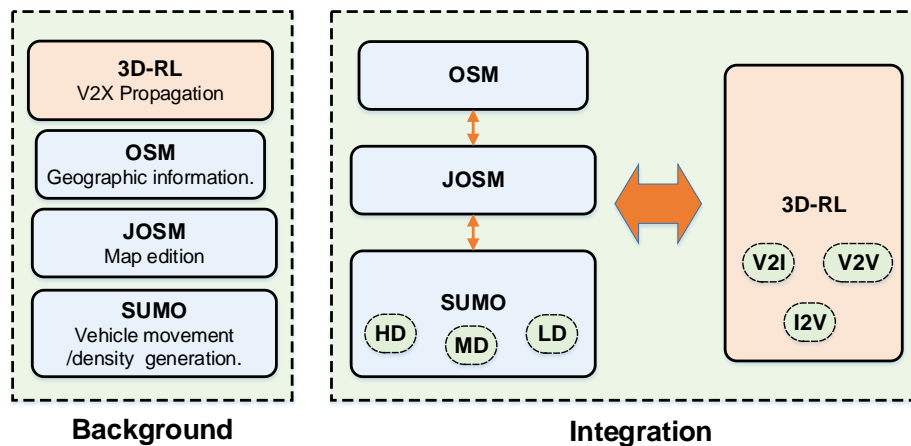
Figure 3. Approach of Chapter 3

3.1 Ray Launching (RL) Technique

The discovery of electromagnetic (EM) waves in 1880's by Hertz started a new era in scientific exploration of EM waves with a breakthrough when radio signals were sent across the Atlantic Ocean by Marconi (1901). Although EM waves are governed, with appropriate boundary conditions, by Maxwell equations, an analytical solution for the EM field is not possible in a realistic propagation environment, [54]. Ray tracing which is based on ray optics, is a numerical method to solve Maxwell's integral equations in high frequency regime which provides estimates of path loss, angle of arrival/departure, Power delay Profile, Doppler profile, time delays. Ray tracing is a member of the computational

EM (CEM) family, where other members are the finite-difference time-domain (FDTD) method, [55], the finite element method (FEM), [56], method of moments (MoM), [57], Multi-level fast multipole method (MLFMM), etc., used in simulation of EM systems as is illustrated in Figure 4.

CEM family:

CEM family	Well suited for:
UTD – Uniform theory of Diffraction	For electrically extremely large, perfect electrically conducting (PEC) structures
PO/RL-GO Physical Optics/Geometric Optics	For electrically very large radiation and scattering analysis
MLFMM Multi-level Fast Multiple Method	Electrically large, full wave analysis
MoM Method of Moments	Radiation and coupling analysis
FEM Finite Element Method	Problems with several dielectrics and waveguides.
FDTD Finite Difference Time Domain	To modelling inhomogeneous materials and simulations over a wide frequency range

Electrical size (vertical axis) — *Complexity of materials* (horizontal axis)

Figure 4. CEM family. Adapted from [58]

Numerical methods as FDTD, FEM, MoM, which are based on the discretization of differential or integral equations face the challenges of prohibitively large computational memory and processor when electrically large scenarios are analyzed, while the ray-tracing method, due to its high frequency approximation, is not so dependent on large computer requirements. Although, ray-launching method let obtain rough analysis results in a short time an inherent disadvantage is the analytical error resulted when the rays that arrive at the RX cannot be obtained rigorously, regardless of how narrow the angular interval of the launched rays be.

The main principle of the RL techniques is the wave front of the radiated wave is identified with several rays that propagate in the space according to optic and electromagnetic theories. There are two main methods for tracing rays. One is the imaging method (or image method), and the other is the ray-launching method (Shooting and bouncing ray (SBR) method or Brute-force ray-tracing method)[59]. In the ray-launching method, multiple rays are uniformly launched (icosahedron polygon) from the

TX in all directions, and then the rays that arrive at the RX are searched by tracing them as is illustrated in Figure 5:
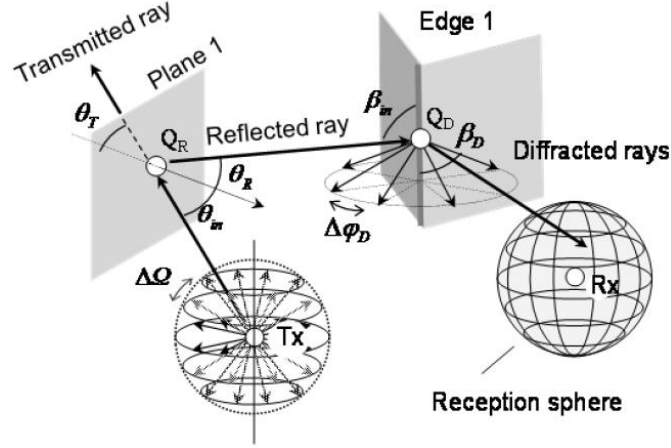
Figure 5: Ray Launching Method [60]

Multiple rays are launched in all directions with an angular interval (horizontal and vertical) of ΔΩ [60]. Each ray is traced until some termination conditions are satisfied. If the ray intersects a plane, the ray is divided into a reflected ray and a transmitted ray. The intersection point is recognized as a reflection point Q$_R$. If the ray intersects an edge, the intersection point is recognized as a diffraction point, Q$_D$, and multiple diffracted rays are conically retransmitted from Q$_D$ in directions with the angular interval of Δφ$_D$. On the Rx side, a reception sphere is set around the RX in advance, and the rays incident inside the sphere are recognized as received rays. The computational burden of the RL method is proportional to the number of traced rays which total number is given by

$$S_{launch} = N_{ray} 2^{N_R} (N_{Dray})^{N_D} , \qquad (1)$$

where

- N_{ray} is the number of launched rays from TX.
- N_{Dray} is the number of retransmitted rays from Q$_D$.
- N_R is the maximum number of reflections.
- N_D is the maximum number of diffractions.

Each ray propagates in the space as a single optic ray. The ray concept can be explained using the high frequency approximation of Maxwell's equations and its concept can be summarized as follows, [54],

- A ray travels in a straight line in a homogeneous medium.
- It obeys the laws of reflection and refraction, as well as the law of diffraction.
- A ray carries energy. It is more intuitive to treat a ray as a tube which electric field can be reduced by reflection, diffraction and when the ray travels further.

The associated electric and magnetic fields can be expressed as

$$\vec{E}(\vec{r}) = \vec{e}(\vec{r})e^{-j\beta_0 S(\vec{r})},$$
$$\vec{H}(\vec{r}) = \vec{h}(\vec{r})e^{-j\beta_0 S(\vec{r})}, \tag{2}$$

where $\vec{e}(\vec{r})$ and $\vec{h}(\vec{r})$ are magnitude vectors, $\beta_0 = 2\pi f_c \sqrt{\varepsilon_0 \mu_0}$, $\varepsilon_0 = 8.854 \times 10^{-12} [F/m]$ is the permittivity of free space, $\mu_0 = 4\pi \times 10^{-7} [H/m]$ is the permeability of the free space, and $S(\vec{r})$ is the optical path length which determines the phase of the light and governs interference and diffraction of light as it propagates and is defined by

$$S(\vec{r}) = \int_A^B n(\vec{r}) \, ds, \tag{3}$$

where $n(\vec{r})$ is the local refractive index as a function of distance, r, along the path $A \, to \, B$ From Maxwell's equations with $\beta_0 \to \infty$ (high frequency regime) the Faraday's law, Ampere's law, and Gauss' laws for electric and magnetic fields in free space are defined by

$$\nabla S \times \vec{e} - \mu_r \eta_0 \vec{h} = 0,$$
$$\nabla S \times \vec{h} - \varepsilon_r \eta_0 \vec{e} = 0,$$
$$\vec{e} \cdot \overrightarrow{\nabla S} = 0,$$
$$\vec{h} \cdot \overrightarrow{\nabla S} = 0, \tag{4}$$

where $\eta_0 = \sqrt{\dfrac{\mu_0}{\varepsilon_0}} = 120\pi \, [Ohms]$ is the impedance of free space.

From (3) it is observed that the electric field, the magnetic field, and the propagation direction are mutually perpendicular, the same relation as in a plane wave in free space. The incident electric field (E$_i$) created by an antenna at a distance r in the free space can be calculated by, [61]

20

$$E_i^{\perp\|} = \sqrt{\frac{P_{rad}D_t(\theta_t,\phi_t)\eta_0}{2\pi}} \frac{e^{-j\beta_0 r}}{r} X^{\perp\|}L^{\perp\|},\tag{5}$$

where P_{rad} is the radiated power with a directivity $D_t(\theta_t,\phi_t)$, where the sub-index t refers to the transmitted angle, and polarization ratio $(X^{\perp}, X^{\|})$. $L^{\perp\|}$ are the path loss coefficients for each polarization. The parameter *j* in (5) refers to the complex number.

A reflected and a transmitted ray are created when the rays impacts with an obstacle in its path, with new angles provided by Snell's law [62]. When a ray hits an edge, a new family of diffracted rays are created provided by formulation of the UTD. The main purpose of these diffracted rays is to remove field discontinuities and to introduce proper field corrections, especially in the zero-field regions predicted by GO. The diffracted field is calculated by [63]

$$E_{UTD} = e_0 \frac{e^{-jks_1}}{s_1} D^{\perp\|} \sqrt{\frac{s_1}{s_2(s_1+s_2)}} e^{-jks_2},\tag{6}$$

where s_1, s_2 are the distances from the source to the edge and from the edge to the receiver point, respectively. $D^{\perp\|}$ are the diffraction coefficients given by [63][64].

The in-house developed Three-Dimensional Ray Launching (3D-RL) code used in this work to analyze the EM propagation, is based on Geometric Optics (GO) and General Theory of Diffraction (GTD) with its uniform extension, the Uniform GTD (UTD). GO approaches considers only direct, reflected and refracted rays. The direct rays are related with the line of sight (LOS) propagation. The reflected rays correspond to the reflection (transmission) of EM waves at interfaces between different mediums and its magnitude is determined by Fresnel´s equations for different polarizations. The diffracted ray results when one incident ray can spawn many diffracted rays which calculation is more complicated than reflection and transmission coefficients, existing different formulations for the diffraction coefficients which may give different field results. The determination of the diffraction points when multiple edges are present is still research topic.

The development of the GTD and later the UTD improved the accuracy for diffraction calculation for wedges. The GTD was developed by Keller in 1960's where the Fermat's

principle of least time (the ray will take a route which consumes the least time possible traveling from one point to another) is applied to the determination of the diffracted ray path [26] and the law of diffraction was formulated: the incident angle is equal to the diffraction angle. A problem with GTD is that its result is not continuous across the shadow boundaries. These problems were solved with uniform solutions to the asymptotic expressions that Keller used to develop his theory. The first one was the UTD, which has been, historically, the most widely used. The RL technique and its combination with the UTD [65] is frequently applied to radio coverage prediction [66][67][68]. These techniques potentially represent the most accurate and versatile methods for urban and indoor multipath propagation characterization and therefore it has been selected to be implemented in the in-house developed 3D RL code.

The 3D-RL algorithm considers spatial resolution, a uniform three-dimensional hexahedral mesh, and parameters such as frequency of operation, radiation patterns of the antennas, number of multipath reflections, and spatial and angular resolution are taken into account. The algorithm is divided into three phases:

- Phase 1: Creating the scenario. This phase sets the scenario, considering all the obstacles within the environment, and the transmitters and receivers.
- Phase 2: Simulation of RL in 3D. In this phase, rays are launched from each transmitter, keeping the parameters in each position in space.
- Phase 3: Analysis of the results. In this phase, the values are obtained from the simulation to calculate the desired parameters.

The advantage of deterministic approaches is that it permits the consideration of all the obstacles within the environment, considering all the material properties, considering the conductivity and dielectric constant at the frequency range of operation of the system under analysis. Electromagnetic phenomena such as reflection, refraction and diffraction have been considered in the algorithm, leading to an efficient and robust technique. Different radiation patterns for the transceivers can be considered, as well as antenna parameters. The frequency of operation, number of multipath reflections, angular and spatial resolution, and cuboids dimension are introduced. In addition, the frequency

dispersive effects due to the movement of the vehicles can be analyzed by means of the Doppler shift and Doppler spread parameters, for different velocities of the vehicles and for the frequency under analysis.

The principle of the algorithm is that the complete 3D scenario is divided into a fixed number of different cuboid sizes. The position of the transmitter antenna is an input parameter of the algorithm; thus, rays are launched from the transmitter position with a fixed angular and spatial resolution, and propagation parameters are calculated for each cuboid along the ray path until the ray reaches the maximum number of reflections considered. The detailed operating mode of the algorithm has been previously published in [69], and it has also been validated in large indoor environments [70], urban and city environments [10], intra vehicle [71] and transportation systems [18], [42], [72]. Figure 6 depicts an example of a 3D urban scenario configured for the 3D-RL simulator.
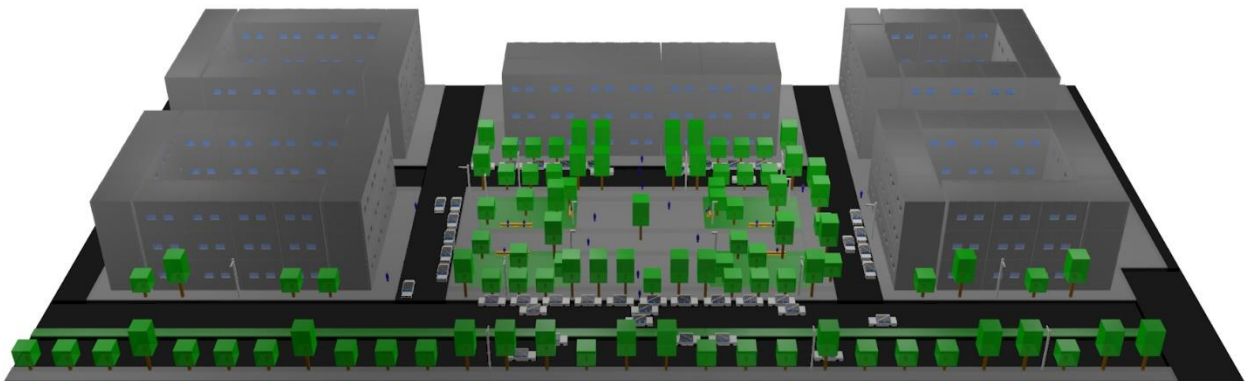
Figure 6. 3D-RL – Example of urban scenario used for simulation [73]

3.2 OpenStreetMap (OSM)

OpenStreetMap (OSM) project, born at University College London (UCL) in July 2004, was founded by Steve Coast. In April 2006, the OpenStreetMap Foundation (OSMF) was established to encourage the growth, development and distribution of free geospatial data and provide geospatial data for anybody to use and share. OSM is called the free wiki world map, a collaborative project to create a free editable map of the world (www.openstreetmap.org) and is one of the most popular examples of a Volunteered Geographic Information (VGI). A digital map can be used in navigation, in research, in development of location based applications, in disasters response [74], etc. As OSM is

open source, its development is rapid and dynamic depending on the volunteer's support. The more volunteers work on it, the faster its development process runs. For this reason, OSM is not equally advanced at all countries: in countries of Europe and North America OSM shows a highly detailed map, but in Asia, Australia and Africa, it is not much developed [75].

The goal of the OSM project is to create a free and editable world map. Within the project volunteers, amateurs and professionals from different social worlds act as sensors and collect geographic data. The motivation for contributing to OSM varies heavily: it ranges from self-expression over manifestation and representation of people's online identity to a simple fun factor. Meaningful extracurricular activities, interesting technologies and a fascinating general project development are further motivational reasons.

The OSM map information can be downloaded in OSM-XML format in convenient packages such by as country, continent, and in some cases administrative regions. An important characteristic of these downloads is that the OSM spatial data contained within the OSM-XML files are close to real-time representations of the spatial data stored in the global OSM database. Since the quality of OSM data can vary strongly, in most cases the data is compared with commercial or administrative datasets which, however, are not always accessible due to the lack of availability, contradictory licensing restrictions or high procurement costs [76]. In general, data for OSM can be derived from multiple sources and edited and imported by means of different freely available editors. One of most popular editors are the Java OpenStreetMap Editor (JOSM) which is described in the next section. Figure 7 shows the OSM map used for simulation.

3.3 Java OpenStreetMap Editor (JOSM)

Java OpenStreetMap Editor (JOSM) an extensible editor for OpenStreetMap for Java (https://josm.openstreetmap.de), is an editing suite with an interface more akin to traditional geographical information systems (GIS) packages. It supports loading GPX (GPS Exchange Format) tracks, background imagery and OSM data from local sources as well as from online sources and allows to edit the OSM data (nodes, ways, and

relations) and their metadata tags [77]. JOSM is open source and licensed under General Public License (GPL).
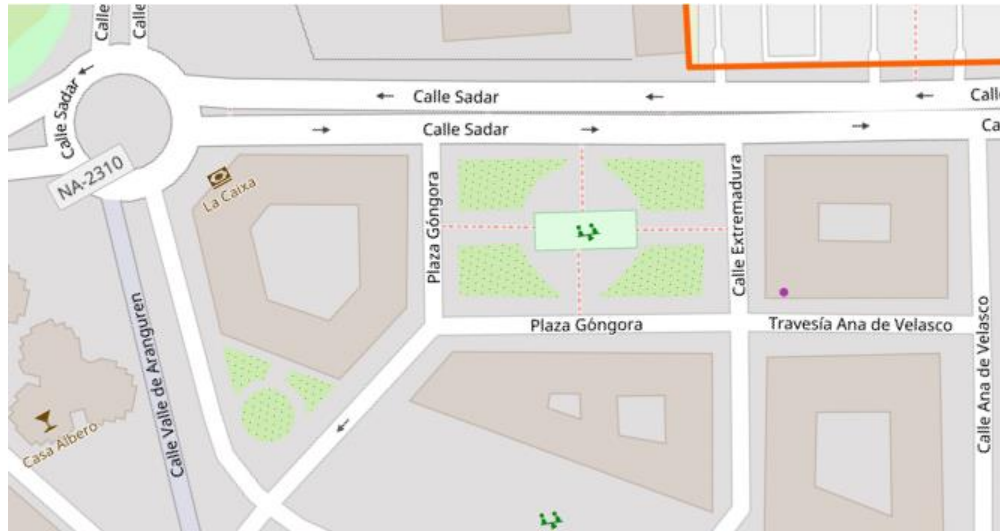
Figure 7. OSM – Example of urban scenario used for simulation

Experienced OSM contributors also use JOSM to import, edit, and tag OSM data offline and allows bulk uploads of OSM updates through the OSM application programming interface (API). JOSM offers advanced functionalities such as linking OSM features to photos and audio notes, supports data conflict resolutions, and can be extended using several independently developed plug-ins. Examples of user-contributed plug-ins include custom Web mapping service (WMS) background imagery and Yahoo aerial imagery, live recording of external GPS data, and a data and tagging scheme validation tool, to name just a few. An educational link to learn about JOSM is available in http://docs.inasafe.org/fr/training/osm/Chapter-04-getting-started-with-josm.html. The JOSM version used in this simulation is 11826. Figure 8 shows the JOSM map used for simulation which has been extracted from OSM platform.

3.4 Simulation of Urban Mobility (SUMO)

Simulation of Urban Mobility (SUMO), is an open source, microscopic, multi-modal traffic simulation based on the microscopic car following model developed by Stefan Krauß in 1998, in his Doctoral Dissertation "Microscopic Modeling of Traffic Flow:

Investigation of Collision Free Vehicle Dynamics" [78], which keeps some similarities with the car following model presented by Gibbs in 1981[79].

Figure 8. JOSM – Example of urban scenario used for simulation

SUMO allows to simulate how a given traffic demand which consists of single vehicles moves through a given road network. The simulation allows to address a large set of traffic management topics. It is microscopic: each vehicle is modelled explicitly, has an own route, and moves individually through the network according to a realistic mobility models where a proposed concept map is showed in Figure 9. Simulations are deterministic by default but there are various options for introducing randomness (http://sumo.dlr.de). It is mainly developed by employees of the Institute of Transportation Systems at the German Aerospace Center. SUMO is open source, licensed under the GPL (General Public License). Main features of SUMO are:

- Space-continuous and time-discrete vehicle movement.
- Different vehicle types.
- Multi-lane streets with lane changing and different right-of-way rules.
- Manages networks with several 10.000 edges (streets).
- Fast execution speed and high portability
- Network-wide, edge-based, vehicle-based, and detector-based outputs

- Microscopic routes - each vehicle has an own one

- Different Dynamic User Assignment algorithms

- High interoperability through usage of XML-data only
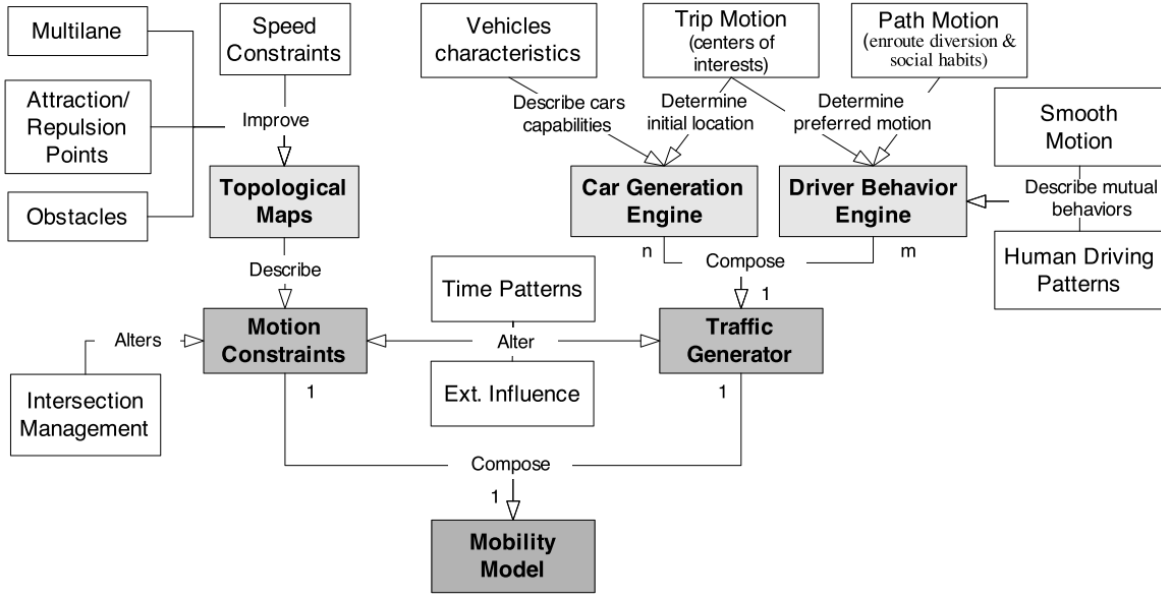
Figure 9. Concept map for the generation of realistic vehicular mobility models, [50]

SUMO car following model is microscopic, space-continuous, based on the safe speed–paradigm: a driver tries to stay away from the driver in his front at a distance and a safe speed that allows him to adapt this leader's deceleration. The model uses restriction parameters as the maximum acceleration and deceleration, maximum velocity, length of the vehicle, and driver's imperfection in holding the wished speed. It can be assumed that, apart from random fluctuations, every vehicle moves at the highest velocity compatible with the restrictions stated above. In this way the model is formulated as follows, [78]

$$v_{safe}(t) = v_l(t) + \frac{g(t) + g_{des}(t)}{\tau_b + \tau},$$

$$v_{des}(t) = min[v_{max}, v(t) + a(v)\Delta t, v_{safe}(t)], \quad (7)$$

$$v(t + \Delta t) = max[0, v_{des}(t) - \eta],$$

$$x(t + \Delta t) = x(t) + \Delta t,$$

where

$v_{safe}(t)$ = safe velocity in time(t),

$v_l(t)$ = maximun velocity velocity in time(t),

$g(t)$ = gap to the leading vehicle in time(t),

$g_{des}(t) = \tau * v_l(t)$ = desired gap to the leading vehicle in time(t),

τ = reaction time of the drivers $[0\ to\ 1]$,

$\tau_b = \dfrac{\bar{v}}{b(v)}$,

$v_{des}(t)$ = desired safe velocity in time(t),

η = random perturbation $[\eta > 0]$. It is assumed decorrelated in time,

$a(v)$ = maximum aceleration of the vehicle,

$b(v)$ = maximum desaceleration of the vehicle.

SUMO has been extensively applied in different projects related to network performance, traffic assignment, vehicle routing, traffic analysis [80], traffic emission, V2X [37] and other diverse traffic issues. SUMO can simulate electric vehicles, busses, pedestrians, bicycles, motorcycles, and their interactions with vehicles to present various traffic-related activities in cities. Since 2001, SUMO has been enhanced to simulate intermodal traffic, and it can be used to simulate the communication between the different entities. Therefore, it allows to simulate new modes in a transport system, and to execute the trips being generated by a demand modelling (which is not part of SUMO, here it relies on external input) and see their effects in terms of time, traffic, energy, pollutants, etc. [81]. Figure 10 illustrates the SUMO map configured for simulation.

3.5 3D-RL and SUMO integration.

The Vehicle-to-Infrastructure, Vehicle-to-Vehicle and Infrastructure-to-Vehicle channel propagation simulations were modeled and implemented in the 3D-RL simulator based on MATLAB (https://www.mathworks.com) platform, while the vehicle movement and its 3 different vehicular traffic densities (high, medium and low) were simulated in SUMO, where a Python platform is needed for the execution of Traffic Control Interface (TraCI) scripts when Windows Operating System is used.
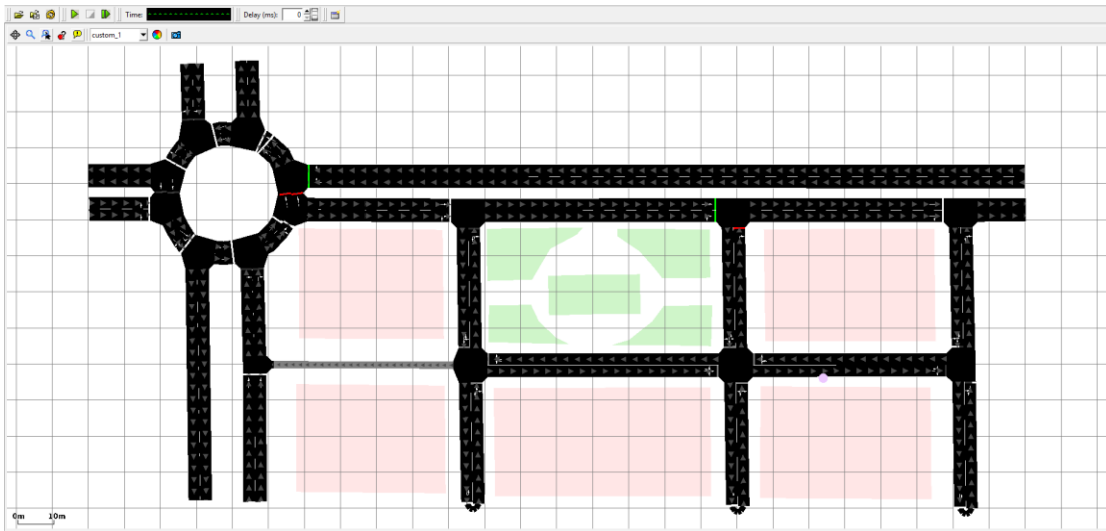
Figure 10. SUMO – Example of urban scenario used for simulation

The analysis results were processed and presented using MATLAB Version: 9.3.0.713579 (R2017b). Figure 11 illustrates a proposed schematic approach of the solution which includes the integration of 4 main stages:

a) the scenario selection and delimitation,
b) the scenario edition,
c) the vehicular density and movement configuration,
d) 3D-RL propagation simulation.

a) Scenario selection and delimitation: for this research a typical urban scenario has been selected which includes: highways, residential streets, parks, roundabouts, buildings, park-bench, lampposts, trees, pedestrians, vehicles, sidewalks, etc. This geographic information was extracted and exported form OSM. All contributed data is stored according to the OSM data model wherein point features are represented by "Nodes" and linear features by "Ways". Polygonal objects are represented by "closed Ways". Additionally, features can be further specified semantically by key-value pairs, so-called tags. There are no restrictions to the usage of tags. Whereas traditional

authoritative and commercial data sets usually follow the Resource Description Framework (RDF) notion, each OSM feature can hold multiple tags or no tags at all.
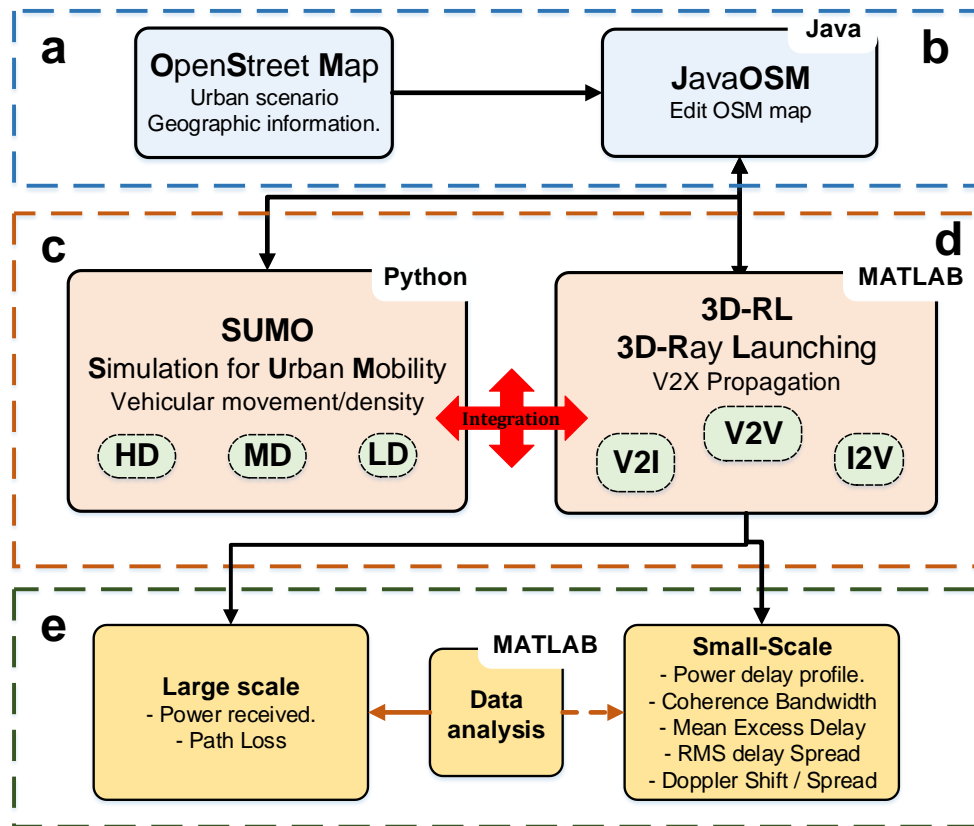
Figure 11. SUMO – 3D-RL integration: schematic approach

The OSM coordinate system is World Geodetic System (WGS 84) [82] which needs to be pre-processed in order to be compatible with SUMO, given that SUMO networks are encoded in Cartesian coordinates (meters) and may contain geo-referencing information to allow conversion to longitude, latitude. By default the Cartesian coordinates use the UTM-projection with the origin shifted to so that the lower left corner of the network is at 0,0 [83].

b) The scenario edition: using the JOSM editor, useless geo-referencing information, non-relevant routes and places were eliminated from the 2D OSM map. Some parameters as velocity limits, lanes number, type of lane (highway, residential,

etc.), lane direction, and axis translations useful for SUMO and 3D-RL compatibility, were configured at this point.

c) The vehicular density and movement configuration: the vehicle movement and density parametrization are described in this stage. The vehicle movement is defined by the default car following model configured in SUMO - Krauss carFollowModel - a modified version of the time-discrete and space-continuous car following model by Krauß [78]. SUMO requires the JOSM files in .net.xml format for scenario simulation; this is achieved whit the use of NETCONVERT tool (refer to Anexo B). Polygons from OSM-data and produce a Sumo-polygon file are generated by POLYCONVERT tool (refer to Anexo B).

Parameters as: vehicle routes, vehicle type, maximum speed, initial and final position, depart and arrive lane, start and final time, vehicles per hour, etc., are defined and configured in the <name>.rou.xml file (refer to Anexo B). The traffic lights parameters, required for the simulation of different vehicle densities, are configured in the <name>.net.xml file (refer to Anexo B). The SUMO simulation output behaves somewhat like a super-accurate high-frequency GPS device for each vehicle when setting the option --fcd-output <FILE>. xml information (refer to Anexo B). The FCD (floating car data) export contains the timestep, Cartesian coordinates and additional information required for the 3D-RL simulator as it is shown in **Table 1**.

With respect to the traffic-stream parameters, these fall into two broad categories: *macroscopic parameters* (volume or rate of flow, speed, and density) characterize the traffic stream as a hole, and *microscopic parameters* (spacing and time headway) characterize the behavior of individual vehicles in the traffic stream with respect to each other [84]. The density a macroscopic measure of traffic stream conditions, is defined as the number of vehicles occupying a given length of highway or lane and is generally expressed in vehicles per mile (vpm) or vehicles per mile per lane (vpmpl). Density is difficult to measure directly and is perhaps the most important of the three traffic-stream parameters because it is the measure most directly related to traffic demand.

In this research, three densities have been defined for SUMO simulation: High Density (HD), Medium Density (MD) and Low Density (LD).

31

Table 1. SUMO – FCD output

Name	Type	Description
timestep	(simulation) seconds	The time step described by the values within this timestep-element
Id	id	The id of the vehicle
type	id	The name of the vehicle type
speed	m/s	The speed of the vehicle
angle	degree	The angle of the vehicle in navigational standard (0-360 degrees)
x	m or longitude	The z value of the vehicle
y	m or longitude	The y value of the vehicle
z	m	The z value of the vehicle
pos	m	The running position of the vehicle measured from the start of the current lane
lane	id	The id of the current lane
slope	degree	The slope of the vehicle.
signals	bitset	The signal state information

Source: http://sumo.dlr.de/wiki/Simulation/Output/FCDOutput

The vehicular traffic density (VTD) was calculated considering two parameters: the total simulated vehicles in the scenario at specific SUMO step time versus the full scenario capacity, this is when all the roads are occupied. Approximately 30% of scenario occupancy is considered for LD, while 50% and 80% are considered for MD and HD respectively. The total scenario occupancy (100%) was calculated as follows

$$Total\ scenario\ occuppancy\ (vehicles\ units) = \frac{Total\ routes\ length\ [m]}{Vehicles\_length[m]\ +minGap[m]}\ ,\quad (8)$$

where

Total routes length [m] = sum of the length of all the vehicular routes in the scenario,

Vehicles_length [m] = default SUMO passenger vehicle length: 5.0 m,

minGap [m] = default SUMO minimum gap between a pair of vehicles, or empty space after leader: 2.5m.

Table 2 shows the VTD for each avenue and street. When all the routes are full occupied, a total of 270 vehicles are simulated simultaneously. Each route has 2 lanes where passenger vehicles (5m large) circulate with a minimum separation of 2.5m between them. The largest route is AV1 (453,60m) with capacity for 58 passenger vehicles.

Table 2. SUMO – Vehicular Traffic density

Route	Total length [m]	Total occupancy [quantity of vehicles]
AV1 (2 lanes)	453,60	58
AV2 (2 lanes)	452,44	58
AV3 (2 lanes)	180,86	22
AV4 (2 lanes)	181,20	22
AV5 (2 lanes)	165.34	20
ST1 (2 lanes)	273.98	34
ST2 (2 lanes)	85.80	10
ST3 (2 lanes)	164.30	20
Roundabout (2 lanes)	203.74	26
Scenario	**2161.26**	**270**

Figure 12 depicts a VTD occupancy simulation for HD (80% occupancy). Each vehicle color is matched with specific assigned route. A uniform vehicle distribution is required along each avenue and street. Traffic lights are useful to simulate different levels of VTD.
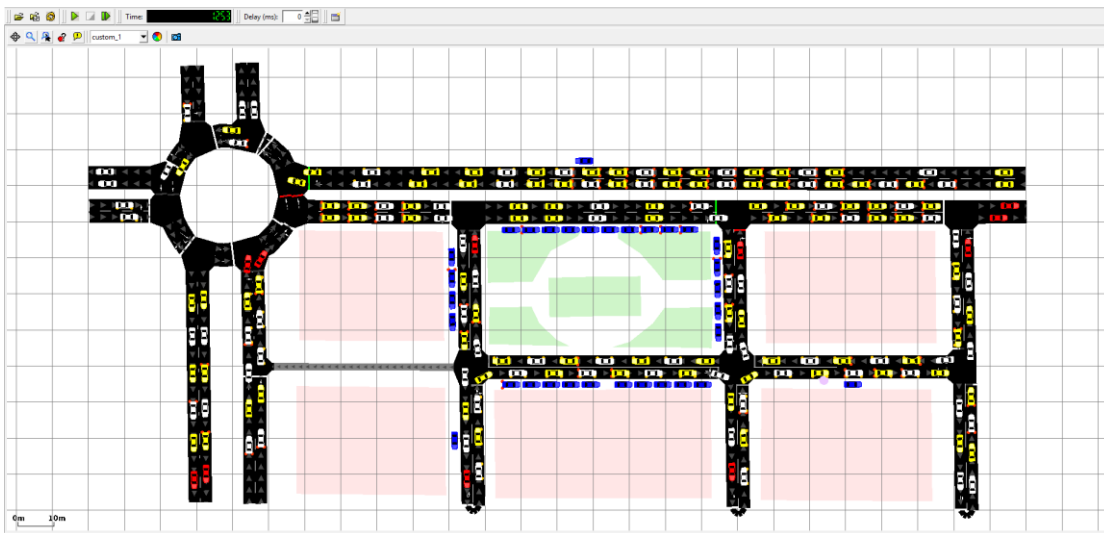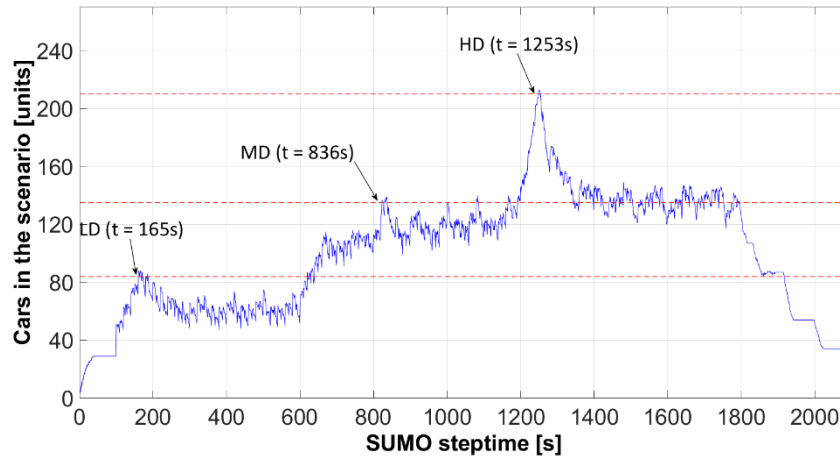

Figure 12. SUMO – VTD scenario occupancy simulation for HD (t = 1253s).

Figure 13 shows a VTD scenario occupancy SUMO simulation where, (a) is the total vehicles simulated and, (b) is the scenario occupancy percentage. Higher levels of occupancy were simulated, almost at 100%, with significant increase in the simulation time.
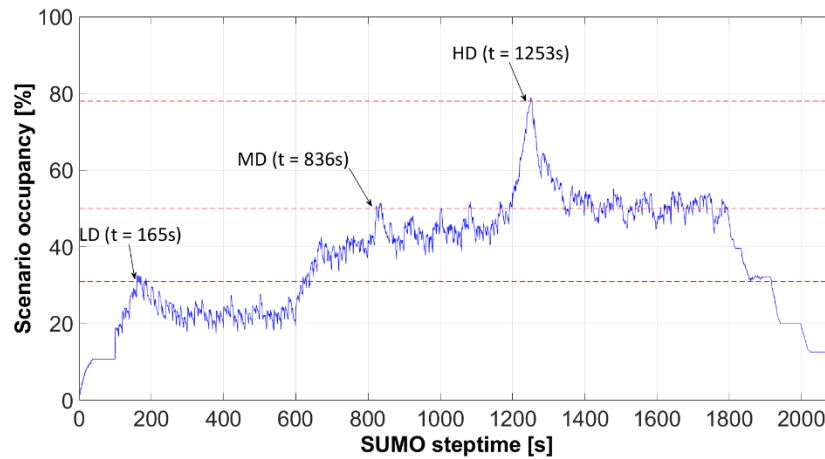
Figure 13. VTD evolution: **(a)** total vehicles simulated, **(b)** scenario occupancy.

d) 3D-RL simulation: the 3D scenario representation and propagation simulation are performed in this stage. From mixed information of OSM, JOSM and SUMO, the 3D scenario is parametrized and building into the 3D-RL simulator. The scenario and vehicular Cartesian coordinates (x, y) [m] must be carefully matched and synchronized between: JOSM, SUMO, and the 3D-RL simulator, while the Cartesian coordinate (z) [m] is matched between OSM and the 3D-RL simulator. The 3D-RL algorithm has three recurrent steps: the first step is to take all the antennas of the same room and introduce them to simulate, the second step is to simulate the room, and the third step is to transform the rays coming out of the room in new antennas in other rooms. Once the point of impact is calculated, it is necessary to follow the straight line joining the initial

point and the final impact point saving the parameters of each ray. Accordingly, the environment is divided into a number of cuboids of a fixed size [85]. The information stored in each hexahedron that the ray passes in its trajectory is:

- Time taken from the ray to arrive.
- Distance traveled by the ray.
- Loss coefficient in each polarization.
- Ray direction in the transmitter.
- Ray direction in the receiver.
- Transmitting antenna.
- Diffraction.

Parameters such as frequency of operation, radiation patterns of the antennas, number of multipath reflections, separation angle between rays and cuboid dimension can be modified in the algorithm. The frequency dispersive effects due to the vehicle's movement can be analyzed by means of the Doppler shift and Doppler spread parameters, for different vehicular velocities and frequency under analysis. The optimal parameters for medium scenarios simulation, to achieve accurate results with an acceptable computational time is to consider six reflections and angular resolution of launching rays of 1º, while for large scenarios an adaptive meshing is necessary, because the algorithm could have divergence zones which lead to neglecting significant contributions [85].

Figure 14 shows an example of 2D map for HD (t = 1253s) which matches the Cartesian coordinates of Figure 12. With the information provided by OSM, JOSM and SUMO, the 3D scenario is parametrized considering:

- The shape and dimensions of the simulated vehicles are given by pre-defined 3D-RL "vehicles-function" which are in close match with the SUMO vehicles, while the dielectric properties of the vehicle components (metal, glass, rubber, etc.) are programed in the 3D-RL code.
- The vehicles position is defined by SUMO. Vehicles can only be oriented in vertical or horizontal position; diagonal position resulted in SUMO simulation must be approximate to vertical or horizontal position in the 3D-RL simulator.
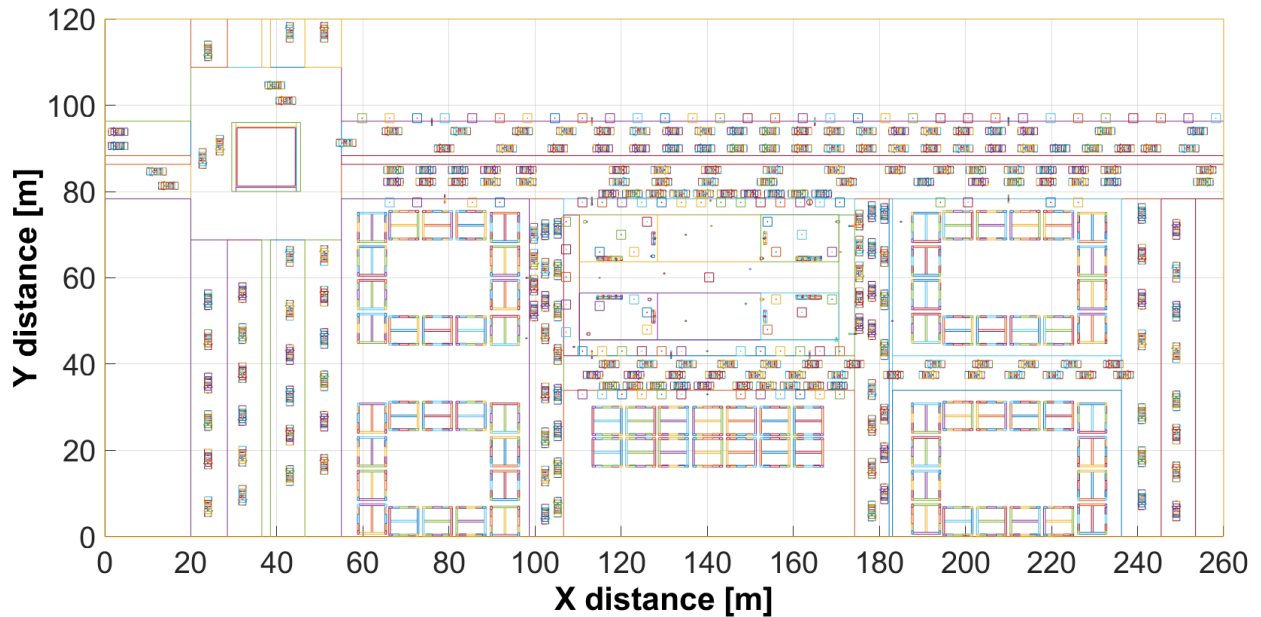
Figure 14. 3D-RL scenario representation for HD (t = 1253s).

- The shape and dimensions of the objects (buildings, lampposts, park-benches, threes, grass, etc.) are given by pre-defined 3D-RL "obstacle-function" in close match with OSM parameters.
- The objects position and objects height are defined by JOSM and OSM respectively.
- Due to scenario cuboid segmentation for 3D-RL analysis, the rounded areas could not be represented accurately. This is the case of the roundabout, where the circular area (refer to Figure 12) is represented by an approximate squared area (refer to Figure 14). Scenario segmentation and spatial TX-RX distance considerations are aimed to minimize this issue.

Figure 15 depicts a 3D scenario prepared for simulation in the 3D-RL. Figure 15(a) illustrates a large-size scenario (260m x 120m x 20m), resulting in 624.000,00 cuboids of useful propagation information, after the 3D-RL simulation. The red circles in Figure 15(b) are TX antennas used in the V2X analysis.
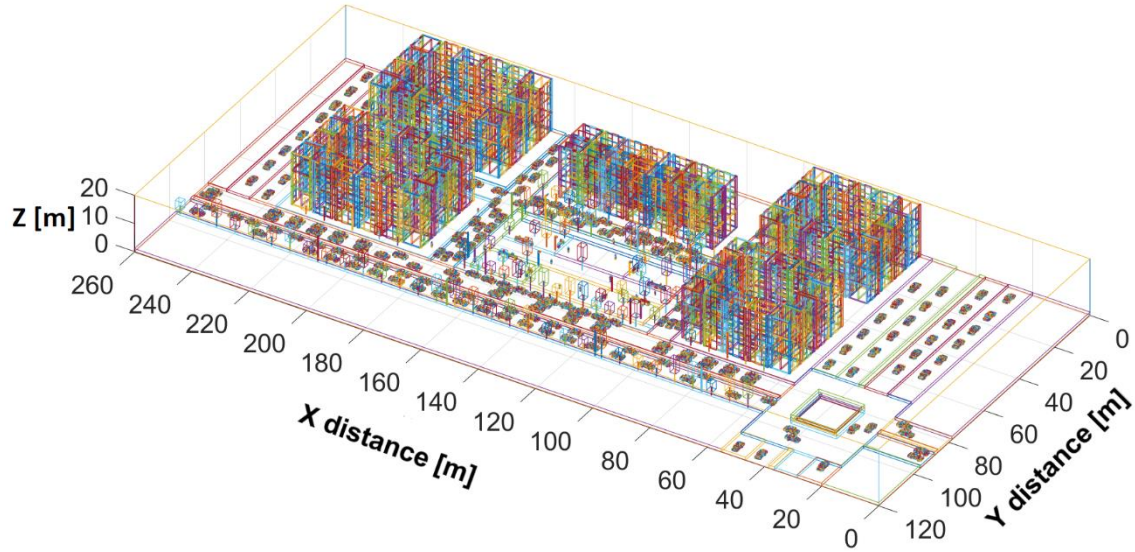
(a)
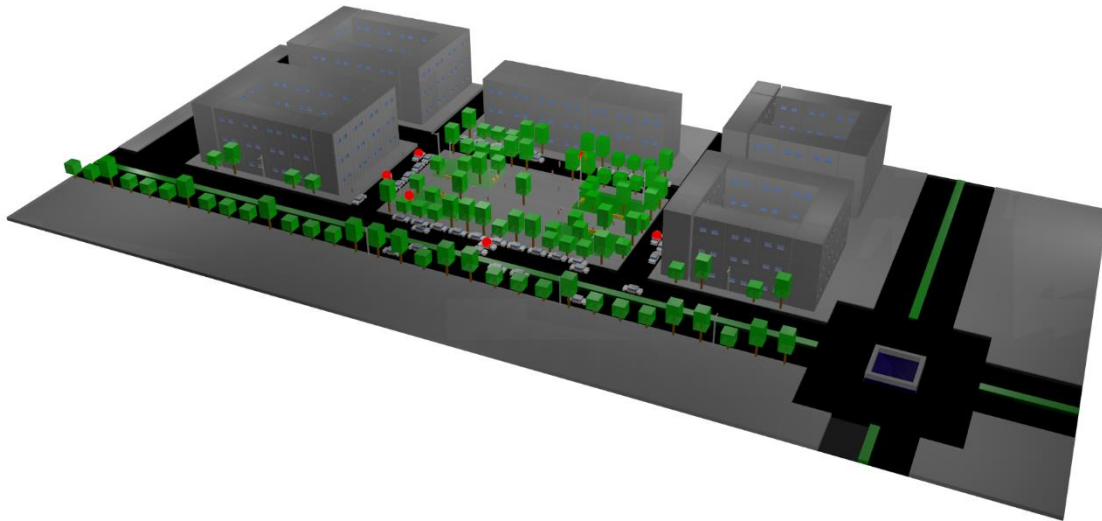
(b)

Figure 15. 3D-RL scenario: **(a)** schematic representation, **(b)** rendered view [18].

In this chapter have been presented the description and the integration of the computational tools used in this research: the geographic database (OSM) and map editor (JOSM), the 3D-RL deterministic algorithm used for the V2X URPC simulation, and the microscopic vehicular movement simulator (SUMO). The integration of these tools is based on three stages: the representation and edition of the urban scenario, the VTD simulation and, the URPC simulation. The URPC data analysis was carried on MATLAB platform, and the results are presented in the next section.

Basic research is what I am doing
when I don't know what I am doing.
Wernher von Braun (Rocket scientist, 1912 - 1977)

4. Results

Small-scale, large scale, coverage and measurement validation are presented and discussed in this Chapter. The description and main simulation parameters of two represented urban scenarios are detailed. Measures such as RSS, spatial Path Loss, coverage map, and multipath metrics as Power Delay Profile, mean excess delay, RMS delay spread, Coherence Bandwidth, Doppler Shift and Doppler Spread are presented. Figure 16 illustrates the approach of this chapter.
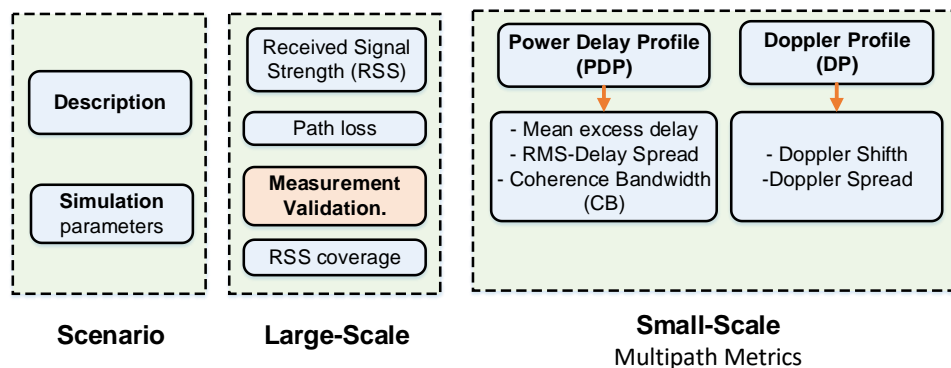
Figure 16. Approach of Chapter 4.

4.1 Urban scenario description

Deterministic models, such as 3D-RL, have the advantage that computer simulations are easier to perform than extensive measurement campaigns, however, the accuracy of the 3D-RL results depends on the detailed geographical description of the scenario together with the electromagnetic properties of the interacting objects. This subsection describes the selected urban scenario with its 2D and 3D representation maps, reference points and main 3D-RL simulation parameters for the V2X propagation simulation and analysis. Three urban scenarios have been used for analysis:

- Scenario 1: a detailed large-scale path loss analysis and measurement validation for V2I is presented.
- Scenario 2: small-scale, multipath metrics, coverage analysis and brief statistical analysis for V2I is analyzed.

4.1.1 Scenario1 description.

The 3D-RL incorporates a database of geographic data such as vegetation, terrain, buildings, park-benches, cars, pedestrians, avenues, streets, roundabouts and sidewalks of an urban scenario modeled and characterized as an approximate replica of Plaza de Gongora (42°47'52.72N, 1°38'21.14W) located in Pamplona, Spain. The area encompasses 624,000 m3 (260m×120m×20m) and includes: one park, one roundabout (with fountain), three secondary streets, five motorway avenues, five buildings (20 m high), eight park benches, eight medium lampposts (7 m high), 13 high lampposts (10 m high), 16 pedestrians, 45 cars, 100 trees and many sidewalks. Figure 17(a) depicts a 3D aerial-view of the modeled scenario. Figure 17(b) displays a 2D aerial-view which identifies the main points and areas of interest and its relative position (x, y), according to Table **3**. Figure 17(c) shows a close-up view of some scenario elements used in the 3D-RL simulation.
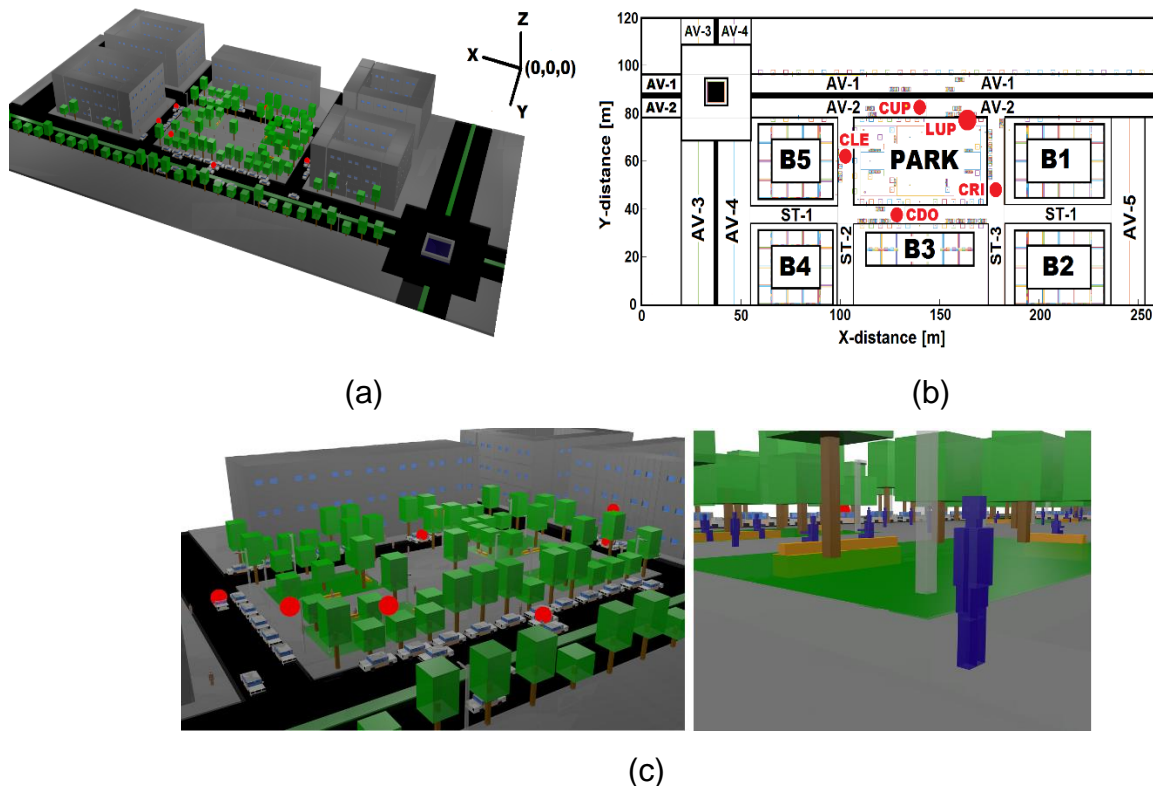

(a)   (b)

(c)

Figure 17. Scenario1: **(a)** 3D frontal-view, **(b)** 2D back-view, **(c)** close-up view, [18].

Table 3. Scenario1 reference.

Description	Abbreviation	Position (x, y, z) [m]
Main Avenues	AV-1/ AV-2/ AV-3 AV-4/ AV-5	(x, 93, 0)/ (x, 82, 0)/ (29, y ,0) (47, y, 0)/ (247, y, 0)
Streets	ST-1/ ST-2/ ST-3	(x, 39, 0)/ (54, y, 0)/ (130, y, 0)
Transmitter antenna	Tx (LUP)	(164, 78, 3.5)
Car antennas	CUP/ CRI CDO/ CLE	(91, 82, 1.5)/ (130, 50, 1.5) /(84, 38, 1.5)/ (54, 62, 1.5)
Buildings	B1, B2, B3, B4, B5	Not applicable.

The simulation parameters are registered in **Table 4**. The simulation information was gathered from 624,000 cuboids of 1 m × 1 m × 1 m evenly distributed. The transmitter antenna (Tx) was located at 3.5 m height in the upper lamppost (LUP). The receiver (Rx) antenna was placed at 1.5 m height. The transmitted power was settled at −10 dBm and the Received Signal Threshold (RST) at −120 dBm. The reference distance d_o = 1 m.

Table 4. Scenario1 simulation parameters.

Parameters	Values
Transmitter (Tx): Power/Gain/Frequency/Height	−10 dBm/3.74 dB/5.9 Ghz/3.5 m
Receiver (Rx): RST/Gain/Frequency/Height	−120 dBm/3.74 dB/5.9 Ghz/1.5 m
Antenna Polarization	Omnidirectional
3D Ray tracing resolution	1 degree
Scenario size/Unitary volume analysis	260 m × 120 m × 20 m/ Cuboids of 1 m

4.1.2 Scenario2 description.

The modeled and simulated urban scenario is a replica of the Pío XII Avenue at the city of Pamplona, Spain (42°48′22.15 N, 1°39′39.14 W) and it was referenced using the Google Maps tool. The scenario encompasses an area of 1,320,000 m^3 (400 × 150 × 22) and includes the typical elements of an urban environment. Each side of the avenue has three lanes, and vehicles park parallel to the pavement on both sides. The parked vehicles coexist with metal and fiberglass garbage containers. Figure 18(a) shows the urban scenario aerial view, 18(b) is the 2D schematic (x, y) map and, 18(c) is the 3D frontal-view map used in the simulation. **Table 5** identifies the Cartesian coordinates (x, y, z) of interest points according to their relative position from the origin (0, 0, 0) [m].

(a)

(b)

(c)
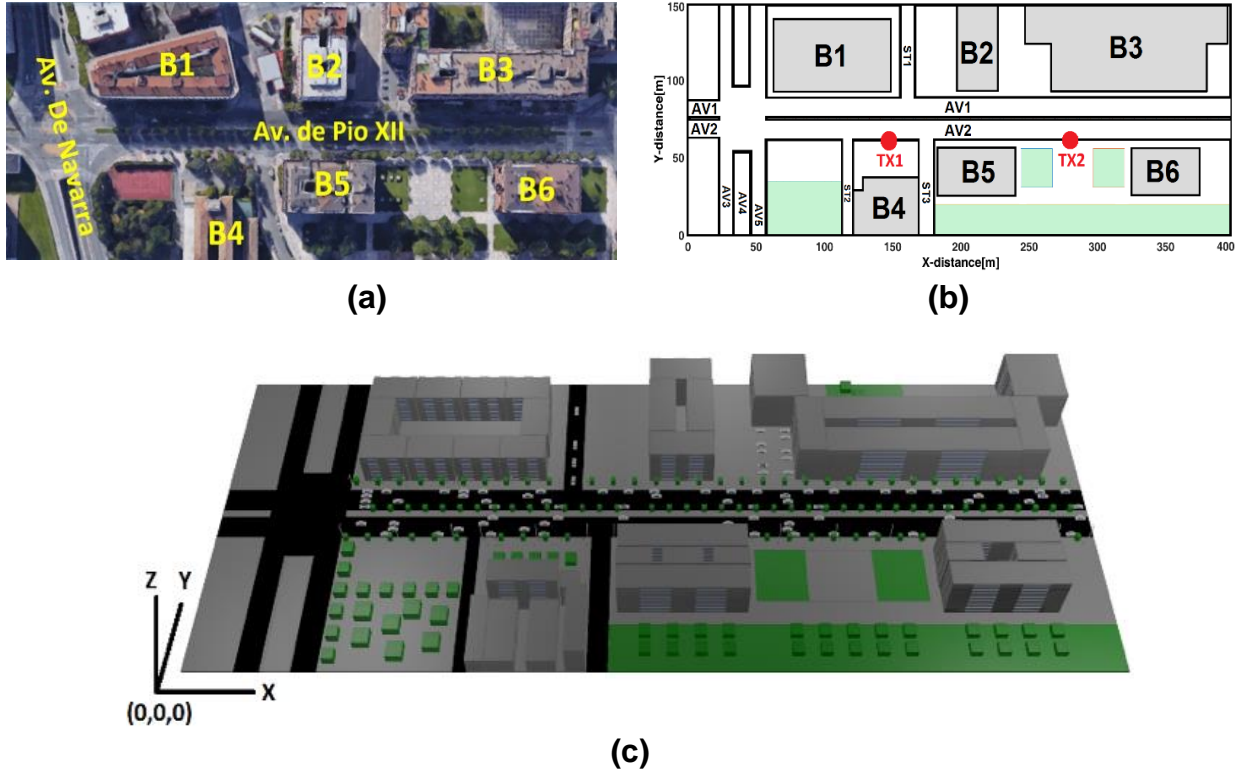
Figure 18. Scenario2: **(a)** google map view, **(b)** 2D-map view, **(c)** 3D-map view [86].

Table 5. Scenario2 reference.

Reference	Abbreviation	Coordinates (x, y, z) m
Main Avenues	AV1/AV2	(x, 83, 0)/(x, 69, 0)
Streets	ST1/ST2/ST3	(161, y, 0)/ (117, y, 0)/ (175, y, 0)
Transmitter antenna (TX)	TX1/TX2	(146, 63, 3.5)/(281, 63, 3.5)
Receiver antenna (RX)	RX	(x, y, 1.5)
Buildings	B1, B2, B3, B4, B5, B6	Not applicable.

Simulation parameters for scenario2 are summarized in Table 6.

Table 6. Scenario2 simulation parameters.

Parameters	Values
TX1, TX2: P_t */$\mathrm{Gain}(G_t)$/Frequency/Height /polarization.	0 dBm/0 dB/5.9 Ghz/3.5 m omnidirectional.
RX: RST **/$\mathrm{Gain}(G_r)$/Frequency /Height. /polarization.	−100 dBm/0 dB/5.9 Ghz/1.5 m omnidirectional.
3D-RL: horizontal and vertical angular resolution	$\pi/180$ rad
Angular resolution of diffracted rays.	$\pi/20$ rad
Maximum permitted reflections.	7 hops
Cuboid segmentation for analysis.	1 m3 (1 × 1 × 1) m
Scenario: dimension.	(400 × 150 × 22) m

Pt *: Power transmitted, RST ** (Received Signal Threshold).

41

The RST was chosen considering the receiver (RX) minimum sensitivity information provided for some manufactures of V2X (IEEE 802.11p) radio-communications products [87], [88], [89].

4.2 Scenario1 - Received Signal Strength (RSS)

Figure 19(a) illustrates a general RSS surf-plot, Figure 19(b) shows a RSS contour map at z-plane of 1.5m, and Figure 19(c) depicts a RSS zone map. From the analysis of Figure 19, four RSS zones are identified:

1. Zone 1 (yellow colored) is mainly under LoS condition without obstruction by buildings, however some obstacles (e.g., trees, cars, lamppost) can cause obstruction. These types of partially obstructed links are sometimes referred to as Quasi-Line-Of-Sight (QLoS) [90]. The average RSS is above −100 dBm, thus V2I communication is feasible. This zone encompasses avenues AV-1 and AV-2 (LoS), the street ST-1, ST-2 around the park (QLoS), and ST-3 (QLoS).

2. Zone 2 (light-green colored) is under LoS, without obstruction by buildings, but with the presence of a roundabout, which causes degradation and high fluctuations in the RSS. The RSS is fluctuating between −100 dBm and −140 dBm. The conditions for V2I are degraded. This zone comprises the roundabout (LoS), AV-1, AV-2 before the roundabout and AV-3, AV-4 after the roundabout.

3. Zone 3 (light-blue colored) is under NLoS conditions caused by buildings. The position of buildings can generate a corridor-configuration at some street segments, where the waveguide effect [91][92] is produced. The average RSS fluctuates between −100 dBm and −120 dBm. The conditions for V2I communications are degraded. This zone encompasses street ST-1 between B5-B4 and B1-B2 and, ST-2 between B4 and B3.

4. Zone 4 (blue colored) is under NLoS caused by buildings. The average RSS is below −120 dBm with high fluctuations. The conditions for V2I communications are unfeasible. This zone encompasses avenues AV-3, AV-4 and the AV-5.
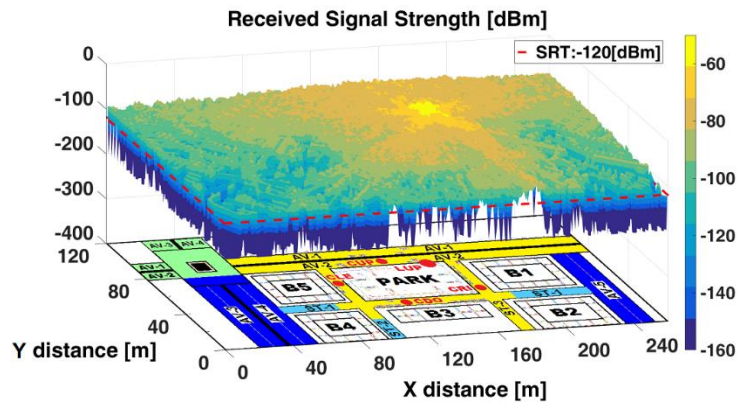
(**a**)
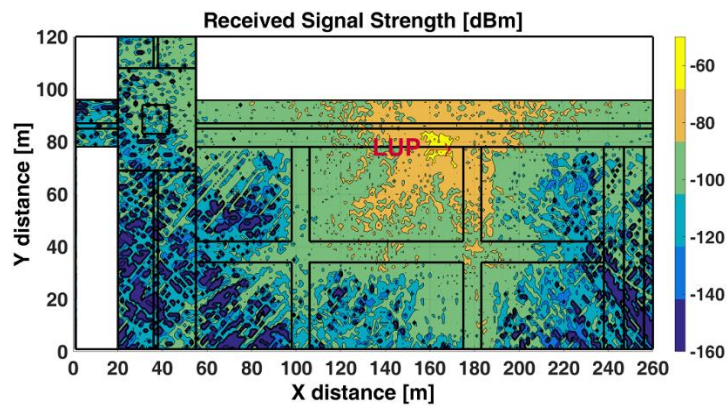
(**b**)
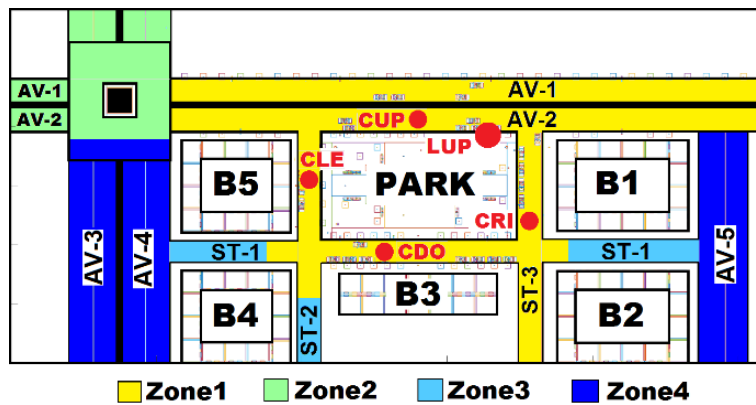
(**c**)

**Figure 19.** Scenario1: **(a)** RSS surf-plot; **(b)** RSS contour map; and **(c)** RSS zone map.

One can observe the impact that distance (TX-RX), factors such as density and material (different electromagnetic properties), geometry and location (the buildings define the LoS and NLoS conditions); and places such as roundabout and intersections

(deteriorate the RSS irrespective of distance) have on the propagation phenomenon. In previous work [22], the impact of the frequency on the propagation in this scenario was shown, the mean RSS at 5.9 GHz is below that at 2.4 GHz. The NLoS caused by buildings generate high path loss and notorious fluctuations in the RSS at AV-3, AV-4 and AV-5. The corridor configuration at streets ST-1 and ST-2 (light-blue colored) causes the waveguide effect when RSU rays impacts upon the lining walls of the buildings where the location of the RSU (angle of incidence) together with factors such as the width and length of the streets define the magnitude of the waveguide effect. A detailed RSS analysis of the propagation along streets and avenues is addressed in the next subsection. With this RSS information, some alternatives of RSU deployment to ensure the V2I communication from the point of view of connectivity (RSS above RST) could be proposed. In terms of radio planning analysis and coverage/capacity estimations, one alternative could be to consider at least four TX distributed as follows:

1. Two TX could be in opposite corners of the park, the first at the intersection of AV-2 and ST-3, and the second at the intersection of ST-1 and ST-2. This configuration ensures RSS above RST at AV-1, AV-2, ST-1, ST-2, and ST-3.
2. One TX could be located at strategic surrounding area of the roundabout to allow coverage for the roundabout, AV-3, AV-4 and part of AV-1 and AV-2.
3. One TX could be placed at intersection of AV-2 and AV-5 so that ensures the coverage for AV-5 and part of AV-1.

4.3. Scenario1 - Large-Scale Spatial Path Loss Characterization

The coverage of WSN in the design phase of V2I communication depends on the accurate estimation of the propagation model parameters. Any error reduction between theoretical or predicted by simulation versus measured RSS have a significant impact in the coverage estimation, identification of undesired power losses, RSU arrangement, size and performance of the WSN network, which have direct implication in quality of service and project viability. The 3D-RL technique is a well-recognized tool for this purpose. Figure 20 depicts a RSS spatial representation (z-plane of 1.5 m) along the avenues and streets. The LoS and NLoS conditions are identified considering the relative spatial distance TX-RX (left, right, up, down).

(**a**)

(**b**)

(**c**)

45
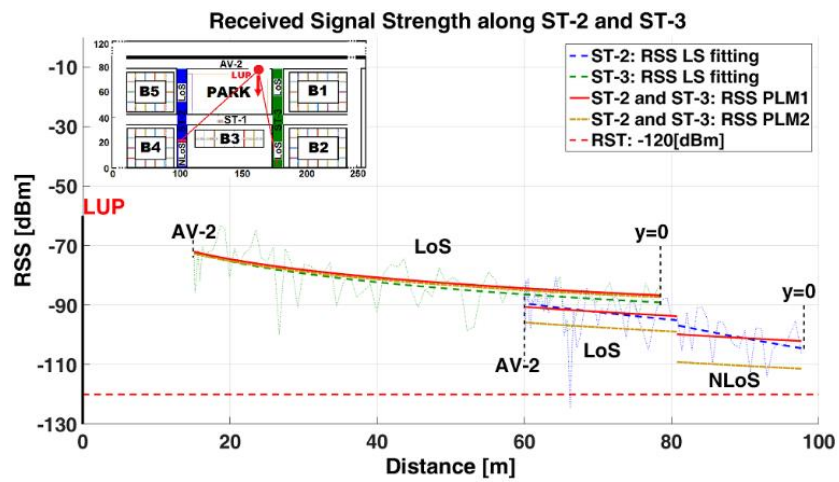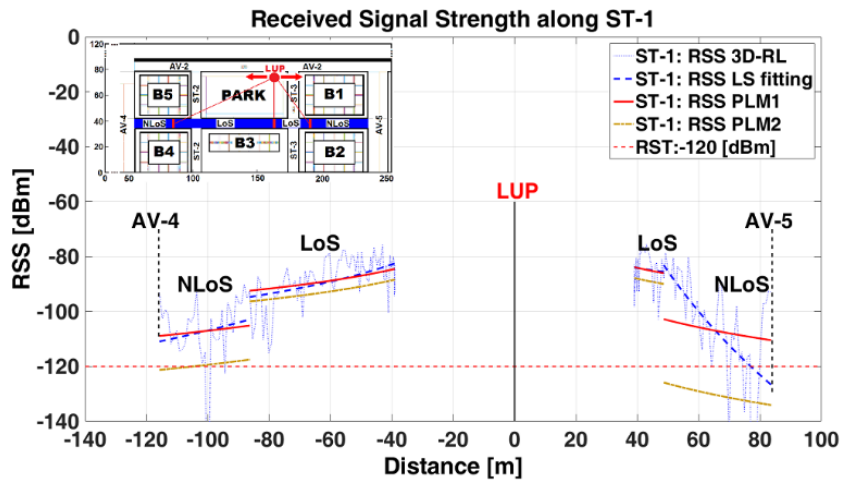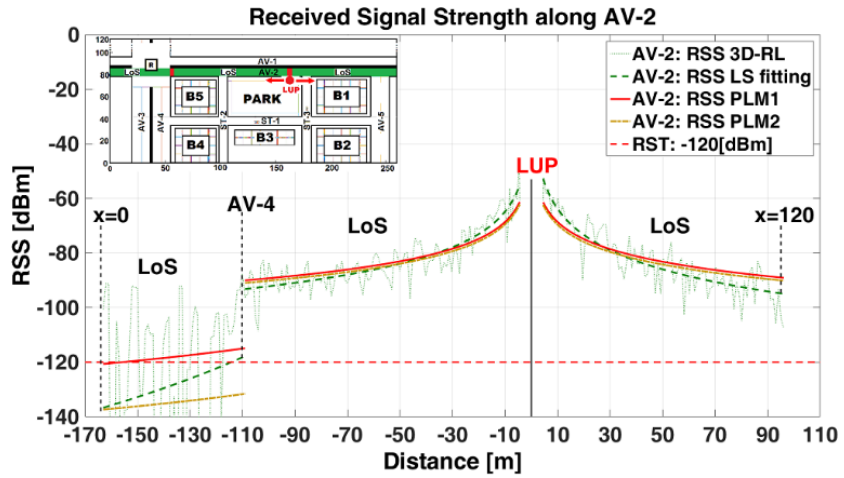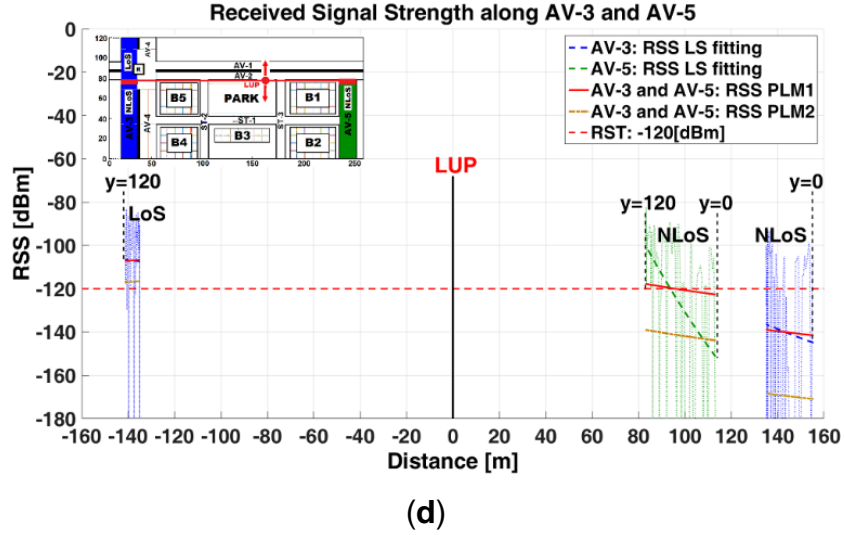
Figure 20. Scenario1 RSS: (**a**) AV-1, (**b**) ST-1, (**c**) ST-2 and ST-3, (**d**) AV-3 and AV-5.

There are four different RSS representations in each image of Figure 20:

1. RSS (dotted-line): 3D-RL technique, is the representation of the raw data obtained from the scenario simulation, organized in an array of 20 matrices (z-plane), each one with dimension of 260 × 120 (x-plane and y-plane).

2. RSS (dashed-line): Fitting of the RSS raw data using a first order polynomial that represents the tendency-line of the raw data. This Least Squares (LS) fitting is robust to minimize the effect of some outliers in the RSS raw data and let us visualize the RSS propagation behavior. It constitutes the comparison point to measure the goodness-of-fit with any path loss model.

3. RSS (continuous-line): Path loss model (PLM1) [53] is used for comparison purposes with the 3D-RL results. This PLM describes the random shadowing effects over many measurements that have the same Tx-Rx separation, but different levels of clutter on the propagation path. The received power P_r; (RSS in this work) is defined by

$$P_r(d)[dBm] = P_t[dBm] + G_t[dB] + G_r[dB] - [\, PL(d_o)[dB] + 10nlog10\left(\frac{d}{d_o}\right)[dB] +$$

$$X_\sigma[dB]], \tag{9}$$

where

- P_t is the power transmitted by TX,

- G_t and G_r are the gain of TX and RX respectively,
- $PL(d_o)$ is the free space path loss (reference distance d_o = 1 m), defined by

$$PL(d)[dB] = -10log_{10}\left(\frac{\lambda^2}{(4\pi)^2 d^2}\right), \tag{10}$$

where

- $\lambda = c/f$ is the wavelength, where $c = 3 \times 10^8$ m/s and $f = 5 \times 10^9$ GHz,
- d_o is the close-in distance from the TX (considered 1 m).

- X_σ is a zero-mean Gaussian distributed random variable with standard deviation σ (STD).
- d is the TX–RX distance.
- n is the path loss exponent (PLE), and together with the standard deviation (STD) were estimated from the 3D-RL raw data, using Maximum Likelihood (ML) [93], according to equations (11) and (12)

$$PLE = \frac{-\sum_{i=1}^{n}(P_i[dBm]-P_0[dBm])\log_{10}\left(\frac{d_i}{d_o}\right)}{\sum_{i=1}^{n}10\left(\log_{10}\left(\frac{d_i}{d_o}\right)\right)^2}, \tag{11}$$

$$STD = \frac{1}{\sqrt{n}}\left\{\sum_{i=1}^{n}\left[P_i[dBm] - P_0[dBm] + 10\log_{10}\left(\frac{d_i}{d_o}\right)\right]^2\right\}^{\frac{1}{2}} \tag{12}$$

4. RSS (dashed-point-line): Path loss model (PLM2), [41] is used for comparison purposes with the 3D-RL results. This analytical PLM2 does not consider either a free space reference distance (do), or free space path loss PL(do). The P_r is defined as

$$P_r(d)[dBm] = P_t[dBm] + G_t[dB] + G_r[dB] - 10log_{10}\left(16\pi^2\frac{d^n}{\lambda^n}\right) \tag{13}$$

For PLM1 and PLM2, P_t is the transmitted power defined at −10 dBm. G_t and G_r are the antenna gains equal to 3.74 dB. Table 7 shows the PLE and STD values for each street and avenue and a measure of goodness-of-fit (GOF) between the LS fitting and the

PLM1, which results in better fit than PLM2, represented by the determination coefficient R^2.

Table 7. Path loss exponent (PLE) and standard deviation (STD).

Description	PLE (n)	STD (σ) [dB]	LS vs. PLM1 GOF (R^2)
AV-2			
Rnd* / left < Tx / Tx >right	3.76/ 2.13/ 2.22	39.12/ 5.59/ 6.59	0/ 0.94/ 0.91
ST-1			
B4 - B5 (NLoS)/ Left< Tx	2.96/ 2.30	18.37/ 7.22/	0.72/ 0.87/
Tx >right / B1 - B2 (NLoS)	2.26/ 3.25	7.21/ 22.43	0.72/ 0.31
ST-2			
Park / B3 - B4 (NLoS)	2.40/ 2.72	7.35/ 6.28	0.77/ 0.48
ST-3	2.07	5.432	0.90
AV-3			
Rnd / B4 - B5 (NLoS)	2.76/ 4.27	31.63/ 42.76	0/ 0.49
AV-5 (NLoS)	3.64	38.01	0.18

Rnd* = Roundabout; left >Tx = left to Tx; Tx > right = Tx to right.

Figure 20 (a–d) illustrates the RSS at 1.5 m height at AV-2, ST-1, ST-2 and ST3, AV-3 and AV-5, respectively, as a function of the Euclidean distance to the Tx (LUP). The left (x-axis) and top (y-axis) distances from the Tx have been spatially differentiated from the right and bottom distances, being prefixed with a negative sign. The dotted-line represents the raw RSS data generated by 3D-RL simulation. The dashed-line represents the LS fitting-line. The continuous-red-line and dashed-dot-line represent the PLM1 and PLM2, respectively.

Figure 20(a) illustrates the RSS at AV-2 avenue and shows good agreement (except for the roundabout sector) between the 3D-RL and the PLM1 (R^2 = 0.94 and 0.91 for the left and right distances from TX, respectively) which can be explained for the optimal LoS conditions. The presence of the roundabout, which can be considered a special type of street intersection, causes a meaningful decay in the RSS becoming evident in the increment of the PLE and STD values resulting in higher path loss and RSS fluctuation that other avenue segments. The roundabout PLE = 3.76 is the highest along the AV-1

with a dramatic increment in its STD = 39.12 dB versus STD = 5.59 dB from the same AV-1 contiguous segment. The PLMs are unable to predict the RSS at the roundabout sector which is illustrated as the lack of agreement between the LS fitting and the PLM1 (R^2 = 0). The conditions for the V2I communications are significantly degraded or are unfeasible at this sector. According to [48], the presence of street intersections and roundabouts are impairment factors that may deteriorate the power signal irrespective of the Tx-Rx distance.

The LoS and NLoS conditions and its effect in the RSS value along ST-1 street are illustrated in Figure 20(b). The obstruction due to the trees in the LoS segments causes an increment in the PLE and STD values which are higher than the reported under LoS optimal conditions in AV-1. However, the coefficient of determination evidences a good agreement between 3D-RL and PLM (R^2 = 0.87 and 0.72, for the left and right distances from Tx, respectively). Under LoS the RSS is above the RST with average STD = 7.22 dB, which means appropriate conditions for V2I communications. Under NLoS condition there are remarkable differences between the left and right ST-1 segments. The right segment, although closer than the left segment to the TX, shows higher PLE and STD values (PLE = 3.25 and STD = 22.43 dB in front of 2.26 and 18.37 dB of the left side respectively) which means higher path loss and signal fluctuations.

The PLMs are unable to predict the behavior of the RSS at the right NLoS segment (R^2 = 0.31). The ST-1-right NLoS segment is more obstructed by the building B1 than the left-ST-1 NLoS segment by the building B5. This behavior is highly influenced by the location of the Tx, which determines the incidence angle of the emitted rays that impinges on the buildings walls and defines the intensity of the waveguide effect in the corridor configuration at ST-1 street. The propagated rays of the transmitter are better guided in the corridor between buildings, where the incidence angle of the main ray is less obstructed. This phenomenon must be considered to define the RSU's placements in the V2I environment. Under NLoS conditions, high fluctuation in RSS causes values below RST and jeopardizes the conditions for V2I communications.

Figure 20(c) depicts the propagation at ST-2 and ST-3 streets. The ST-3 street is under LoS with PLE = 2.07 and STD = 5.34 dB. The PLMs show good agreement with the LS fitting 3D-RL with R^2 = 0.90. The V2I communication is workable at this segment.

The RSS at ST-2 street under LoS is influenced by obstacles in the park sector (QLoS) which causes a PLE = 2.40 higher than in free-space and a STD = 7.35 dB. The GOF (R^2 = 0.77) indicates an acceptable level of agreement with PLM1. The V2I communications are feasible considering some outliers in the 3D-RL raw data that can affect the results. Under ST-2 NLoS condition, there is a slight increment in the PLE = 2.72. The GOF (R^2 = 0.48) for PLM1 indicates the low agreement with the LS fitting mainly due to the phenomena of diffraction in B3 and reflection on B4. The conditions for V2I communications are in the limit, near to the RST. The waveguide effect is not present in this corridor-configuration segment.

Figure 20(d) illustrates the propagation at AV-3 and Av-5 avenues. Buildings, as the most significant obstacles for the LoS in this urban scenario, cause the highest PLE values: 4.27 and 3.64 for AV-3 and AV-5, respectively. However, the most dramatic increment is represented by the STD: 42.76 dB and 38.01 dB, respectively. The PLMs are unable to represent the RSS behavior with R^2 values of 0.49 and 0.18 for AV-3 and AV-5, respectively. The RSS is below −120 dBm with high fluctuations and totally degraded V2I communications conditions.

In general, these results are coherent with reported in the literature [53][93][94][23]. PLE ranges from 2.07 to 3.25 for LOS and QLOS, and 3.64 to 4.27 for NLOS; higher values have been derived from building obstruction. V2I communication is suitable at zone 1, zone 2 (excepting the roundabout area) and zone 3 (LoS and left-NLoS). Under LoS, PLM1 is more accurate than PLM2 to predict the RSS, nonetheless, under NLoS caused by buildings, both PLMs are incapable to predict the RSS behavior. The emplacements of the TX have great influence on the creation of the LoS, NLoS conditions and the corridor-configuration with its inherent waveguide effect.

4.4. Scenario1- measurement validation

An RSS measurement in zone 1 was performed to establish a comparison versus the 3D-RL technique and the two analytical PLM. The TX was connected to a signal generator at 5.9 GHz and has been located at the upper lamppost LUP (x = 164 m, y = 78 m, z = 3.5 m) at 3.5 m height. The receiver antenna was placed in the compartment of a sedan-car, just below the front windshield at 1.30 height. TX and RX antennas were ACA-

4HSRPP-2458 from ACKme Networks (Los Gatos, CA, USA), both omnidirectional, with a gain of 3.74 dB. The employed signal generator was a portable N1996A (Agilent Technologies, Santa Clara, CA, USA) unit and the spectrum analyzer was an Agilent N9912 Field Fox. The measurements were performed with 100 MHz bandwidth at 5.9 GHz frequency and the measurement time at each point was 60 s. RSS in each point is the highest peak (Max-Hold function) of power shown by the spectrum analyzer. Figure 21 depicts the measurement validation results.
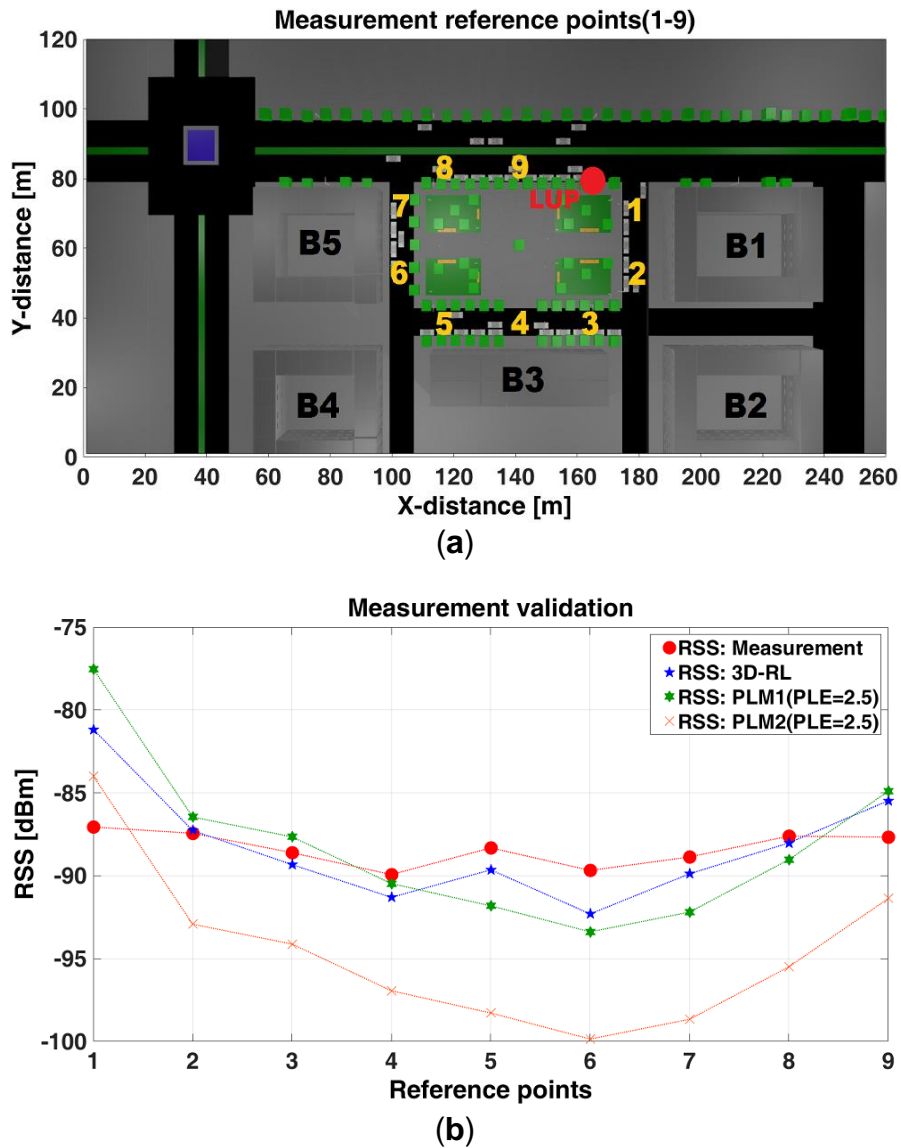

Figure 21. Scenario1 measurement: (a) reference points, (b) measurement validation [18].

Figure 21(a) shows the nine points used as reference for the measurements campaign at zone 1: points 1 and 2 are along ST-3, points 3–5 are along ST-1, points 6 and 7 are along ST-2 and points 8 and 9 are along AV-2.

Figure 21(b) depicts a comparison between measurements versus the 3D-RL technique and versus PLMs defined in Section 3.3. RSS values estimated by 3D-RL were obtained taking as reference the same spatial coordinates of the points (real measurements) and evaluating the resulting distance in a first order polynomial that represent a LS fitting of a 10 m street or avenue segment that include the same coordinates in the three-dimensional mesh of cuboids in which the scenario was divided. PLM1 was evaluated according to equations (11) and (12), and PLM2 was evaluated according to Equation (13).

Figure 21(b) shows better agreement of the 3D-RL than PLMs with the measured points, which means more accurate representation of propagation phenomena. A mean error of 1.75 dBm and standard deviation of 2.54 dB corresponds to the 3D-RL simulation, while mean error of 3.0 dBm and standard deviation of 4.18 dB correspond to the PLM1 when compared against measurements. A mean error of 6.96 dBm and standard deviation of 4.18 dB results for PLM2. These results (zone 1) validate the 3D-RL technique as more accurate than the used PLMs in this urban environment. The effect of the obstacles in the propagation is more accurate represented with less variability in comparison with measurements. PLM1 shows better fit with the measurements than PLM2.

The applicability of this results and the accuracy needs of the mean error or standard deviation is related with the V2I service or application requirement. As it can be seen from the results, received power level values are within the sensitivity range of conventional wireless transceivers, with values above −100 dBm. It also worth noting that an increase in transceiver density can be directly considered, given that each connection can be independently modeled and superimposed to overall estimations, in terms of received power estimations as well as time domain components, given that in principle their operation is uncorrelated. Overall effect of transceiver node density increase is requirement of lower transmit power to reduce overall interference and hence, increase coverage/capacity ratios.

4.5. Scenario2 - RSS and coverage

Figure 22 illustrates the RSS map of TX1 and TX2 at z-plane of 1.5m.

(a)

(b)

(c)
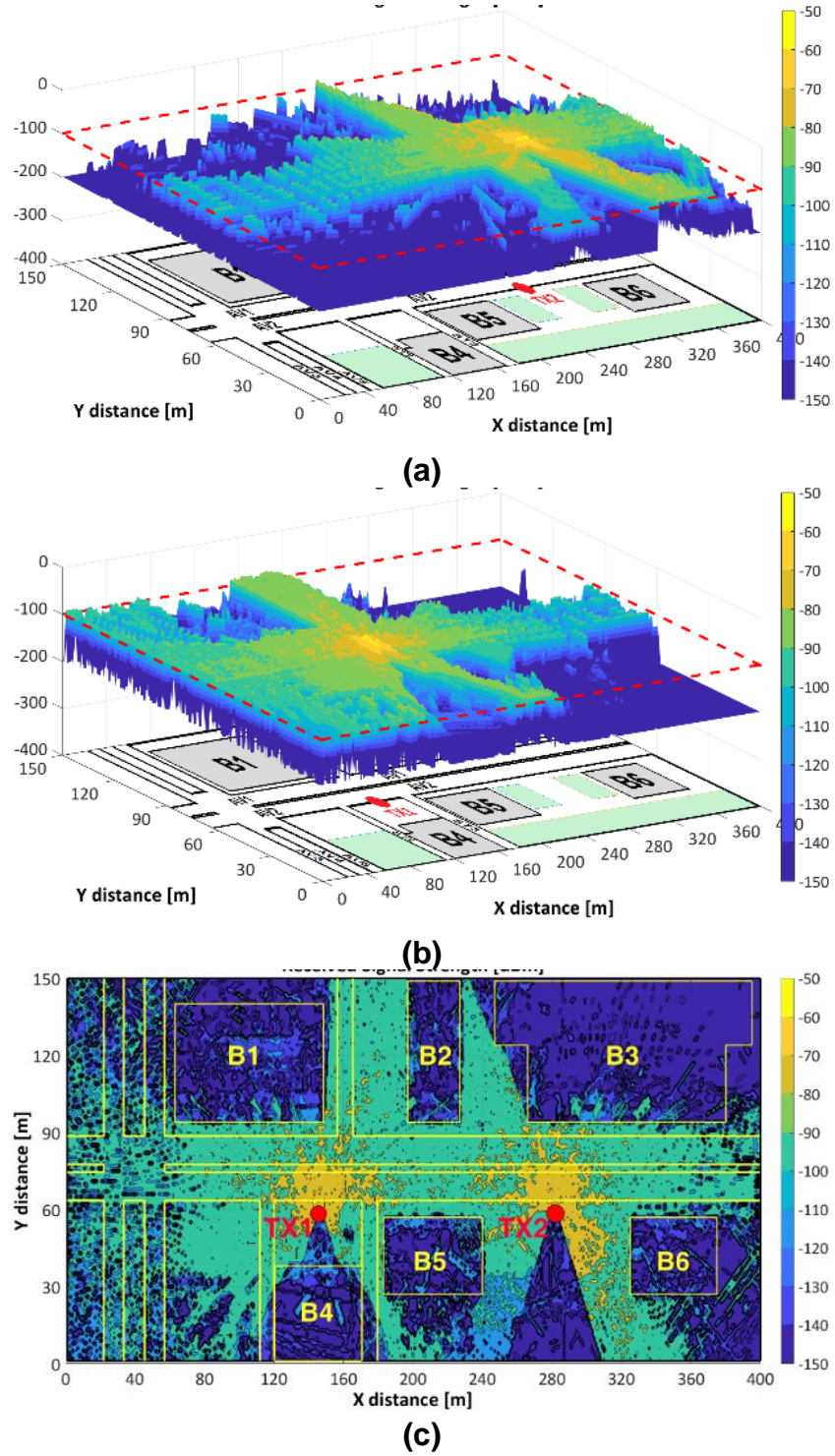
Figure 22. Scenario2 RSS: (**a**) TX1 RSS; (**b**) TX2 RSS; (**c**) TX1&TX2 RSS [86]

Figure 22(a),(b) show an RSS surf-plot of TX1 and TX2 respectively. Figure 22(c) depicts the jointly TX1 and TX2 contour-plot where RSS values above the RST are observed along AV1, AV2, ST1 and upper sector of ST2 and ST3 making feasible the V2I communication.

4.5.1 Scenario2 - Coverage

Figure 23 depicts the coverage map for the joint configuration of TX1 and TX2.

(a)

(b)
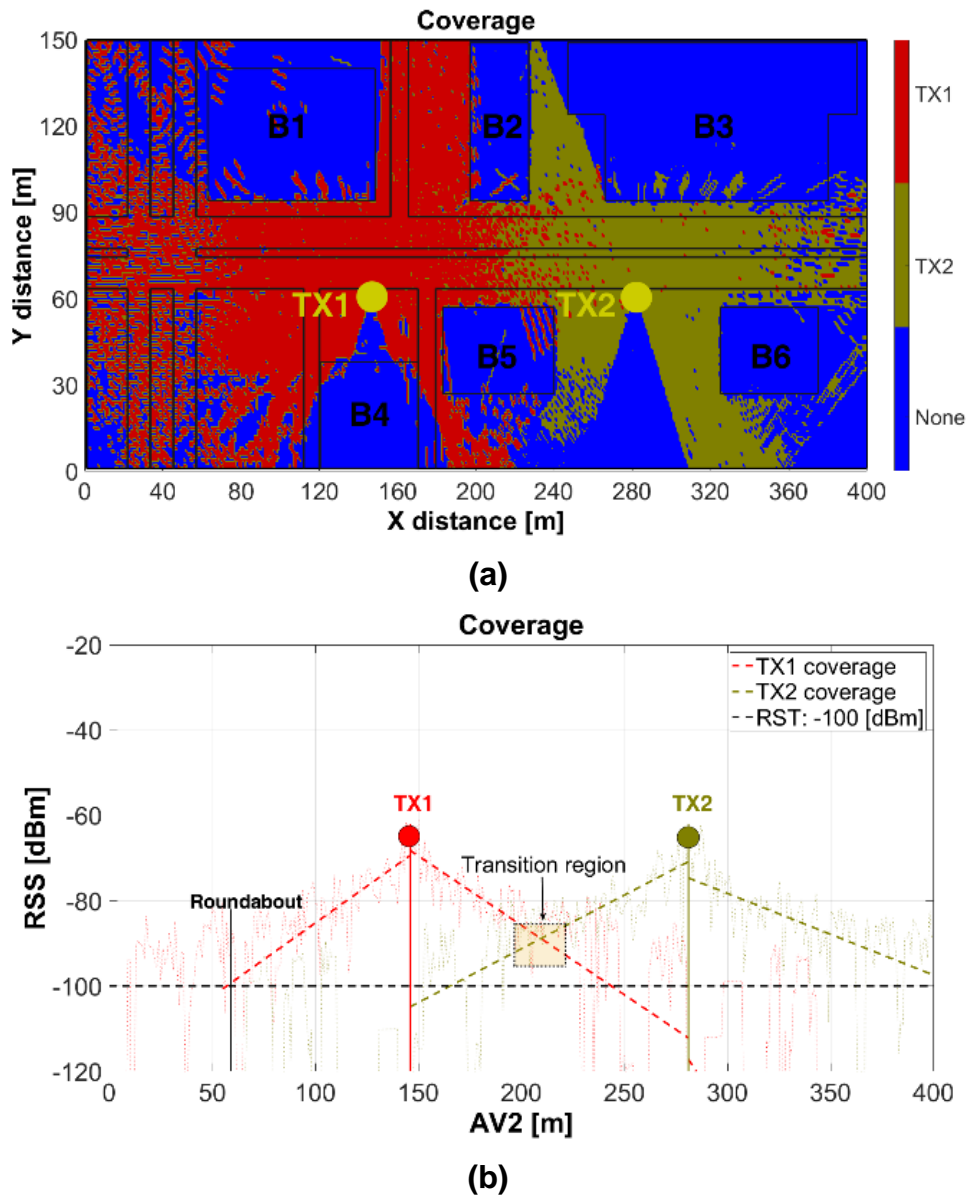
Figure 23. Scenario2 coverage map: **(a)** scenario; **(b)** along AV2. [86]

The coverage map was based on the selection of the highest TX1 or TX2 RSS (above the RST of -100 dBm) at each point of the scenario when both antennas are transmitting. RSS values below the RST were identified with "None". Figure 23(a) shows that the TX1 coverage encompasses AV1–AV2 (left-segment), ST1, ST2 (LoS) and ST3 (LoS), while the TX2 coverage embrace AV1–AV2 (right-segment). Figure 23(b) illustrates the AV2-RSS as function of the coverage-distance (x-axis) for each TX and, the transition region where the RX defines the point-to-point link either with TX1 or TX2, based on the sensing of the highest power received. Each TX has an approximate total coverage distance of 170m (asymmetric). The transition point is located approximately at the half distance between the TXs. The roundabout, AV3, AV4, AV5, ST2–ST3 (NLoS) is out of coverage.

The effectiveness of cooperative systems using RSUs for V2I communications is dependent on how efficiently RSUs are being deployed [43]. In this way, based on the simulated results, different TX placement configurations could be suggested to achieve RSS coverage levels above the RST; one of these configurations could be as follows:

- TX1 and TX2 in the same simulated placement to give coverage to AV1, AV2, ST1.
- Tree additional TXs: one for coverage of ST2, one for coverage of ST3 and, one for coverage the roundabout, AV3, AV4 and AV5 areas.

4.6. Scenario2 - Multipath Metrics

The analysis of multipath metrics as Power Delay Profile (PDP), Mean excess delay, Root Mean Square Delay Spread (RMS delay spread) and Coherence Bandwidth (CB) has great importance in WSN to design some general guidelines for deployment. To mention, the cyclic prefix (CP) of adaptive algorithms aimed to increase the spectral efficiency is determined by the maximum excess delay or by the RMS delay spread of that environment [95] . Environments with high RMS delay spread cause inter-symbol interference (ISI), and affect the guard interval in OFDM systems, alike small coherence bandwidth affect the OFDM pilot spacing [96].

The multipath metrics must be understood and determined for different environments to develop a proper scheme for communications requirements. This subsection presents the analysis of multipath metrics, required parameters to develop a proper scheme for

communications and determined for different environments to design some general guidelines for WSN deployment.
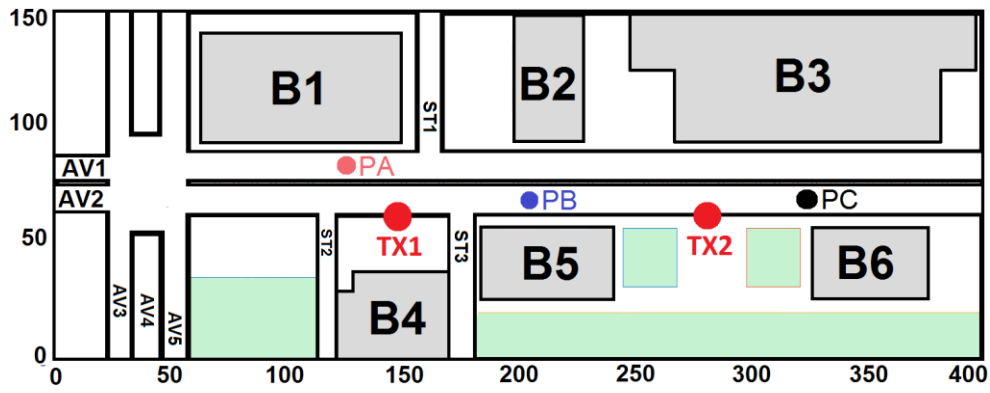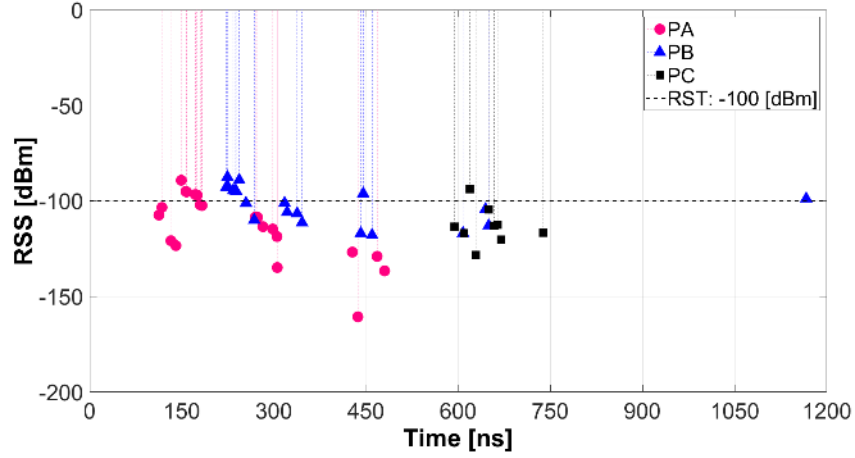
Figure 24. Scenario2 Power Delay Profile: **(a)** measured points; **(b)** TX1, **(c)** TX1&TX2 [86].

4.6.1. Scenario2 - Power Delay Profile (PDP)

The PDP is used to calculate various multipath statistics (mean excess delay, RMS delay spread, maximum excess delay, CB) and quantifies the number and severity of power rays (echoes) in the wireless channel.

Figure 24 illustrates the PDP at z-plane of 1.5 m for 3 different locations represented in Figure 24(a), while Figure 24b,c depicts the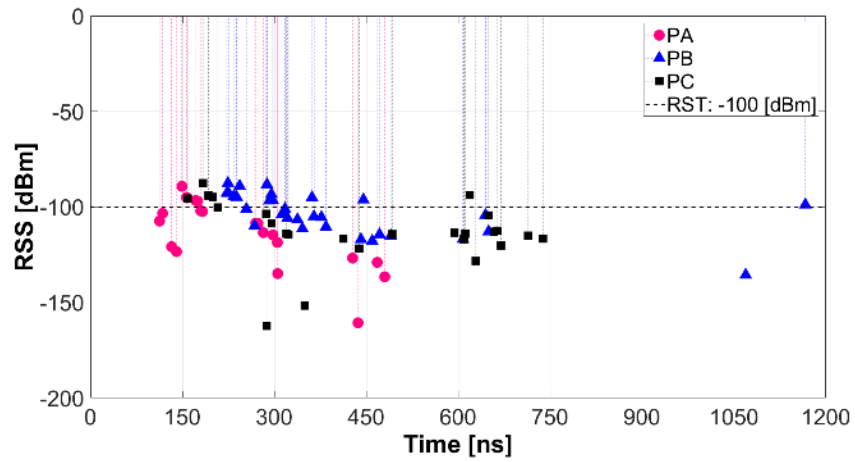 PDP when TX1 or both TX1 and TX2 are transmitting. Figure 24(b) shows many power rays (echoes) in a time span of 0 to 1200 ns showing a high dispersive nature of this environment causing reflected, refracted, and diffracted rays that arrive to PA, PB and PC points. The highest density of rays arrives to PA which is in LoS and closest (first ray arrives at 100 ns) to TX1; conversely the lowest density is at PC, which farthest from TX1. Figure 24(c) illustrates the increase in the number of power rays arriving to PB and PC as a contribution effect of TX2 to the jointly PDP mainly at the transition region (refer to Figure 23(b)). The presence of power rays with low RSS values are mainly those reflected and diffracted by obstacles and the line of trees among AV1 and AV2.

4.6.2. Mean Excess Delay, RMS Delay Spread, and Coherence Bandwidth

The mean excess delay (the first moment of the PDP) and the RMS delay spread (the square root of the second central moment of PDP) quantify the time dispersive properties of multipath channels while the Coherence Bandwidth (CB) is the range of frequencies over which two frequency components have a strong potential for amplitude correlation[53]. The NLoS scenarios have much higher mean excess delay than LoS scenarios given that the transmitted signals encounter many reflections along their path to the receiver. Figure 25 shows the mean excess delay, RMS delay spread and CB (for frequency correlation of 0.9). Figure 25 (a1), (a2) depict the mean excess delay for TX1 and TX2 respectively, where higher values in the extent of distance is increased from the TX are observed, while lower values are related to low RSS due to the blocking of the propagated signal by concrete walls (signal absorption) and glass windows (signal reflection) of the buildings. The roundabout, AV3, AV4, AV5, ST3 and the rightmost segment of AV1–AV2 display the highest mean excess delay for TX1, while the leftmost segment of AV1–AV2 display this behavior for TX2.
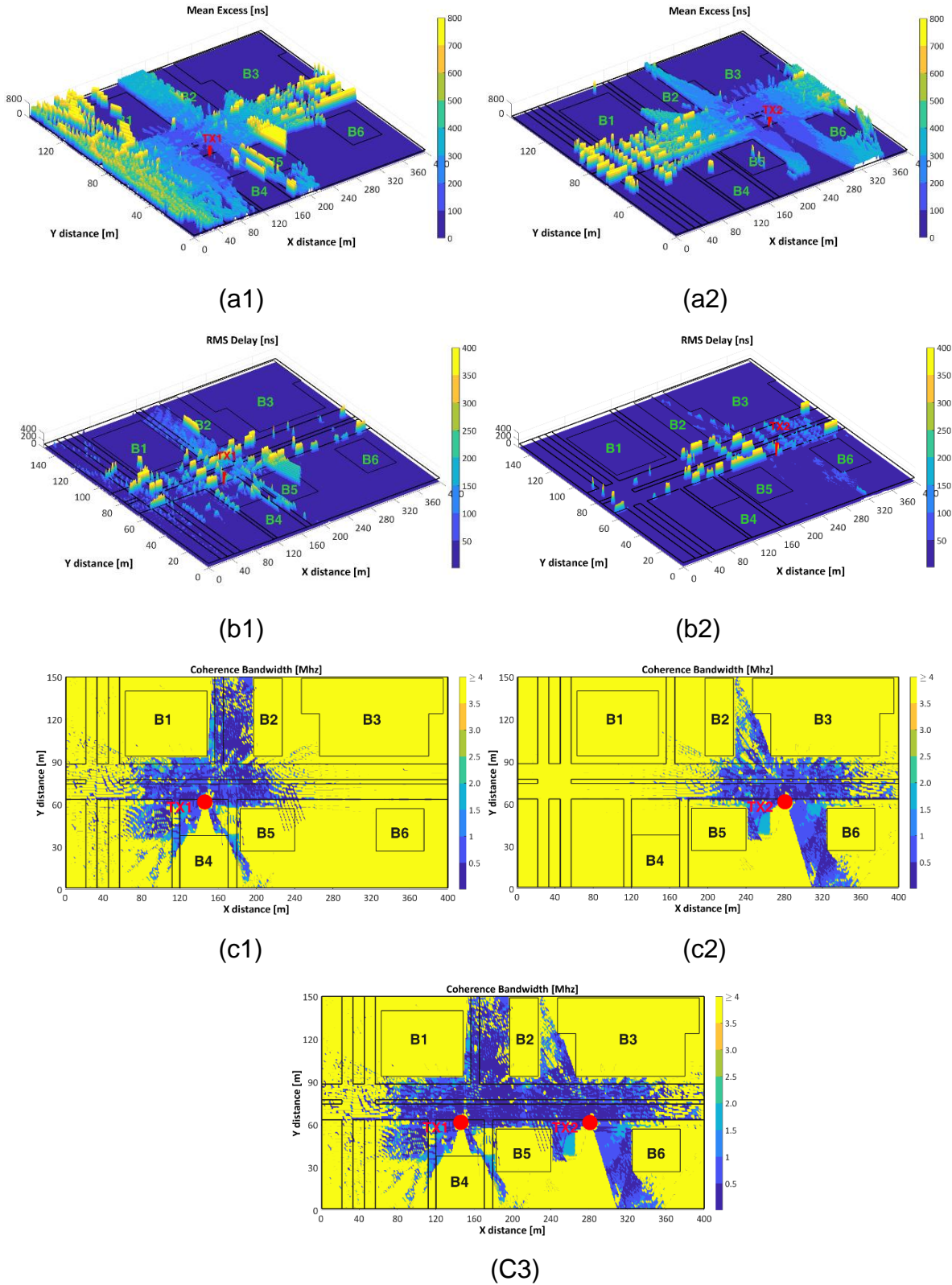
(a1)

(a2)

(b1)

(b2)

(c1)

(c2)

(C3)

Figure 25. (a1–a2) Mean Excess Delay, (b1–b2) RMS delay spread, (c1–c3) Coherence Bandwidth [86]

Figure 25(b1) and 25(b2) illustrate the RMS delay spread. Lowest values keep a close relationship with lowest values of RSS due to the NLoS conditions. Some factors such as the presence of obstacles (trees, lampposts, cars) and the LoS conditions cause high RMS delay spread values near the TXs. As the TX-RX distance is increased, the amplitudes of the reflected signals relative to the direct path become larger, and this produces the increase of the mean excess and RMS delay spread as is depicted in Figure 25(a) and 25(b).

Figure 25(c1), 25(c2), 25(c3) depict the CB values of TX1, TX2 and TX1 and TX2 respectively. High CB values, in areas such as AV3, AV4, AV5, ST2–ST3 (NLoS), etc., correspond with low RMS delay spread (given its inverse relationship) and high CB could be considered as an indicator of channel availability for TXs other than TX1 or TX2. On the other hand, low CB values are present at the vicinity of the TXs due to its multipath environment, which means high channel occupancy. Figure 25(c3) illustrates a superimposed CB contour map of TX1 and TX2 to gain insight of the joint CB and low CB values along AV1–AV2 and ST1 are observed. The CB analysis must be complementary with the analysis of RSS, and coverage and RMS delay spread mentioned above.

4.6.3. Doppler Spread (B_D) and Doppler Shift (fd)

Doppler Spread (B_D) and coherence time (T_C) describe the time-varying nature of the channel, caused by either relative motion between the mobile and base station or by the movement of objects in the channel, in the small-scale region. B_D is defined as the range of frequencies (spectral broadening) over which the received Doppler Spectrum is essentially non-zero (if the baseband signal bandwidth is much greater than B_D, the effects of Doppler spread are negligible at the receiver—slow fading channel). Doppler Shift (fd) is the Doppler spectrum of the received signal in the range fc – fd to fc + fd, where fc is the transmitted frequency [53].

Figure 26 shows the effect of the relative velocity on the maximum Doppler Shift, which is when $\cos\theta = 1$ (θ is the angle between the direction of motion of the mobile and direction of arrival of scattered waves).

Figure 26(a) and 26(b) depicts Doppler Shift with respect to TX1 of three different cars PA, PB and PC (see Figure 24(a)) which are traveling at constant velocities (v) of 40

km/h and 60 km/h respectively. The relative motion between cars and TX, results in random frequency modulation due to different Doppler Shifts on each of the multipath components. If the Doppler Shift is given by, [53]

$$fd = \frac{1}{2\pi} \cdot \frac{\Delta\emptyset}{\Delta t} = \frac{v}{\lambda} \cdot Cos\theta \,, \tag{14}$$

where

- $v =$ is vehicle velocity with respect to TX,
- $\lambda = c/f$ is the wavelength, where $c = 3 \times 10^8$ m/s and $f = 5 \times 10^9$ GHz,
- $\theta =$ spatial angle between the vehicle and TX,

the theoretical fd_{max} (40 km/h) = 218.52 Hz and f_{dmax} (60 km/h) = 327.78 Hz, when $Cos\theta = 1$
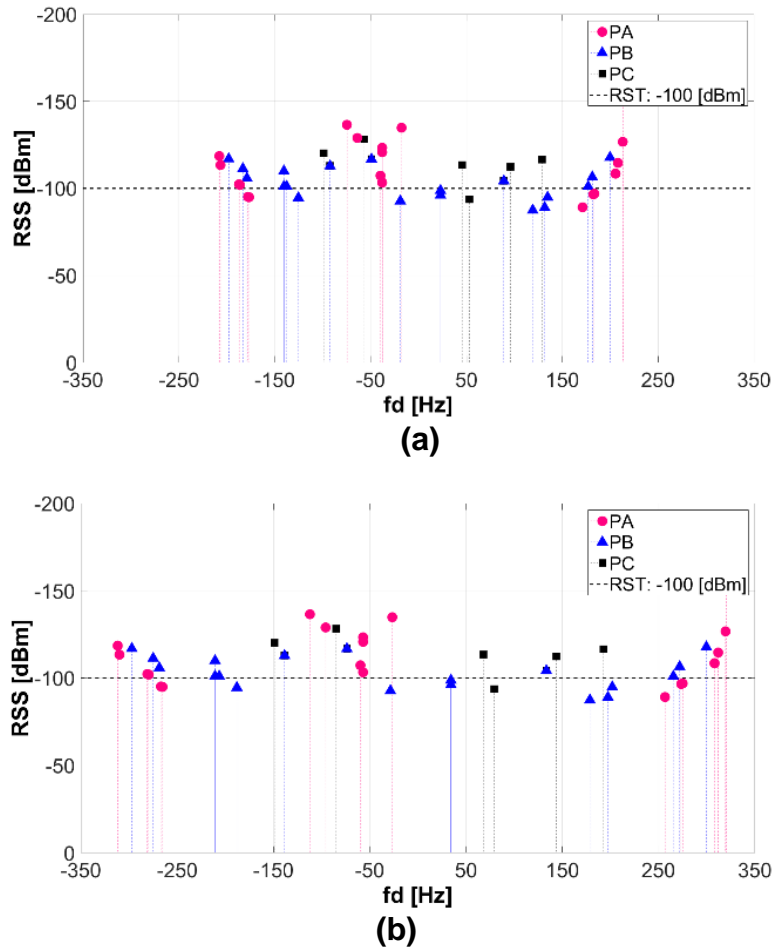
Figure 26. Scenario2 Doppler Shift (fd): **(a)** car velocity, 40 km/h, **(b)** car velocity, 60 km/h [86].

When PA is traveling at a constant velocity of 40 km/h, the simulated fd_{max} were reported between −207,821 and 213.33 Hz, while for 60 km/h the simulated fd_{max} were reported between −311.72 and 319.99 Hz. The reported fd positive values is an indicator that PA is moving directly toward the TX and the apparent received frequency is defined by: f = (fc + fd) Hz, meanwhile negative fd values means that PA is moving directly away the TX and the apparent received frequency is f = (fc − fd) Hz.

According to this definition and simulation results, the received signal spectrum has components in the range f = (5.9×10^9 − 311.72 to 5.9×10^9 + 319.99) Hz. Additional simulation shows that the signal spectrum components for PB and PC (traveling at constant velocity of 60 km/h) are in the range of f_{PB} = (5.9×10^9 − 297.05 to 5.9×10^9 + 299.42) Hz and f_{PC} = (5.9×10^9 − 148.80 to 5.9×10^9 + 192.65) Hz respectively.

(a)

(b)
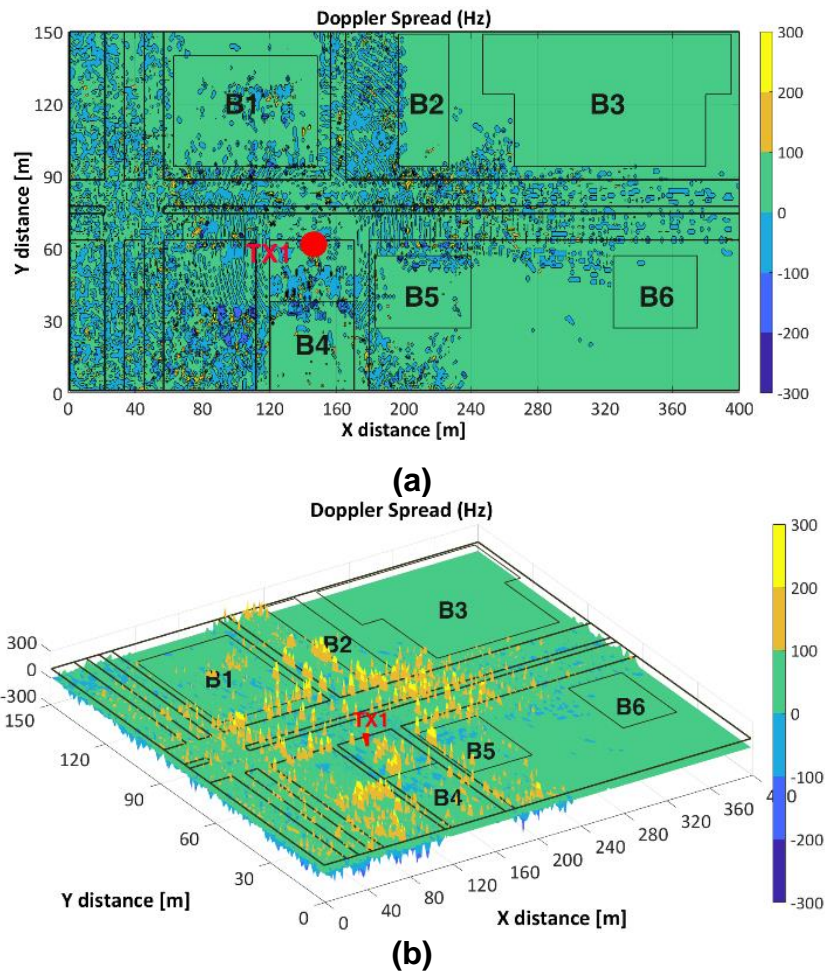
Figure 27: Scenario2 Doppler Spread (B_D): (**a**) car velocity,40 km/h, (**b**) car velocity,60 km/h [86].

Figure 27(a) and 27(b) shows the TX1-B_D for velocities of 40 km/h and 60 km/h respectively. Higher B_D values are observed in the vicinity of the TX1 and higher B_D values are depicted for velocity of 60 km/h. Figure 27(a) clearly illustrates the positive and negative range of received frequencies when the PA is traveling at 40 km/h. Factors such as the relative velocity and direction of motion respect to TX, have an impact on the apparent received frequency which impact B_D, T_C and fd values, as aforementioned.

The large-scale and small-scale results are presented and discussed in this chapter. The RSS analysis identify the coverage zones and the measurement validation for I2V-RSS shows more accurate results from 3D-RL simulation than a theoretical PLE for vehicular environments presented in the bibliography. The multipath metrics evidence a highly multipath environment where factors as distance and NLoS and QLoS conditions, causes variation in the Mean Excess Delay, RMS Delay Spread and CB. The Doppler Spread and Doppler Shift, show that factors such as the relative velocity and direction of motion respect to TX, causes significantly impact on the apparent received frequency. These results are useful to understand the RSS behavior which lead us to find strategies to choose homogeneous data information segments for statistical analysis, which are presented in the next section.

5. Statistical Analysis

The impact of the VTD into the URPC for V2X communication is presented and discussed. A brief overview of fading models, Goodness-of- fit, dispersion measures and graphical and descriptive statistic tools, required for statistical characterization is presented. The description and simulation parameter of two urban environments is laid out. Some theoretical fading distributions, widely used in multipath environments, as Lognormal, Gamma, Weibull and other are used to find the best fit with the V2X-RSS, to shape and explain the impact of different VTD levels have in the URPC. The approach of this chapter is illustrated in Figure 28.
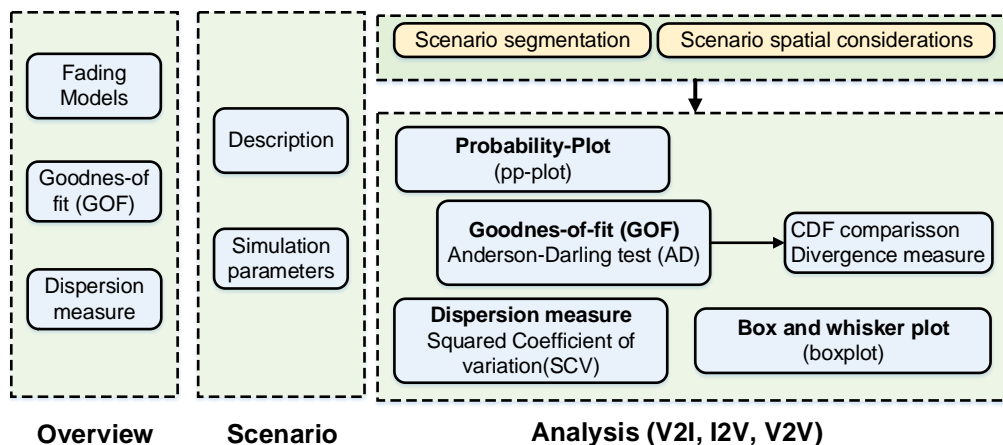
Figure 28. Approach of Chapter 5

5.1. Fading models, GOF, and dispersion measure.

The fading channel in vehicular environments could be a combination of different fading channel types that changes over distance, time, and mobility. Different fading models have been proposed and utilized in literature as Gamma, Lognormal, Rician [97], Rayleigh, Nakagami, Weibull, composite fading models as Weibull-Gamma [98], Nakagami-Lognormal, K distribution (mixture of Rayleigh and Gamma), mixtures of Gamma distributions [99], etc. In this multipath environment, identification of some statistical fading model able to fit and characterize the fading level of this urban scenario is required, as well as the adoption of a descriptive statistic to measure it. To validate the

closeness of the theoretical distribution (Gamma, Lognormal, Weibull, etc.) function to the empirical distribution function (RSS 3D-RL), a Probability Plot (pp-plot) and GOF tests are used.

Pp-plot is a graphical technique and powerful tool for determining if two data sets come from populations with a common distribution [100] where the data density distribution (the cumulative density function CDF) is transformed into a linear plot. A 45-degree reference line is also plotted. If the two sets come from a population with the same distribution, the points should fall approximately along this reference line. The greater the departure from this reference line, the greater the evidence for the conclusion that the two data sets have come from populations with different distributions, nonetheless, the natural variation in the data causes some departures from the straightness. Pp-Plot keeps similarity with the Quantile-to-Quantile Plot where the quantiles of the first data set are plotted against the quantiles of the second data set [101].

The Anderson-Darling (AD) test, which is a test along with Kolmogorov-Smirnov(K-S), Cramer-von Mises (C-vM), Chi_Square(C-S), etc., to evaluate the GOF for nonparametric data sets. The AD statistic provides robustness and flexibility compared to other GOF measures because it gives more weight to the tail of the distribution, and it has been employed to quantify the difference between the observed and expected values [102], as a type of divergence or discrepancy measurement. The AD statistic gives heavy weight to the tails and should be powerful against alternatives in which the true distribution and the data disagree near the tails of the data distribution. The parameters of the fitted distributions were estimated from the data, and the critical value depend on the sample size. In applications such as Cognitive Radio, a proposed AD sensing has much higher sensitivity to detect a transmission signal than energy detector-based sensing, especially for small samples [103], however, in applications such as hydrological statistics, the results show most powerful GOF results for K-S and C-S test than AD [104].

Given the multipath nature of the urban environments, a measure to quantify the data variability is needed, and, one descriptive statistics to measure it, is the squared coefficient of variation (SCV) defined as, [105]

$$SCV = \frac{Var}{\mu^2} = \frac{E((x-\mu)^2)}{\mu^2} = \frac{E(x^2)}{(E(x))^2} - 1 \, , \qquad (15)$$

where x is a random variable and E (·) is expectation operator. According to [106], for a given distribution of strength, a, of a received signal, the amount of fading (AF) is defined by the ratio of the variance of the received energy to the square of the mean of the received energy as follows,

$$AF = \frac{Var(a^2)}{(E(a^2))^2} \, , \qquad (16)$$

According to equations (15) and (16), the SCV of received signal power characterizes the amount of fading (AF) of signal power and are used in this section to describe the data variability and AF. In order to have as much as possible consistent data for analysis in terms of data variability, symmetric and equidistant data segments from the TX, were organized for analysis in order to have reliable GOF results. This kind of segmentation was chosen for three reasons:

a) *To consistently identify the statistical differences between symmetric and equidistant areas from TX (spatial considerations):* left and right RSS segments of TX (x-axis), should be symmetric and equidistant. Upper and lower RSS segments of TX (y-axis), should be symmetric and equidistant.

b) *To get a reasonable balance between maximum segment-length and significant statistical fit when compared with theoretical distributions:* it is noted that RSS areas in the vicinity of the TX are characterized by high data variability which decreases in the measure the distance increases; data segments in the vicinity should be shorter than in remote locations.

c) *To organize the data into homogeneous segments, avoiding as much as possible extreme 3D-RL RSS values*: symmetric and equidistant RSS segments exhibit homogeneous values when are grouped under LoS, QLoS or NLoS criteria. Segments under QLoS and NLoS conditions are prone to high data dispersion and multipath effect.

5.2. Scenario description

5.2.1 Scenario2

The scenario2 was previously described in section 4.1.2 (Pag. 40).

5.2.2 Scenario3

Figure 29 shows the scenario3, which geometry was previously described in scenario1, section 4.1.1 (Pag. 39), however some modifications in the TX/RX location and simulation parameters differentiate it from scenario1. Two transmitter antennas TX1 and TX2, and three vehicles C1, C2, C3 were considered. **Table 8** identifies the Cartesian coordinates (x, y, z) of interest points according to their relative position from the origin (0, 0, 0) [m].
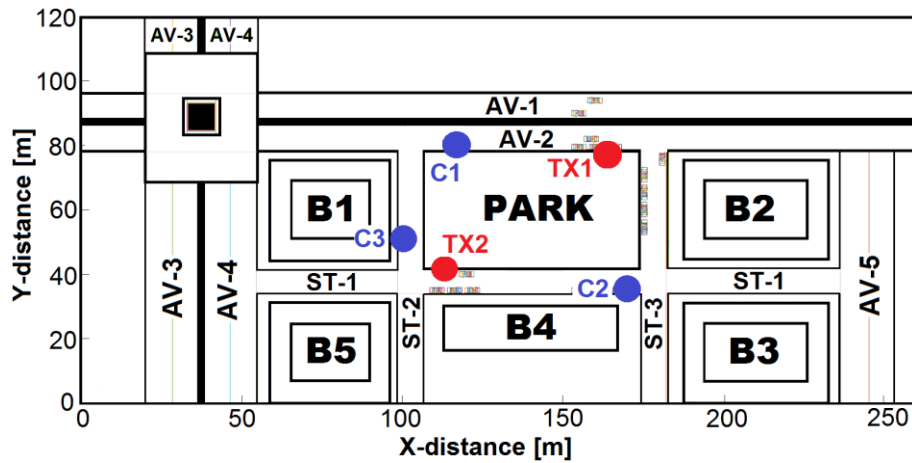
Figure 29. Scenario3.

Table 8 shows the scenario reference for scenario3.

Table 8. Scenario3 reference.

Description	Abbreviation	Position (x, y, z) [m]
Main Avenues	AV-1/ AV-2/ AV-3 AV-4/ AV-5	(x, 93, 0)/ (x, 82, 0)/ (29, y ,0) (47, y, 0)/ (247, y, 0)
Streets	ST-1/ ST-2/ ST-3	(x, 39, 0)/ (54, y, 0)/ (130, y, 0)
Transmitter antenna	TX1 /TX2	(164, 78, 3.5) / (114, 43, 3.5)
Car antennas	C1/ C2/ C3	(118, 80, 1.5)/ (171,35, 1.5) /(100, 53, 1.5)
Buildings/Park	B1, B2, B3, B4, B5	Not applicable.

Table 9 shows simulation parameters for scenario3.

Table 9. Scenario3 simulation parameters.

Parameters	Values
TX1, TX2: P_t */ Gain(G_t)/Frequency/Height /polarization.	0 dBm/0 dB/5.9 GHz/3.5 m omnidirectional.
RX: RST **/Gain (G_r)/Frequency /Height. /polarization.	−100 dBm/0 dB/5.9 GHz/1.5 m omnidirectional.
3D-RL: horizontal and vertical angular resolution	π/180 rad
Angular resolution of diffracted rays.	π/20 rad
Maximum permitted reflections.	7 hops
Cuboid segmentation for analysis.	1 m^3 (1 × 1 × 1)m
Scenario: dimension.	(260 × 120 × 20)m

Pt *: Power transmitted, RST ** (Received Signal Threshold).

5.3. I2V and V2V statistical characterization

5.3.1 I2V statistical characterization of scenario2.

To analyze the I2V-RSS statistical behavior, distance segmentation and spatial position from the transmitter were considered. In this sense, TX1-RSS coverage area along AV2 was divided into 6 segments: S1 to S3 (left to TX1) and S4 to S6 (right to TX1) where S1 is symmetric and equidistant with S6, S2 with S5 and S3 with S4, as is depicted in Figure 30. These segments are under LoS conditions.
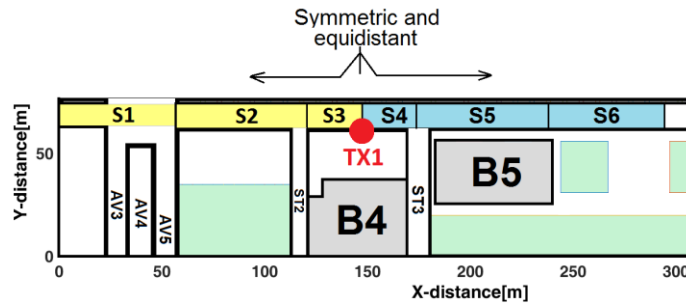
Figure 30. Symmetric and equidistant segments for analysis.

Figure 31 depicts the TX1-RSS Cumulative Distribution Function (CDF) along the AV2 and its statistical comparison with theoretical distributions widely used in the description of multipath fading environments. Figure 31(a-d) show the CDF comparison between the ECDF of S1(60m), S2(60m), and S3 (26m) with Gamma, Lognormal, Nakagami and Weibull distributions.
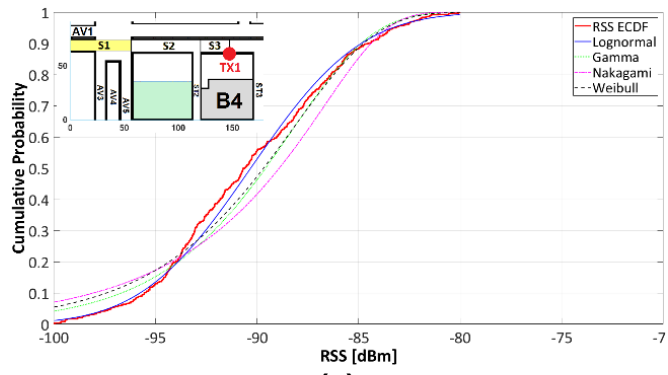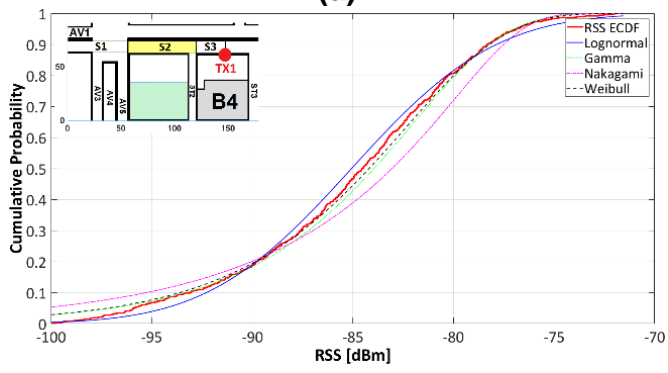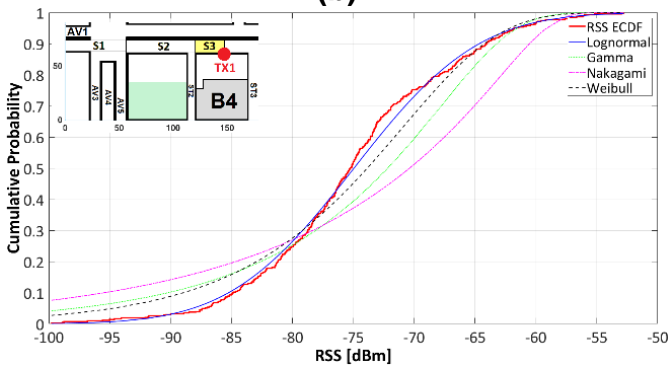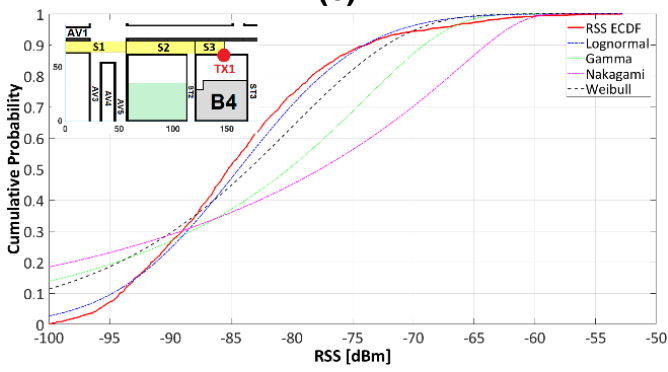
Figure 31. S2 CDF (S1-to-S3) along AV2. **(a)** S1, S2, S3 (x: 1m to 146m); **(b)** S1 (x: 1m to 60m); **(c)** S2 (x: 60m to 120m); **(d)** S3 (x: 120m to 164m) [86].

Complementary to this, Table 10 **Error! Not a valid bookmark self-reference.** summarizes:

- the 3D-RL data Squared Coefficient of Variation (SCV) a statistical measure of the data dispersion level and the PLN as a measure of RSS attenuation.
- the GOF between theoretical distributions and the 3D-RL data, using AD test with 5.0% for a significance level of the hypothesis (H_0) test.
- the AD statistics as a measure of divergence.
- the input parameter (shape) for the tested distributions.

Table 10 items (a) and (c) show that S1 and S3 can be described in terms of Lognormal distribution while S2, item (b) is better fitted by Weibull distribution. The SCV of each individual segment is significantly lower than the joint segment S1-S3 which is an indicator of data homogeneity that can lead to consistent statistical GOF test. Analogous statistical behavior was obtained for the symmetric and equidistant segments S5, S6 and S7 (**Table 10**, items f, g, h).

Table 10. Data dispersion measurements and GOF test for TX1.

| Description	SCV **	n ***	Lognormal	Gamma	Nakagami	Weibull
(a) S1: (x: 1 to 60) m CDF-GOF: (AD-H/ AD-S) Input parameter: Shape	1.126	3.099	**F/** 1.817 0.072	T/ 8.029 1.210	T/ 19.552 0.391	T**/** 7.485 1.058
(b) S2: (x: 60 to 120) m AD (AD-H/ AD-S) Shape factor	1.715	2.345	T/ 3.951 1.136	T/ 3.558 0.842	T/ 23.013 0.289	**F/** 1.936 0.870
(c) S3: (x: 120 to 146) m AD (AD-H/ AD-S) Shape factor	8.473	2.449	**F/** 1.051 3.466	T/ 20.25 0.396	T/ 44.186 0.139	T/ 7.907 0.541
(d) S1, S2, S3 (x: 1 to 146) m AD (AD-H/ AD-S)	34.268	2.764	T/ 11.261	T/ Inf	T/ Inf	T/ 70.462
(e) S4, S5, S6 (x: 146 to 290) m AD (AD-H/ AD-S)	27.526	3.041	T/ 0.313	T/ 4.544	T/ 46.353	T/ 2.495
(f) S4: (x:146 to 170) m AD (AD-H/ AD-S) Shape factor	6.691	2.377	**F/** 0.878 3.987	T/ 19.259 0.479	T/ 46.353 0.161	T/ 8.437 0.609
(g) S5: (x: 170 to 230) m AD (AD-H/ AD-S) Shape factor	1.826	2.284	**F/** 1.639 1.507	T/ 7.946 0.827	T/ 34.403 0.282	T/ 4.809 0.855
(h) S6 (x: 230 to 290) m AD (AD-H/ AD-S) Shape factor	1.225	3.610	**F/** 1.342 0.013	T/ 4.658 1.149	T/ 18.919 0.370	T/ 4.668 1.029

SCV ** (Squared Coefficient of Variation), n *** (Path loss exponent).

AD-H: Anderson-Darling hypothesis test, T=True, F = False (for hypothesis test).
AD-S: Anderson-Darling statistic.

Figure 31(d) depicts the CDF for the joint data segment S1-S3 (146 m), and its comparison with Gamma, Lognormal, Nakagami, and Weibull distributions where the best fit is observed for the Lognormal distribution; however, the AD-GOF test resulted in the rejection of the null hypothesis (H_0) which means that the RSS statistical behavior of this segment does not fit with any of the tested distribution. The S1-S3 GOF test results for Gamma, Lognormal, Nakagami and Weibull distributions is registered in Table 10, item (d). This S1-S3 segment is characterized by a high data dispersion level measured by the SCV index (34.268), indicator of heterogeneity in the RSS data. This heterogeneity could be a possible factor that causes the rejection of the null hypothesis. Consequently, it makes necessary an analysis with smaller segments where the RSS data is distributed homogenously. Analogous results were obtained for joint segment S4-S6 (144m) according to the results in Table 10, item (e).

When the GOF test indicates the non-rejection of the null hypothesis for two or more distributions, the best distribution fit are defined for the lower "AD-statistic" given that this statistic represents a divergence or discrepancy measurement [107]. The input parameter (shape)—estimated from the 3D-RL RSS data using Maximum Likelihood Estimation MLE—that characterizes the Gamma, Lognormal, Nakagami and Weibull distributions, shows slight variations for the shape parameter when the individual segments are compared; for the joint segments these parameters were not reported given the lack of fit between the data and the proposed distributions.

5.3.2 V2V statistical characterization for scenario2.

To analyze the V2V-RSS statistical behavior, segmentation and spatial position were considered as is depicted in Figure 32. Three horizontal segments along AV-1(S1, S2, S3) and two vertical segments along ST-2(S4, S5) were selected, considering C1 as the transmitter. Figure 33 shows the Probability Plot (pp-plot) - a graphical technique for assessing whether or not a data set follows a given distribution [100] - for segments S1 to S3 (S1-S3) and S4-S5. The RSS data were plotted against a theoretical Weibull (Figure 33(a)) and Lognormal(Figure 33(b)) distributions which are represented by the black-

dotted straight line as a reference line. Departures from this straight line indicate departures from the specified distribution.
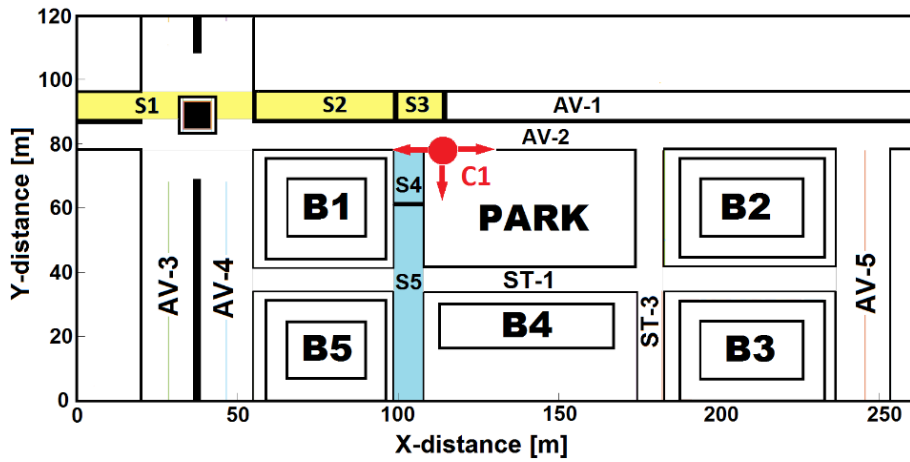

Figure 32. Scenario segmentation for V2V analysis

(a)

(b)
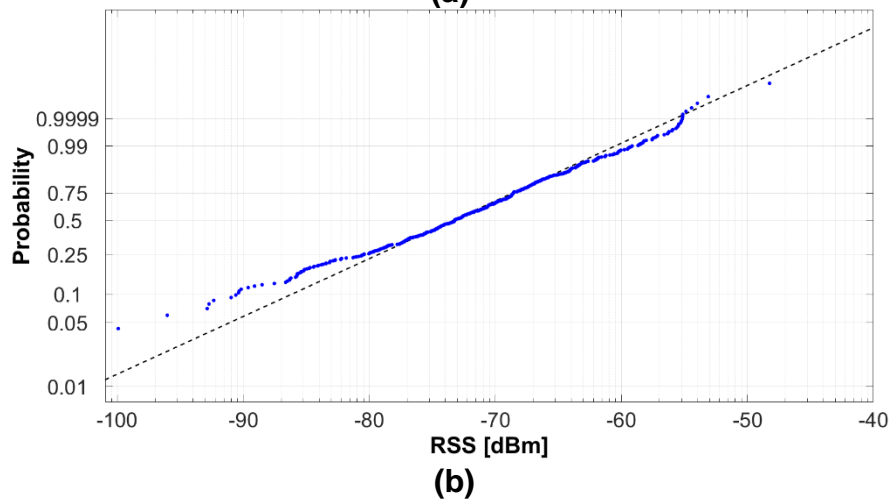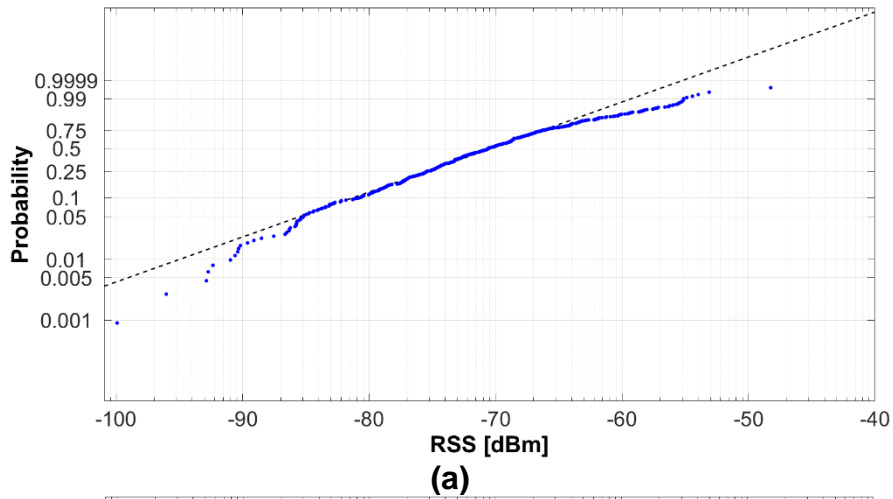
Figure 33. pp-plot for C1-RSS: **(a)** S1-S3 for Weibull distribution, **(b)** S4-S5 for Lognormal Distribution.

From Figure 33(a) and 34(b), it is noted the RSS departure from the proposed distributions, mainly at the right-sided and left-sided tails, which is an indicator that RSS do not follow the theoretical distributions; in other words, those distributions do not provide good fit to the RSS data. Additional pp-plot analysis for Exponential, Rician and Lognormal distributions for S1-S3 and S4-S5 segments, resulted in similar departure of the RSS data to those distributions. These results give insight into the necessity to evaluate individual segments and define metrics to find the statistical distribution able to represent the RSS data. Figure 34 illustrate the S1-RSS pp-plot for Weibull distribution where is observed the RSS data lie closer the straight line; the S1-RSS behavior would be characterized by Weibull distribution. The natural variation in the RSS (outliers), could be the cause of the data departure from the left-side tail.
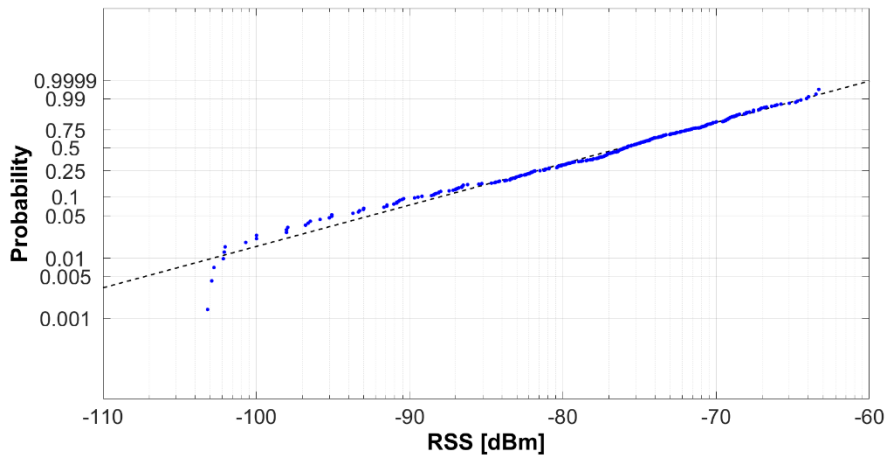
Figure 34. S1 pp-plot for Weibull distribution

Figure 35 depicts the CDF of C1-RSS along AV-1, when C1 is transmitting, and its statistical comparison with distributions used in the description of multipath fading environments as Gamma, Lognormal, Nakagami and Weibull. Figure 35 (a), 36(b), 36(c) represents the S1(60m), S3(17m), and S1-S3 (160m) respectively. According to Figure 35(a), S1 is best described by Weibull distribution, while from Figures 36(b) and 36(c) is observed that S3 and the join segment S1-S3 are best described by Lognormal

distribution. Figure 36(a), 37(b), 37(c) represents the S4(60m), S5(20m), and S4-S5 (160m) segments respectively and its statistical comparison with the aforementioned distributions.
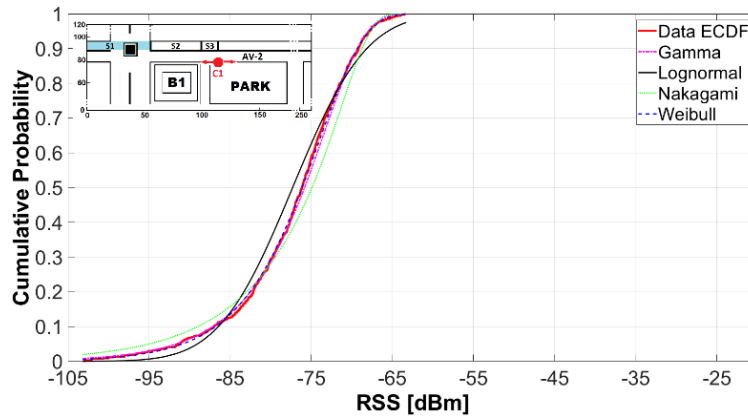
(a)
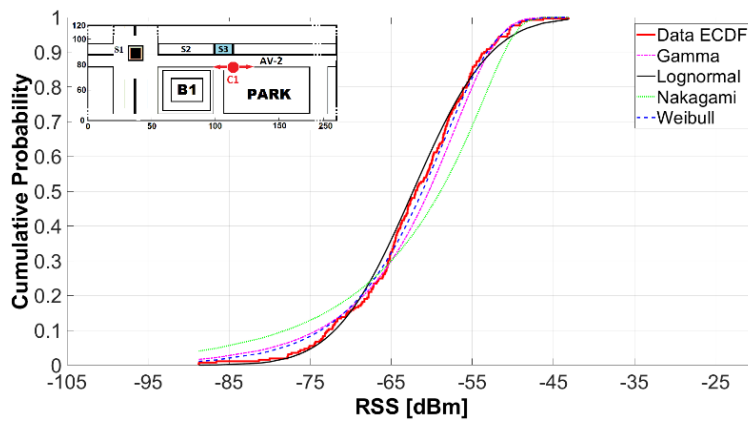
(b)
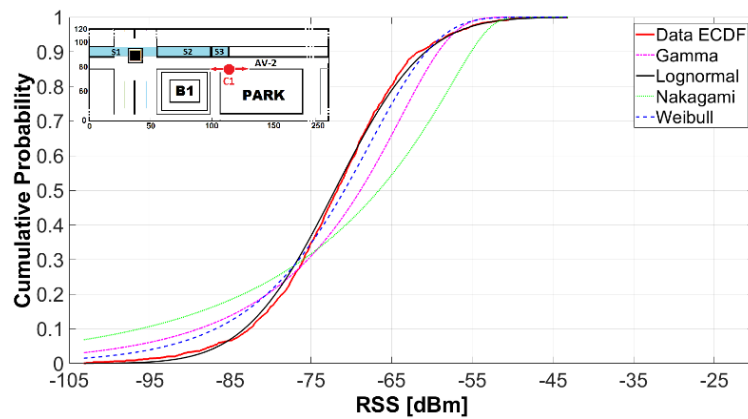
(c)

Figure 35. CDF of C1-RSS along AV1. **(a)** S1(60m); **(b)** S3 (17m); **(c)** S1-S3 (160m)

From Figure 36(a) and 37(b), it is observed that S4 and S5 are best described by a Weibull distribution, while the joint segment S4-S5 is best described by a Lognormal distribution as is depicted in Figure 37(c).
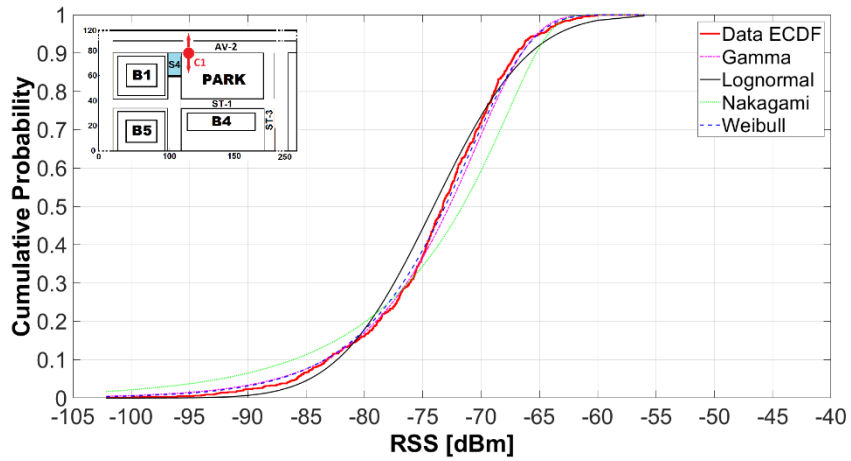
(a)
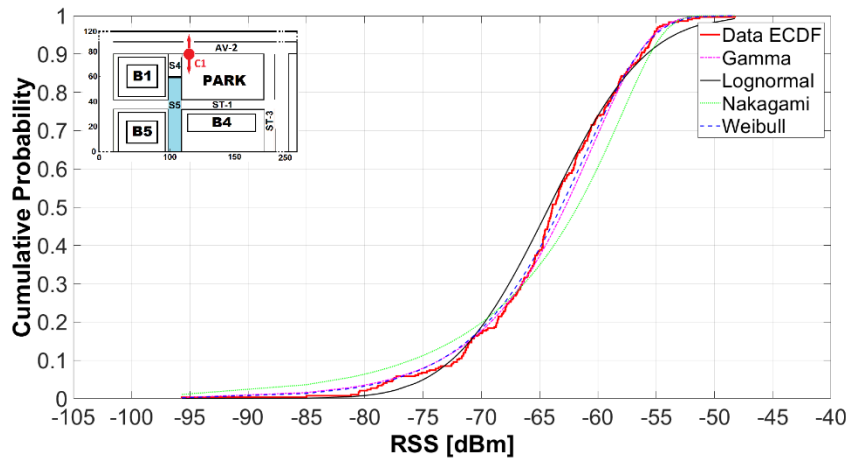
(b)
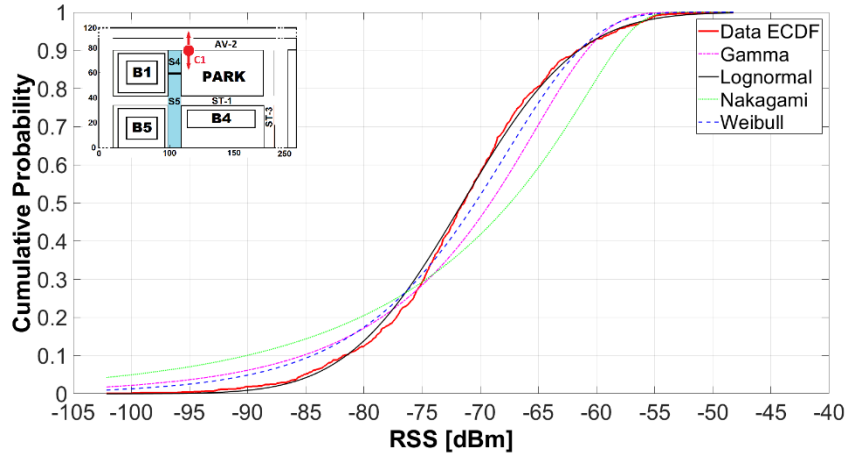
(c)

Figure 36. CDF of C1-RSS along ST1: **(a)** S4(20m); **(b)** S5 (60m); **(c)** S4-S5 (80m)

Error! Not a valid bookmark self-reference. summarizes some statistical measurement referent to Figure 35 and Figure 36 as: SCV, GOF (with 5.0% for a significance level of the hypothesis (H_0) test), AD statistics and the input parameter (shape) for the tested distributions. According to the hypothesis test results, the Weibull distribution can describe the statistical behavior of the individual segments S1, S2, S3, S4, S5 while Lognormal distribution can describe the jointly segment S4-S5. On the other hand, the jointly segment S1-S3, although cannot be described, under stringent statistical sense, by anyone of the tested distribution, nonetheless, would be "fitted" by a Lognormal distribution given its lowest AD-statistic when compared with other distributions.

Table 11. Data dispersion measurements and GOF test for C1.

Description	SCV **	n ***	Lognormal	Gamma	Nakagami	Weibull
(a) S1 (AV-1): (x: 1 to 60) m CDF-GOF: (AD-H/ AD-S) Input parameter: Shape	1.953	2.065	T/ 10.017 2.922	F/ 1.220 0.671	T/ 12.587 0.249	F/ 0.399 0.766
(b) S2 (AV-1): (x: 60 to 100) m AD (AD-H/ AD-S) Shape factor	1.956	1.355	T/ 2.924 4.833	T/ 2.973 0.860	T/ 19.573 0.285	F/ 2.091 0.876
(c) S3 (AV-1): (x: 100 to 117) m AD (AD-H/ AD-S) Shape factor	6.030	1.174	F/ 1.061 6.376	T/ 2.980 0.532	T/ 13.793 0.183	F/ 0.887 0.652
(d) S1 – S3 (x: 1 to 117) m AD (AD-H/ AD-S)	23.776	1.799	T/ 3.127	T/ Inf.	T/ Inf	T/ 18.879

75

(e) S4 (ST-2): (y:60 to 80) m						
AD (AD-H/ AD-S)	2.515	1.228	**F**/ 2.239	**F**/ 1.745	T/ 9.288	**F**/ 0.941
Shape factor			5.942	0.711	0.246	0.609
(f) S5 (ST-2): (y: 1 to 60) m						
AD (AD-H/ AD-S)	2.869	1.528	T/ 7.971	T/ 3.432	T/ Inf	**F**/ 1.716
Shape factor			3.666	0.722	0.241	0.786
(g) S4 – S5 (y: 1 to 80) m						
AD (AD-H/ AD-S)	7.131	1.479	**F**/ 2.087	T/ 37.136	T/ Inf	T/ 13.436
Shape factor			4.251	0.447	0.154	0.583

5.4. VTD impact for I2V, V2I and V2V.

Figure 37 depicts a I2V-V2I RSS plot under two VTD levels: LD and HD.
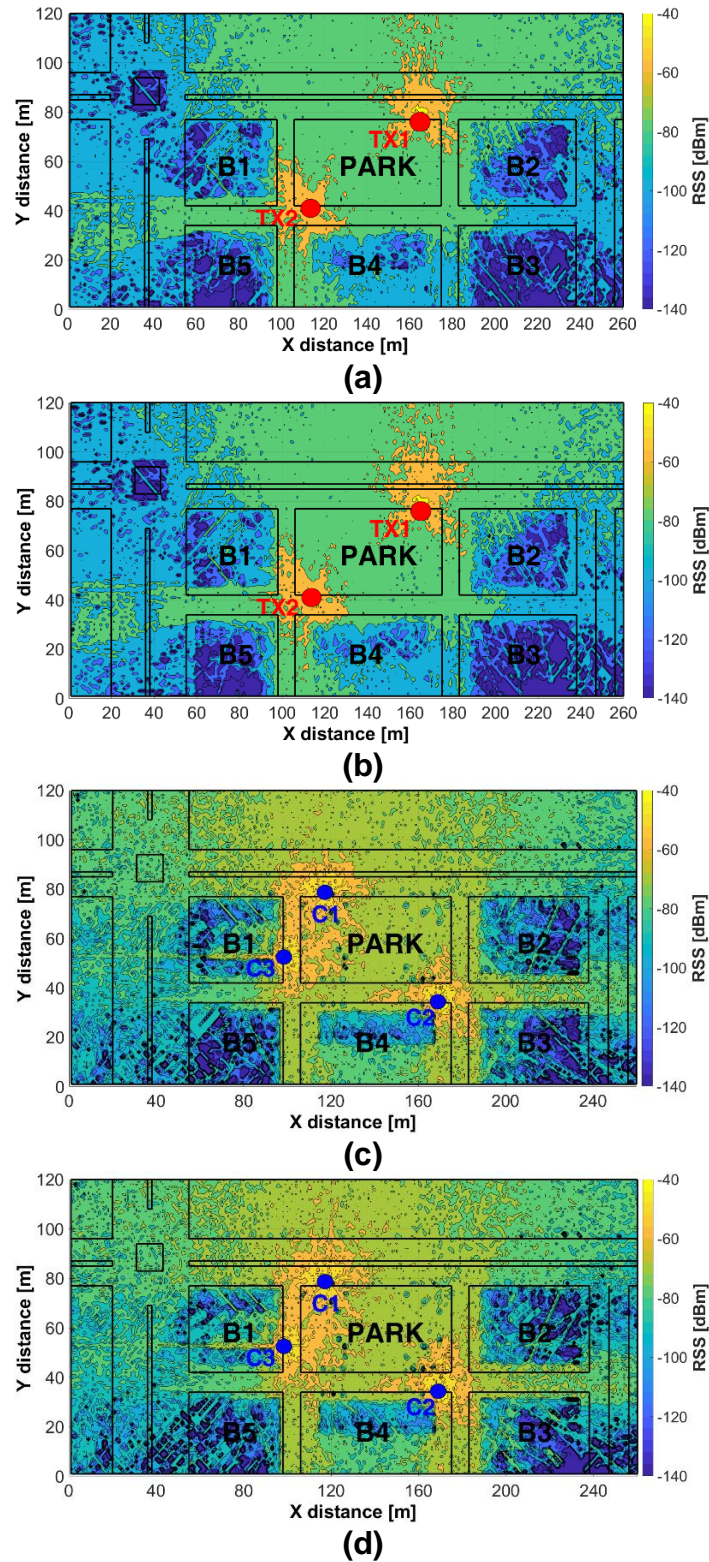
Figure 37. I2V and V2I RSS: (a), (b) I2V for LD, HD; (c), (d) V2I for LD, HD

In order to have a better understanding of the VTD impact into the V2X links, a RSS and VTD analysis together with statistics measurements have been carried on scenario S4. Up to three RSU has been considered for V2I and I2V analysis while three vehicles have been considered for V2V analysis, placed in different locations of the scenario S4.

5.4.1 VTD analysis for I2V and V2I.

Figure 37(a) and 38(b) shows the I2V-RSS for LD and HD respectively for the join transmission of TX1&TX2 when the RX´s are located at vehicles height (1.5m). Subtle variations in the RSS are noted in the vicinity of the TX, however, the RSS values seem to be similar in both figures. Figure 37(c, d) shows the V2I-RSS for LD and HD respectively for the join transmission of C1&C2&C3 when the RX´s are located at RSU height (3.5m). For both configurations I2V and V2I, a subtle increase in the RSS values are noted in the vicinity of the transmitters.

At first glance, the RSS is minimum affected by the VTD for I2V and V2I links, however, this supposition must be complemented with additional measures as statistical measures. One of these measures is the box and whisker plot (boxplot), a five-number summary statistic (median, upper and lower quartile, higher and lower observation) measure to compare two or more datasets when many observations are involved, and useful for indicating whether a distribution is skewed and whether there are potential unusual observations (outliers). A boxplot analysis is used to complement the analysis of the VTD impact in the I2V-V2I RSS for areas located in the vicinity and remote to TX (Figure 38).
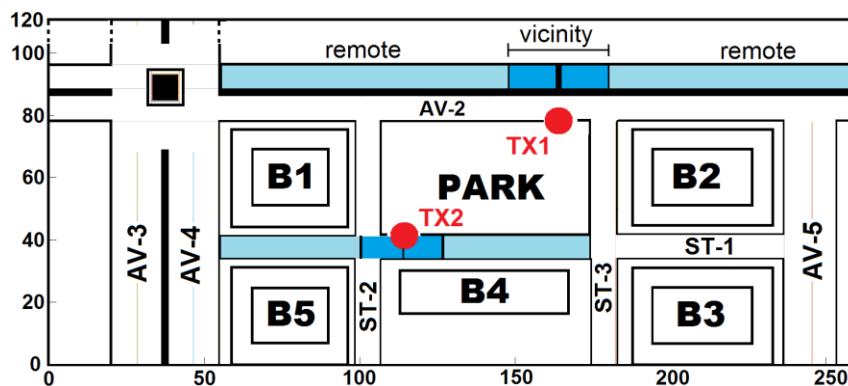
Figure 38. I2V-V2I boxplot analysis areas

Figure 39 shows a boxplot of the V2I- RSS in the vicinity and remote areas to TX´s. Figure 39(a) shows the RSS boxplot in the vicinity of TX1 and TX2, while Figure 39(b) display the RSS boxplot for remote areas. In the extent, the TX-RX distance increases and the segment length for analysis enlarges, the median RSS decreases and, outliers appear as a result of the presence of extreme values due to the multipath effect and data variability.
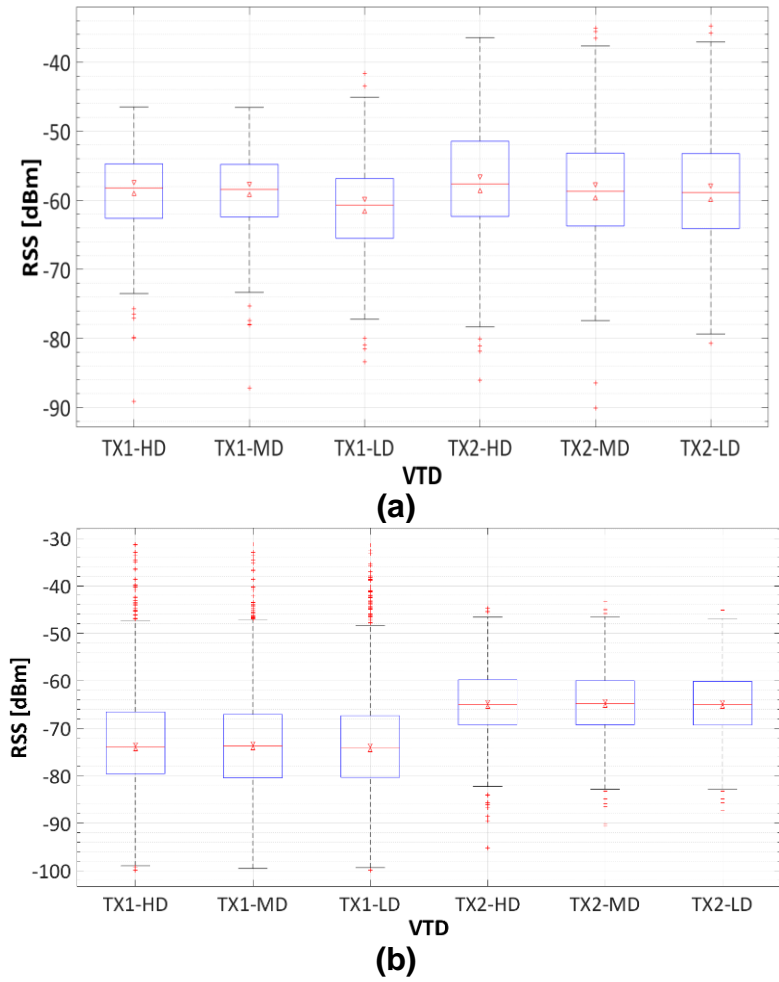
Figure 39. I2V- RSS: **(a)** vicinity to TX´s, **(b)** remote to TX´s

Figure 39(b) (TX1) shows a decrease in the RSS media value when TX remote areas are compared with the TX vicinity (Figure 39(a)) for HD, MD and LD due to the distance factor. From Figure 39(a), it is observed differences in the media values and trend is out looked where high RSS values are correspondent with HD, while from Figure 39(b) it is observed slightly variation in the media values but without trend. Additional

measurements where performed for TX2 with similar outcomes. These results suggest that for I2V links, in the vicinity areas of the TX, higher RSS values area related with HD.

With respect to V2I, Figure 40 illustrates the average TX's-RSS (TX1, TX2, TX3) when vehicles C1, C2 and C3 are transmitting (refer to Figure 29), under different VTD levels. TX3 was an additional RSU placed in the roundabout area because the 3D-RL simulator permits to place an indefinite number of additional RSU for V2I analysis. According to Figure 40, while more distant are the cars to the TX´s or more significant are the obstacles in the LoS, the mean RSS at the receiver is lower. For instance, in TX3, its greatest distance to the cars, causes the lowest RSS values for C1, C2 and C3 for all VTD levels, when compared with TX1 and TX2. Otherwise, although C3 is nearest to TX3, its RSS is below than C1 and C2 due to the significant obstruction of B1.
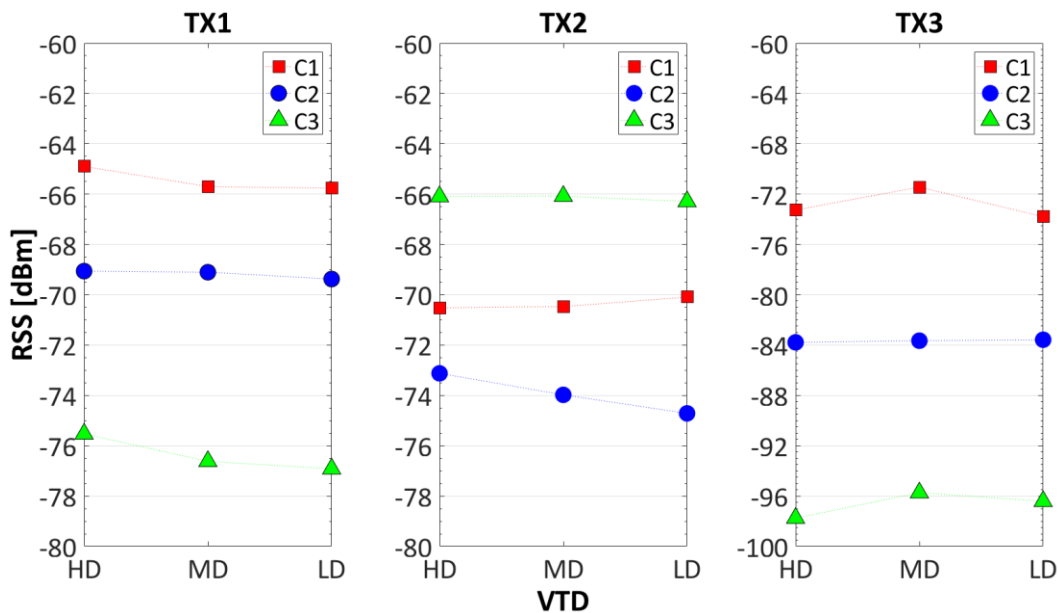
Figure 40. V2I- RSS

The most significant RSS variation due to VTD is correspondent with C2 - TX2 where the difference between HD and LD is 2dBm approximately, however, this difference is not the trend for different VTD levels at TX´s.

From the analysis and comparison between TX1, TX2 and TX3, there are not significant differences in the RSS mean or some trend is evident under different VTD

levels. These results suggest that VTD is a factor that does not cause a significant impact in the TX-RSS for V2I links.
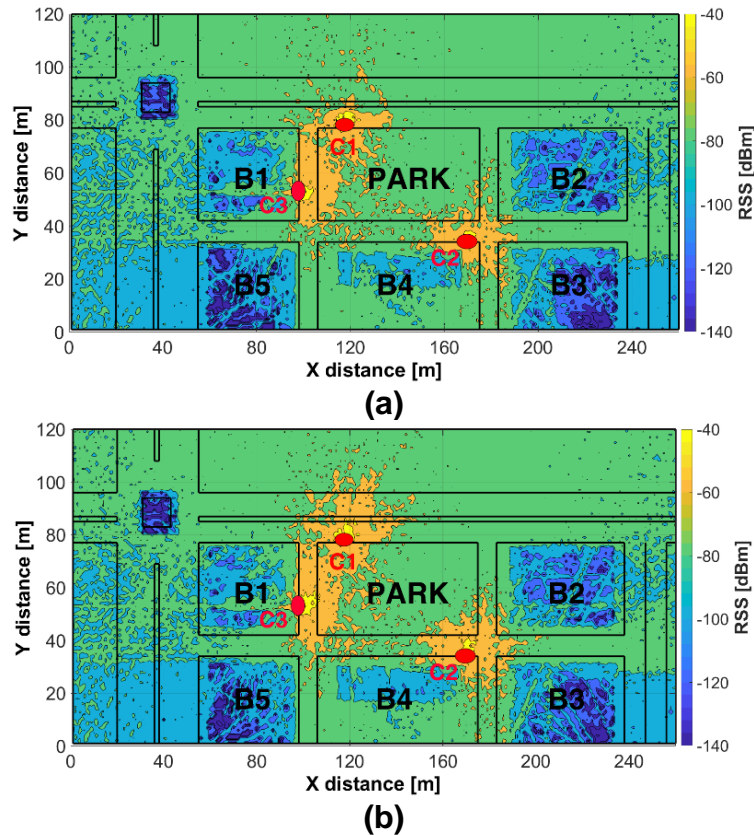
Figure 41. V2V-RSS: **(a)** LD, **(b)** HD

5.4.2 VTD analysis for V2V

Figure 41(a) and 42(b) show the V2V-RSS for the join transmission of C1&C2&C3 under LD and HD respectively. The V2V communication is feasible along AV1, AV2, ST1, ST2, ST3 given that the RSS values are above the RST for both VTD conditions, nonetheless, higher RSS values are noted in the vicinity of C1, C2, C3 for HD (Figure 41(b)) when compared with LD (Figure 41(a)) which suggest that higher VDT levels are related with higher RSS levels (in the Cx's vicinity area). There are not observable RSS variations for remote areas.

Figure 42 shows a boxplot of the V2V-RSS in the vicinity (Figure 42(a)) and remote areas (Figure 42(b)) to the CX´s (C1, C2, C3) under HD, MD and LD. From Figure 42(a) is observable a trend where higher RSS values are related to HD and lower RSS values

are related to LD for each one of the analyzed CX´s, while there are not significant differences or observable trend for remotes areas from CX's (Figure 42(b)). These results suggest that higher VTD levels are related with higher RSS values for V2V links in the vicinity of the CX´s.
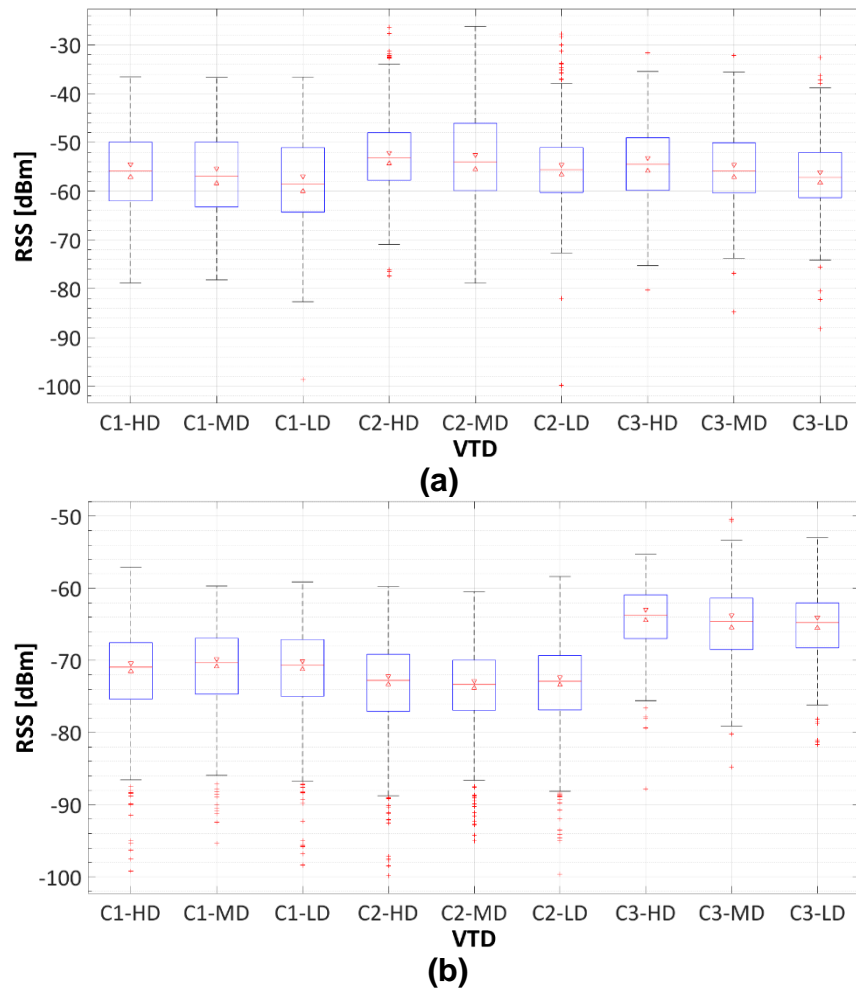
Figure 42. V2V- RSS: **(a)** vicinity to CX´s, **(b)** remote to CX´s

Table 12 and Table 13 show some RSS statistics in the vicinity and remote areas of C1, C2, C3, respectively, for different VTD levels. From Table 12 , the more noticeable difference and trend is for the second quartile (Q2) - the median of the RSS data - where higher RSS values are related with higher VTD levels: approximate 3 dBm difference between C3-HD and C3-LD. The first quartile (Q1) and third quartile (Q3) show the same

trend as Q2, with exception for C2 when its Q3 is analyzed: C2-HD RSS value is below than C2-MD. Measures as mean, STD and PLE do not show apparent RSS tendency when different VTD values are compared.

For remote areas there are not observable differences or trends in the RSS values due to the influence of the VTD, as is illustrated in Figure 42(b) and described by RSS statistics from Table 13

Table 12. RSS statistics for V2V in the vicinity of CX's

CX – VTD	Q1[dBm]	Q2[dBm]	Q3[dBm]	Mean[dBm]	STD[dB]	SCV	PLE
C1- HD	-62.021	-55.799	-49.923	-48.135	18.800	5.252	2.48
C1- MD	-63.241	-56.895	-49.946	-48.121	20.600	4.448	2.54
C1- LD	-64.302	-58.484	-51.094	-48.401	19.601	4.860	2.69
C2- HD	-57.780	-53.230	-47.997	-42.080	16.557	13.264	2.32
C2- MD	-59.895	-54.011	-46.094	-41.992	14.892	12.338	2.44
C2- LD	-60.279	-55.598	-51.068	-42.853	18.170	14.208	2.51
C3- HD	-59.828	-54.494	-49.059	-46.680	29.002	8.914	2.54
C3- MD	-60.368	-55.857	-50.091	-47.955	29.327	12.769	2.46
C3- LD	-61.348	-57.204	-52.065	-48.479	30.866	14.208	2.53

Q1 = Quartile1 (25%), Q2 = Quartile2 (50%), Q3 = Quartile3 (75%)
SCV = Squared Coefficient of variation

Table 13. RSS statistics for V2V for remote areas of the CX's

CX – VTD	Q1[dBm]	Q2[dBm]	Q3[dBm]	Mean[dBm]	STD[dB]	SCV	PLE
C1- HD	-75.367	-70.924	-67.535	-68.342	51.058	2.112	1.82
C1- MD	-74.674	-70.323	-66.922	-68.351	57.621	1.272	1.86
C1- LD	-74.973	-70.669	-67.094	-68.434	52.536	1.307	1.86
C2- HD	-77.055	-72.759	-69.152	-69.974	15.113	1.892	1.45
C2- MD	-76.903	-73.314	-69.955	-70.777	15.891	1.767	1.50
C2- LD	-76.867	-72.882	-69.319	-70.276	15.803	1.977	1.46
C3- HD	-66.964	-63.711	-60.910	-62.099	29.833	1.014	1.15
C3- MD	-68.479	-64.569	-61.349	-61.798	25.799	2.874	1.87
C3- LD	-68.251	-64.745	-62.018	-62.620	29.827	1.977	1.22

The impact of the VTD for V2X communication is represented and discussed in this section. Graphical and statistical tools have been used to identify the fading model able to characterize the implications that different VTD levels induce in the RSS - URPC. Considerations of spatial distance, and symmetric and equidistant distances from TX

were taken into account to organize the data into homogeneous segments to easy the statistical analysis. Lognormal and Weibull distributions can characterize the RSS of V2I, I2V and V2V links. The statistical evidence suggests significant RSS differences (in terms of the median) and consistent trend for V2V and I2V links in areas located in the vicinity of the TX, where the highest RSS values keep relationship with HD. Further analysis and measurement campaigns are needed to validate these results.

6. Conclusions, Research Strands, and Future Work

The potential to improve different aspects in the roads are being conducted on ITS and has attracted the commercial, governmental and research interest for technologies related with VANET's The IEEE 802.11p standard was developed to operate at 5.9GHz band for V2V and V2I, which provides a low-latency, short-to-medium-range wireless in urban environments which have two remarkable characteristics: they are time dispersive, due to the multipath effect, and they present rapid changes between LoS, QLoS and NLoS. The channel characterization of this environments must be quantitative as thorough as possible but not excessively complex as to limit its usefulness.

This research work, based on simulation tools, is aimed to characterize the URPC for V2X under different VTD levels and make use of three computational tools: a deterministic 3D Ray-Launching algorithm, a detailed geographic database and a microscopic vehicular movement simulator, which integration is an important contribution for V2X URPC research. The methodology considers three stages: the accurate and detailed scenario representation, the channel propagation and vehicular movement (3 density levels) simulation, and, the V2I and V2V Large Scale, Small scale metrics and statistical characterization. The resulted volumetric power estimation together with volumetric power delay profile and delay spread values, can provide insight in coverage/capacity radios, equalization requirements, parameterization of adaptive modulation and coding schemes.

The 3D scenario is delimited and represented from OSM geospatial data, an open source platform and collaborative project to create a free editable map of the world. The OSM map information is downloaded in OSM-XML format and edited in JOSM, an extensible editor for OSM. The edited map is represented in an open source, microscopic, multi-modal traffic simulator SUMO to mimic and evaluate the vehicular movement and different VTD levels. Information as vehicle position, velocity, routes, etc., is shared to the 3D-RL algorithm for URPC simulation. The URPC data analysis and representation results was carried on MATLAB platform. The analysis with the aid of hybrid deterministic

code based on 3D Ray Launching enables evaluation of complex vehicular scenarios with affordable computational cost, opening a path for the analysis of issues such as scalability or heterogeneous network operation. The operating mode of the algorithm has been previously published in it has also been validated in transportation systems.

Three different urban scenarios were used for analysis of the large-scale and small-scale parameters: RSS, spatial Path Loss, multipath metrics as Power Delay Profile, mean excess delay, RMS delay spread, Coherence Bandwidth, Doppler Shift and Doppler Spread. Propagation zones where LoS, QLoS and NLoS conditions were identified resulted from the RSS map analysis. The measurement validation for I2V- RSS shows more accurate results from 3D-RL simulation than a theoretical PLM for vehicular environments presented in the bibliography. The coverage analysis of the scenario1, results in a suggested configuration of at least four TX for complete I2V- RSS coverage. Multipath metrics as PDP shows a highly multipath environment with high levels of Mean Excess Delay, RMS Delay Spread. Channel availability was suggested for areas with high CB values, as located in NLoS. The Doppler Spread and Doppler Shift, which describe the time-varying nature of the channel, show that factors such as the relative velocity and direction of motion respect to TX, have an impact on the apparent received frequency. Two velocities where used for analysis, 40km/h and 60km/h.

To shape and characterize the implications that different VTD levels induce in the RSS – URPC, useful graphical statistical tools as pp-plot and Boxplot, or analytical as GOF, SCV, AF has been used to identify the theoretical fading model, from the proposed and utilized in multipath environments as Gamma, Lognormal, Rician, etc., or composite models as Weibull-Gamma, Nakagami-Lognormal, etc., that best fit the RSS-V2X data. The statistical analysis considers spatial distance, and symmetric and equidistant distances from TX, so as to organize the data into homogeneous segments to easy the fitting test when compared with theoretical fading distributions. Lognormal and Weibull distributions are able to characterize the RSS of V2I, I2V and V2V links. Weibull distribution best fit individual RSS-V2X segments, while Lognormal distribution explain in a better way the jointly RSS-V2X segments. The statistical evidence suggests significant mean RSS differences and consistent trend where the highest RSS values keep

relationship with HD for V2V and I2V for areas in the vicinity of the TX. Further analysis and measurement campaigns are needed to validate these results.

The approach, methodology and solution of this proposal, could raise new strands for the vehicular communications field, as follows:

- URPC characterization for different vehicle types: further studies are needed to investigate URPC for vehicles other than personal cars (e.g. motorcycles, bicycles, trucks, buses, etc.). For V2P communications, URPC for different communication technologies that can enable (e.g., DSRC, Wi-Fi, and cellular-based systems) need to be explored further.

- URPC characterization, measurements and modeling studies for under-explored environments as tunnels, parking, overpasses, bridges, roundabouts, bus-stop, etc.

- URPC characterization for vehicle-to-X and 5G: Device-to-Device (D2D) concept in 5G systems shares many similarities with V2X communications; efforts on characterize the URPC in V2I /V2X channels can benefit from the existing D2D channel characterization and vice versa.

- URPC characterization using beamforming: With beamforming, a vehicle can focus the antenna beam only on a specific region and can minimize interference[108]. Directional antennas let to reuse space through beamforming by focusing the antenna pattern on a specific vehicle or RSU. Therefore, beamforming is a direction to explore in the URPC.

As a future work, an extensive measurement campaign should be considered to validate the obtained results. The identification and characterization of significant areas (i.e., different density of obstacles such as buildings, vegetation, etc.) could lead us to the proposal of an empirical or statistical propagation model that accounts for more environmental variables with the aim of precise results. The zones with high CB and low RSS levels where the V2X communication is unfeasible could be of special interest in research fields such as cognitive radio and V2P, among others. The detailed and quantitative impact of street intersections and roundabout on the RSS

87

have special interest for V2V communications. Massive V2X WSN deployments are not only technological matters, but also ones for governments, manufacturers and customers. The offer of developing services and applications for which customers are willing to pay, car manufacturers are willing to offer, and government policies are willing to permit will define the future deployment of V2X technology.

References

[1]   World Health Organization, "Road traffic injuries." [Online]. Available: http://www.who.int/mediacentre/factsheets/fs358/en/. [Accessed: 04-Feb-2017].

[2]   K. D. Kochanek, J. Xu, S. L. Murphy, A. M. Minino, and H.-C. Kung, "National Vital Statistics Reports Deaths : Final Data for 2009," *Natl. Cent. Heal. Stat.*, vol. 60, no. 3, pp. 1–117, 2012.

[3]   Instituto Nacional de Estadística y Geografía-INEGI, "Accidentes de tránsito terrestre en zonas urbanas y suburbanas," 2015. [Online]. Available: http://www.beta.inegi.org.mx/proyectos/registros/economicas/accidentes/default.h tml. [Accessed: 10-Mar-2017].

[4]   The Institute of Electrical and Electronics Engineers., "IEEE Std 802.11 p-2010. Part 11: Wireless LAN Medium Access Control (MAC) and Physical Layer (PHY). Specifications-Amendment 6: Wireless Access in Vehicular Environments.," New York, USA, 2010.

[5]   C. Sommer and F. Dressler, *Vehicular networking*. United Kingdom: Cambridge University Press, 2015.

[6]   S. B. Raut and L. G. Malik, "Survey on vehicle collision prediction in VANET," *2014 IEEE Int. Conf. Comput. Intell. Comput. Res. IEEE ICCIC 2014*, no. Idm, pp. 735–751, 2015.

[7]   D. W. Matolak, "Channel modeling for vehicle-to-vehicle communications," *IEEE Commun. Mag.*, vol. 46, no. 5, pp. 76–83, 2008.

[8]   D. Vlastaras, T. Abbas, M. Nilsson, R. Whiton, M. Olback, and F. Tufvesson, "Impact of a truck as an obstacle on vehicle-to-vehicle communications in rural and highway scenarios," *2014 IEEE 6th Int. Symp. Wirel. Veh. Commun. WiVeC 2014 - Proc.*, 2014.

[9]   M. G. Nilsson, C. Gustafson, T. Abbas, and F. Tufvesson, "A Measurement Based Multilink Shadowing Model for V2V Network Simulations of Highway Scenarios," vol. 66, no. 10, pp. 1–10, 2017.

[10]   L. Azpilicueta, P. López-Iturri, E. Aguirre, C. Martínez, J. J. Astrain, J. Villadangos, and F. Falcone, "Evaluation of deployment challenges of wireless sensor networks at signalized intersections," *Sensors (Switzerland)*, vol. 16, no. 7, 2016.

[11]   F. Granda, L. Azpilicueta, C. Vargas-rosales, P. López-iturri, E. Aguirre, J. J. Astrain, J. Villandangos, and F. Falcone, "Characterization of radio propagation channel in Urban Vehicle to Infrastructure environments to support WSNs," in *Proceedings of the 3rd Int. Electron. Conf. Sens. Appl.*, 2016, vol. 3, no. November, pp. 1–6.

[12]   W. Viriyasitavat, M. Boban, H. M. Tsai, and A. Vasilakos, "Vehicular communications: Survey and challenges of channel and propagation models," *IEEE Veh. Technol. Mag.*, vol. 10, no. 2, pp. 55–66, 2015.

[13]   I. Rodriguez, E. Almeida, M. Lauridsen, D. A. Wassie, L. Chavarria, H. Nguyen, T.

Sorensen, and P. Mogensen, "Measurement-based Evaluation of the Impact of Large Vehicle Shadowing on V2X Communications," in *European Wireless*, 2016, pp. 142–149.

[14]   N. Akhtar, S. C. Ergen, and O. Ozkasap, "Vehicle mobility and communication channel models for realistic and efficient highway VANET simulation," *IEEE Trans. Veh. Technol.*, vol. 64, no. 1, pp. 248–262, 2015.

[15]   R. Fujimoto and G. Riley, "Analytical models for information propagation in vehicle-to-vehicle networks," *IEEE 60th Veh. Technol. Conf. 2004. VTC2004-Fall. 2004*, vol. 6, no. C, pp. 4548–4552, 2004.

[16]   J. A. Sanguesa, M. Fogue, P. Garrido, F. J. Martinez, J. C. Cano, C. T. Calafate, and P. Manzoni, "An infrastructureless approach to estimate vehicular density in urban environments," *Sensors (Switzerland)*, vol. 13, no. 2, pp. 2399–2418, 2013.

[17]   M. Fogue, P. Garrido, F. J. Martinez, J. C. Cano, C. T. Calafate, and P. Manzoni, "Analysis of the most representative factors affecting warning message dissemination in VANETs under real roadmaps," *IEEE Int. Work. Model. Anal. Simul. Comput. Telecommun. Syst. - Proc.*, pp. 197–204, 2011.

[18]   F. Granda, L. Azpilicueta, C. Vargas-rosales, P. Lopez-iturri, E. Aguirre, J. Astrain, J. Villandangos, and F. Falcone, "Spatial Characterization of Radio Propagation Channel in Urban Vehicle-to-Infrastructure Environments to Support WSNs Deployment," *Sensors*, vol. 17, no. 6, p. 1313, 2017.

[19]   D. W. Matolak and A. Chandrasekaran, "5 GHz Intra-Vehicle Channel Characterization," in *IEEE Vehicular Technology Conference*, 2012, pp. 1–5.

[20]   M. Boban, W. Viriyasitavat, and O. K. Tonguz, "Modeling vehicle-to-vehicle line of sight channels and its impact on application-layer performance," *Proceeding tenth ACM Int. Work. Veh. inter-networking, Syst. Appl. - VANET '13*, p. 91, 2013.

[21]   N. Akhtar and C. Science, "Vehicle Mobility , Communication Channel Modeling and Traffic Density Estimation in VANETs," Koç University, 2013.

[22]   R. Nagel and S. Eichler, "Efficient and realistic mobility and channel modeling for VANET scenarios using OMNeT++ and INET-framework," *Proc. 1st Int. Conf. Simul. tools Tech. Commun. networks Syst. Work.*, p. 89:1--89:8, 2008.

[23]   H. Fernandez, V. M. Rodrigo-Penarrocha, L. Rubio, and J. Reig, "Path loss characterization in vehicular environments under LOS and NLOS conditions at 5.9 GHz," *8th Eur. Conf. Antennas Propagation, EuCAP 2014*, vol. 13, pp. 3044–3048, 2014.

[24]   R. F. Atallah, M. J. Khabbaz, and C. M. Assi, "Vehicular networking : A survey on spectrum access technologies and persisting challenges," *Veh. Commun.*, vol. 2, no. 3, pp. 125–149, 2015.

[25]   U.S. Department of Transportation, "Estimated Benefits of Connected Vehicle Applications. Dynamic Mobility Applications, AERIS, V2I Safety, and Road Weather Management Applications.," Noblis Inc., Washington DC., 2015.

[26] W. Manfe and D. Turgay, "HYBRIST Mobility Model - A Novel Hybrid Mobility Model for VANET Simulations," *Int. J. Comput. Appl.*, vol. 86, no. 14, pp. 15–21, 2014.

[27] Massachuset Institute of Technology - News, "SMART automation," 2017. [Online]. Available: http://news.mit.edu/2017/smart-automation-daniela-rus-0119. [Accessed: 04-Feb-2017].

[28] University of Michigan, "Transportation Research Institute-ITS Publications." [Online]. Available: http://www.umtri.umich.edu/our-focus/intelligent-transportation-systems. [Accessed: 04-Feb-2017].

[29] TESLA-motors., "All Tesla Cars Being Produced Now Have Full Self-Driving Hardware." [Online]. Available: https://www.tesla.com/blog/all-tesla-cars-being-produced-now-have-full-self-driving-hardware?redirect=no. [Accessed: 04-Feb-2017].

[30] WAYMO., "Technology-We're building a safer driver that is always alert and never distracted." [Online]. Available: https://waymo.com/tech/. [Accessed: 30-Apr-2018].

[31] World Bank Group, "Intelligent Transport Systems - Toolkit for European Union." [Online]. Available: https://ppp.worldbank.org/public-private-partnership/library/intelligent-transport-systems-its-toolkit-european-union. [Accessed: 30-Apr-2018].

[32] U.S. Department of Transportation USDOT, "Vehicle-to-Infrastructure (V2I) Safety Applications. Concept of Operation Document," 2013.

[33] F. Basma, Y. Tachwali, and H. H. Refai, "Intersection collision avoidance system using infrastructure communication," in *In Proceedings of the 14th International IEEE Conference on Intelligent Transportation Systems (ITSC)*, 2011, pp. 422–427.

[34] V. Milanes, S. E. Shladover, J. Spring, C. Nowakowski, H. Kawazoe, and M. Nakamura, "Cooperative adaptive cruise control in real traffic situations," *IEEE Trans. Intell. Transp. Syst.*, vol. 15, no. 1, pp. 296–305, 2014.

[35] E. Belyaev, A. Vinel, A. Surak, M. Gabbouj, M. Jonsson, and K. Egiazarian, "Robust vehicle-to-infrastructure video transmission for road surveillance applications," *IEEE Trans. Veh. Technol.*, vol. 64, no. 7, pp. 1–1, 2014.

[36] U.S. Department of Transportation (USDOT), "Transit Vehicle-to-Infrastructure (V2I) Assessment Study Project Report," Washington, DC 20590, 2015.

[37] B. Aygun, M. Boban, J. P. Vilela, and A. M. Wyglinski, "Geometry-based propagation modeling and simulation of vehicle-to-infrastructure links," in *IEEE Vehicular Technology Conference*, 2016, pp. 3–7.

[38] United States Department of Transportation (U.S. DOT), "Smart Columbus : Systems Engineering Management Plan for the Smart Columbus Demonstration Program," Washington, DC 20590, 2018.

[39] L. Shen, L. Du, X. Yang, X. Du, J. Wang, and J. Hao, "Sustainable Strategies for Transportation Development in Emerging Cities in China : A Simulation Approach," *Sustainability*, vol. 10, no. 3, 2018.

[40] IEEE Vehicular Technology Society, "IEEE Standard for Wireless Access in Vehicular Environments (WAVE)— Multi-Channel Operation," New York, NY, USA, 2016.

[41] C. Sommer and F. Dressler, *Vehicular Networking*. United Kingdom: Cambridge University Press, 2015.

[42] L. Azpilicueta, C. Vargas-Rosales, and F. Falcone, "Deterministic Propagation Prediction in Transportation Systems.," in *IEEE Vehicular Technology Magazine*, 2016, vol. 11, pp. 29–37.

[43] J. Gozalvez, M. Sepulcre, and R.Bauza, "IEEE 802.11p Vehicle to Infrastructure Communications in Urban Environments," *Top. Automot. Netw. Appl.*, no. May, pp. 176–183, 2012.

[44] A. H. Souley and S. Cherkaoui, "Realistic Urban Scenarios Simulation for Ad Hoc Networks," *Second Int. Conf. Innov. Inf. Technol.*, pp. 1–10, 2005.

[45] M. Boban, J. Barros, and O. K. Tonguz, "Geometry-Based Vehicle-to-Vehicle Channel Modeling for Large-Scale Simulation," *IEEE Trans. Veh. Technol.*, vol. 63, no. 9, pp. 4146–4164, 2014.

[46] D. W. Matolak, "Modeling the vehicle-to-vehicle propagation channel: A review," *Radio Sci.*, vol. 49, no. 9, pp. 721–736, 2014.

[47] M. Shemshaki, G. Lasser, L. Ekiz, and C. Mecklenbrauker, "Empirical path loss model fit from measurements from a vehicle-to-infrastructure network in Munich at 5.9 GHz," *IEEE Int. Symp. Pers. Indoor Mob. Radio Commun. PIMRC*, vol. 2015–Decem, no. 1, pp. 181–185, 2015.

[48] Z. Wang, E. Tameh, and A. Nix, "Statistical peer-to-peer channel models for outdoor urban environments at 2GHz and 5GHz," vol. 10, no. 1, pp. 5101–5105, 2004.

[49] C. Campolo, H. A. Cozzetti, A. Molinaro, and R. Scopigno, "Vehicular connectivity in urban scenarios: effectiveness and potential of roadside, moving WAVE providers and hybrid solutions," *EURASIP J. Wirel. Commun. Netw.*, vol. 1, no. 146, p. 10, 2011.

[50] J. Harri, F. Filali, and C. Bonnet, "Mobility models for vehicular ad hoc networks: a survey and taxonomy," *IEEE Commun. Surv. Tutorials*, vol. 11, no. 4, pp. 19–41, 2009.

[51] D. Krajzewicz, M. Hartinger, G. Hertkorn, P. Mieth, C. Rössel, J. Zimmer, and P. Wagner, "Using the Road Traffic Simulation ``SUMO'' for Educational Purposes," in *Traffic and Granular Flow '03*, 2005, pp. 217–222.

[52] Z. Sun and I. F. Akyildiz, "A mode-based approach for channel modeling in underground tunnels under the impact of vehicular traffic flow," *IEEE Trans. Wirel. Commun.*, vol. 10, no. 10, pp. 3222–3231, 2011.

[53] T. Rappaport, *Wireless communications: principles and practice.*, 2nd ed. United States: Prentice Hall PTR, Upper Saddle River, NJ, 2002.

[54] Z. Yun and M. F. Iskander, "Ray tracing for radio propagation modeling: Principles and applications," *IEEE Access*, vol. 3, pp. 1089–1100, 2015.

[55] A. Taflove and S. C. Hagness, *Computational Electrodynamics: The Finite-difference Time-domain Method*, 3rd ed. Norwood, MA, USA: Artech House, 2005.

[56] J. Jin, *The Finite Element Method in Electromagnetics*, 3rd ed. New York, NY, USA: Wiley-IEEE Press, 2014.

[57] R. F. Harrington, *Field Computation by Moment Methods*. New York, NY, USA: Wiley-IEEE Press, 1993.

[58] Hyperworks, "Numerical Methods in FEKO," 2018. .

[59] T. K. Sarkar, Z. Ji, K. Kim, A. Medouri, and M. Salazar-Palma, "A Survey of Various Propagation Models for Mobile Communication," *IEEE Antennas Propag. Mag.*, vol. 45, no. 3, pp. 51–82, 2003.

[60] T. Imai, "A survey of efficient ray-tracing techniques for mobile radio propagation analysis," *IEICE Trans. Commun.*, vol. E100B, no. 5, pp. 666–679, 2017.

[61] A. Cardama, *Antenas*. Barcelona, Spain: Editions Universitat Politécnica de Catalunya, 1993.

[62] H. D. Hristov, *Fresnel Zones in Wireless Links, Zone Plate Lenses and Antennas*, 1st ed. Artech House Inc.: 685 Canton Street: Norwood, MA, USA, 2000.

[63] R. Luebbers, "A Heuristic UTD Slope Diffraction Coefficient for Rough Lossy Wedges," *IEEE Trans. Antennas Propag.*, vol. 37, pp. 206–211, 1989.

[64] R. Luebbers, "Comparison of Lossy Wedge Diffraction Coefficients with Application to Mixed Path Propagation Loss Prediction," *IEEE Trans. Antennas Propag.*, vol. 36, no. 7, pp. 1031–1034, 1988.

[65] R. G. Kouyoumjian and P. H. Pathak, "A uniform GTD for an edge in a perfectly conducting surface," *Proc. IEEE*, vol. 62, no. 11, pp. 1448–1461, 1974.

[66] G. Gennarelli and G. Riccio, "A uapo-based model for propagation prediction in microcellular environments," *Prog. Electromagn. Res. B*, vol. 17, pp. 101–116, 2009.

[67] H. Son and N. Myung, "A Deterministic Ray Tube Method for Microcellular Wave Propagation Prediction Model," *IEEE Trans. Antennas Propag.*, vol. 47, no. 8, pp. 1344–1350, 1999.

[68] A. Tayebi, J. Gomez, F. S. De Adana, and O. Gutierrez, "The Application of Ray-Tracing to Mobile Localization using the Direction of Arrival and Received Signal Strength in Multipath Indoor Environments," *Prog. Electromagn. Res.*, vol. 91, pp. 1–15, 2009.

[69] L. Azpilicueta, M. Rawat, K. Rawat, F. Ghannouchi, and F. Falcone, "Convergence analysis in deterministic 3D ray launching radio channel estimation in complex environments," *Appl. Comput. Electromagn. Soc. J.*, vol. 29, no. 4, pp. 256–271, 2014.

[70] P. Lopez-Iturri, E. Aguirre, J. Trigo, J. Astrain, L. Azpilicueta, L. Serrano, J. Villadangos, and F. Falcone, "Implementation and Operational Analysis of an Interactive Intensive Care Unit within a Smart Health Context," *Sensors*, vol. 18, no. 2, pp. 2838–2850, 2018.

[71] L. Azpilicueta, P. López Iturri, E. Aguirre, J. J. Astrain, J. Villadangos, C. Zubiri, and F. Falcone, "Characterization of Wireless Channel Impact on Wireless Sensor Network Performance in Public Transportation Buses," *IEEE Trans. Intell. Transp. Syst.*, vol. 16, no. 6, pp. 3280–3293, 2015.

[72] L. Azpilicueta, J. J. Astrain, P. Lopez-Iturri, F. Granda, C. Vargas-Rosales, J. Villadangos, A. Perallos, A. Bahillo, and F. Falcone, "Optimization and Design of Wireless Systems for the Implementation of Context Aware Scenarios in Railway Passenger Vehicles," *IEEE Trans. Intell. Transp. Syst.*, vol. 18, no. 10, 2017.

[73] F. Granda, L. Azpilicueta, C. Vargas-rosales, P. Lopez-iturri, E. Aguirre, J. Astrain, J. Villandangos, and F. Falcone, "Characterization of Radio Propagation Channel in Urban Vehicle to Infrastructure Environments to support WSNs," in *Proceedings of the 3rd Int. Electron. Conf. Sens. Appl.*, 2016, vol. 3, pp. 2–7.

[74] M. Zook, M. Graham, T. Shelton, and S. Gorman, "Volunteered Geographic Information and Crowdsourcing Disaster Relief: A Case Study of the Haitian Earthquake," *World Med. Heal. Policy*, vol. 2, no. 2, pp. 6–32, 2010.

[75] S. Latif, K. M. R. Islam, M. M. I. Khan, and S. I. Ahmed, "OpenStreetMap for the disaster management in Bangladesh," in *2011 IEEE Conference on Open Systems, ICOS 2011*, 2011, pp. 435–439.

[76] C. Barron, P. Neis, and A. Zipf, "A Comprehensive Framework for Intrinsic OpenStreetMap Quality Analysis," *Trans. GIS*, vol. 18, no. 6, pp. 877–895, 2014.

[77] M. Haklay and P. Weber, "OpenStreet map: User-generated street maps," *IEEE Pervasive Comput.*, vol. 7, no. 4, pp. 12–18, 2008.

[78] S. Krauß, "Microscopic Modeling of Traffic Flow: Investigation of Collision Free Vehicle Dynamics," University of Cologne, 1998.

[79] P. G. Gipps, "A behavioural car-following model for computer simulation," *Transp. Res. Part B*, vol. 15, no. 2, pp. 105–111, 1981.

[80] W. M. Griggs, R. H. Ordonez-Hurtado, E. Crisostomi, F. Hausler, K. Massow, and R. N. Shorten, "A Large-Scale SUMO-Based Emulation Platform," *IEEE Trans. Intell. Transp. Syst.*, vol. 16, no. 6, pp. 3050–3059, 2015.

[81] F. Grimaldo, M. Lozano, F. Barber, and A. Guerra-Hernández, "Towards a model for urban mobility social simulation," *Prog. Artif. Intell.*, vol. 1, no. 2, pp. 149–156, 2012.

[82] G. N.-I. Agency, "World Geodetic System 1984 (WGS 84)." [Online]. Available: https://www.nga.mil/ProductsServices/GeodesyandGeophysics/Pages/WorldGeodeticSystem.aspx. [Accessed: 18-Jun-2018].

[83] Institute of Transportation Systems at the German Aerospace Center, "SUMO-Geo-

Coordinates." [Online]. Available: http://sumo.sourceforge.net/userdoc/Geo-Coordinates.html. [Accessed: 18-Jun-2018].

[84] R. Roess, W. McShane, and E. Prassas, *Traffic Engineering*, 2nd ed. New Jersey: Prentice Hall PTR, Upper Saddle River, NJ, 1998.

[85] L. Azpilicueta, "Characterization of wireless propagation in complex indoor scenarios," Universidad Pública de Navarra, 2015.

[86] F. Granda, L. Azpilicueta, C. Vargas-Rosales, M. Celaya-Echarri, P. Lopez-Iturri, E. Aguirre, J. J. Astrain, P. Medrano, J. Villandangos, and F. Falcone, "Deterministic propagation modeling for intelligent vehicle communication in smart cities," *Sensors (Switzerland)*, vol. 18, no. 7, 2018.

[87] RedPine Signals., "Driving Wireless Convergence. WaveCombo Module. 802.11p V2X," 2018. [Online]. Available: http://www.redpinesignals.com/Products/802.11p_V2X_Connectivity/802.11p_V2X_Module.php. [Accessed: 28-Feb-2018].

[88] Kapsch TrafficCom., "In-vehicle products (5.9 Ghz). EVK-3300. V2X Evaluation Kit.," 2018. [Online]. Available: https://www.kapsch.net/ktc/downloads/. [Accessed: 28-Feb-2018].

[89] Ublox, "VERA-P1 series. Host-based V2X transceiver modules. Product Information.," 2018. [Online]. Available: https://www.u-blox.com/en/product/vera-p1-series. [Accessed: 28-Feb-2018].

[90] M. Toeltsch, S. Member, J. Laurila, and K. Kalliola, "Statistical Characterization of Urban Spatial Radio," vol. 20, no. 3, pp. 539–549, 2002.

[91] N. Blaunstein, "Average Field Attenuation in the Nonregular Impedance Street Waveguide," *IEEE Trans. Antennas Propag.*, vol. 46, no. 12, pp. 1782–1789, 1998.

[92] D. Porrat, "Radio Propagation in Hallways and Streets for UHF Communications," Thesis Dissertation-Stanford University, 2002.

[93] G. Mao, B. D. O. Anderson, and B. Fidan, "Path loss exponent estimation for wireless sensor network localization," *Comput. Networks*, vol. 51, no. 10, pp. 2467–2483, 2007.

[94] V. Shivaldova, M. Sepulcre, A. Winkelbauer, J. Gozalvez, and C. F. Mecklenbrauker, "A model for vehicle-to-infrastructure communications in urban environments," *2015 IEEE Int. Conf. Commun. Work. ICCW 2015*, pp. 2387–2392, 2015.

[95] K. Hassan and T. A. Rahman, "The Mathematical Relationship Between Maximum Access Delay and the R . M . S Delay Spread," in *The seventh international conference on wireless and mobile communications*, 2011, pp. 18–23.

[96] R. Sevlian, C. Chun, I. Tan, A. Bahai, and K. Laberteaux, "Channel Characterization for 700 MHz DSRC Vehicular Communication," *J. Electr. Comput. Eng.*, vol. 2010, pp. 1–9, 2010.

[97] L. Bernado, T. Zemen, F. Tufvesson, A. F. Molisch, and C. F. Mecklenbräuker,

"Time- and Frequency-Varying K-Factor of Non-Stationary Vehicular Channels for Safety-Relevant Scenarios," *IEEE Trans. Intell. Transp. Syst.*, vol. 16, no. 2, pp. 1007–1017, 2015.

[98] P. S. Bithas, "Weibull-gamma composite distribution: alternative multipath/shadowing fading model," *Electron. Lett.*, vol. 45, no. 14, p. 749, 2009.

[99] S. Atapattu, C. Tellambura, and H. Jiang, "Representation of composite fading and shadowing distributions by using mixtures of gamma distributions," in *IEEE Wireless Communications and Networking Conference, WCNC*, 2010.

[100] NIST/SEMATECH e-Handbook of Statistical Methods., "Probability Plot," 2018. [Online]. Available: https://www.itl.nist.gov/div898/handbook/eda/section3/probplot.htm. [Accessed: 27-Jul-2018].

[101] NIST/SEMATECH e-Handbook of Statistical Methods., "Quantile-Quantile Plot," 2018. [Online]. Available: https://www.itl.nist.gov/div898/handbook/eda/section3/qqplot.htm. [Accessed: 10-Jul-2018].

[102] N. U. Rehman, K. Naveed, S. Ehsan, and K. McDonald-Maier, "Multi-scale image denoising based on goodness of fit (GOF) tests," in *European Signal Processing Conference (EUSIPCO)*, 2016, pp. 1548–1552.

[103] H. Wang, E.-H. Yang, Z. Zhao, and W. Zhang, "Spectrum Sensing in Cognitive Radio Using Goodness of Fit Testing," *IEEE Trans. Wirel. Commun.*, vol. 8, no. 11, pp. 5427–5430, 2009.

[104] X. Zeng, D. Wang, and J. Wu, "Evaulating the Three Methods of Goodness of Fit Test for Frequency Analysis," *J. Risk Anal. Cris. Response*, vol. 5, no. 3, pp. 178–187, 2015.

[105] H. Abdi, "Coefficient of variation in N.J. Salkind, D.M., Dougherty, & B. Frey (Eds.)," *Encyclopedia of Research Design.* SAGE Publications, Inc., pp. 169–171, 2010.

[106] U.Charash, "Reception Through Nakagami Fading Multipath Channels," vol. 27, no. 4, pp. 645–670, 1979.

[107] E. Liebscher, "Approximation of distributions by using the Anderson Darling statistic," *Commun. Stat. - Theory Methods*, vol. 45, no. 22, pp. 6732–6745, 2016.

[108] K. D. Singh, P. Rawat, and J. Bonnin, "Cognitive radio for vehicular ad hoc networks (CR-VANETs): approaches and challenges," *EURASIP J. Wirel. Commun. Netw.*, p. 49, 2014.

Appendix A

Abbreviations and acronyms

Table A.1 Abbreviations

Abbreviation	Description
3D-RL	Three Dimensional-Ray Launching.
CR	Cognitive Radio.
D2D	Device-to-Device.
FCC U.S.	Federal Communications Commission.
GBDM	Geometric Based Deterministic Models.
GPS	Global Positioning System.
HVT	Heavy-flow Vehicular Traffic.
IEEE	Institute of Electrical and Electronics Engineers.
ITMS	Intelligent Traffic Management Systems.
ITS	Intelligent Transportation Systems.
I2V	Infrastructure-to-vehicle
LTE	Long Term Evolution.
NHTSA	National Highway Traffic Safety Administration.
NGBDM	Non-Geometric Based Deterministic Models.
NLoS	Non Line of Sight.
PDP	Power Delay Profile
QLoS	Quasi Line of Sight.
RMS-Delay Spread	Root Mean Square delay spread.
RSU	Road Side Unit.
UHF	Ultra High Frequency.
URPC	Urban Radio Propagation Channel.
V2I	Vehicle-to-Infrastructure.
V2P	Vehicle-to-Pedestrian.
V2V	Vehicle-to-Vehicle.
VDSA	Vehicular Dynamic Spectrum Access.
VHF	Very High Frequency.
VTD	Vehicular Traffic Density.
WCS	Wireless Communication Systems.

Table A.2 Acronyms

Acronym	Description
CIR	Channel Impulse Response.
LoS	Line of Sight.
OBU	On Board Unit.
SISO	Single-Input Single-Output.
SUMO	Simulation of Urban Mobility
VANET	Vehicular Ad-Hoc Network.
WAVE	Wireless Access in Vehicular Environment.

Appendix B

SUMO files and scripts

Netconvert, Polyconvert, routes and output files generation.

netconvert --osm <name>.osm -o <name>.net.xml

polyconvert --osm-files <name>.osm --net-file <name>.net.xml --type-file osmPolyconvert.typ.xml -o <name>.poly.xml

python C:/…/sumo3/tools/randomTrips.py -n <name>.net.xml -r <name>.rou.xml -e 10 -l

sumo-gui -c <name>.sumo.cfg --fcd-output <name>.xml

SUMO polygons definition1
File <name>.typ.xml (this script is only a portion of the complete file)

```
<polygonTypes>

   <polygonType id="waterway"        name="water"      color=".71,.82,.82" layer="-4"/>
   <polygonType id="natural"         name="natural"    color=".55,.77,.42" layer="-4"/>
   <polygonType id="natural.land"    name="land"       color=".98,.87,.46" layer="-4"/>
   <polygonType id="landuse"          name="landuse"    color=".76,.76,.51" layer="-3"/>
   <polygonType id="landuse.forest"    name="forest"     color=".55,.77,.42" layer="-3"/>
   <polygonType id="landuse.park"      name="park"       color=".81,.96,.79" layer="-3"/>
   <polygonType id="tourism"         name="tourism"    color=".81,.96,.79" layer="-2"/>
   <polygonType id="leisure.park"      name="tourism"    color=".81,.96,.79" layer="-2"/>
   <polygonType id="building"        name="building"   color="1.0,.90,.90" layer="-1"/>
   <polygonType id="power"           name="power"      color=".10,.10,.30" layer="-1" discard="true"/>

   <polygonType id="boundary" name="boundary"    color="1.0,.33,.33" layer="0" fill="false"
discard="true"/>

 </polygonTypes>
```

SUMO polygons definition2
File <name>.poly.xml (this script is only a portion of the complete file)

```
<additional xmlns:xsi="http://www.w3.org/2001/XMLSchema-instance"
xsi:noNamespaceSchemaLocation="http://sumo.dlr.de/xsd/additional_file.xsd">

   <location netOffset="-611133.89,-4739237.76" convBoundary="-0.00,-130.00,1355.92,124.10"
origBoundary="-1.640977,42.796260,-1.624445,42.798740" projParameter="+proj=utm +zone=30
+ellps=WGS84 +datum=WGS84 +units=m +no_defs"/>

   <poly id="-31486" type="building" color="255,230,230" fill="1" layer="-1.00" shape="57.68,34.41
57.68,4.55 99.18,4.16 98.92,34.01 57.68,34.41"/>

   <poly id="248062271" type="leisure" color="207,245,201" fill="1" layer="-2.00" shape="127.61,64.44
127.71,60.26 127.87,53.48 140.29,53.80 153.31,53.91 153.19,59.07 153.06,64.86 140.48,64.76
127.61,64.44"/>

   <poly id="90645872" type="building" color="255,230,230" fill="1" layer="-1.00" shape="187.49,77.32
187.92,46.36 235.15,46.35 234.80,77.49 187.49,77.32"/>
```

```xml
<poi id="2377499802" type="shop" color="237,199,255" layer="4.00" x="203.97" y="36.08"/>

</additional>
```

SUMO Routes definition
File <name>.rou.xml (this script is only a portion of the complete file)

```xml
<routes xmlns:xsi="http://www.w3.org/2001/XMLSchema-instance"
xsi:noNamespaceSchemaLocation="http://sumo.dlr.de/xsd/routes_file.xsd">

<vType id="av1parked" vClass="passenger"/>
<vType id="low-vel1" vClass="passenger" maxSpeed="1" />

<vTypeDistribution id="typedist1">

    <vType id="type1" probability="1.0" vClass="passenger" speedFactor="normc(1,0.1,0.2,2)" />
            <vType id="type3" probability="0.0" vClass="motorcycle" />
            <vType id="type4" probability="0.0" vClass="emergency" />
  </vTypeDistribution>

<!-- Parked vehicles -->
        <!-- AV1 -->
<route id="av1-stop" edges="164011290">
        </route>
        <vehicle id="av1-stop1" type="av1parked" depart="00.00" route="av1-stop" departLane="best"
        color="0,0,1">
        <stop lane="164011290_1"  endPos="125"  parking="true" />
        </vehicle>

</routes>

<!-- ST2 -->
        <route id="st2-stop" edges="478652698 -31484 ">
        </route>
        <vehicle id="st2-stop1" type="st2parked" depart="00.00" route="st2-stop" departLane="best"
        color="0,0,1">
        <stop lane="478652698_0"  endPos="10"  parking="true" />
        </vehicle>

<!-- Define the routes with probabilities -->
        <routeDistribution id="av1a-dist">
        <!--Route1: Av1-r -->
        <route id="route1" edges="-31490" probability= "1" />
        </routeDistribution>

        <routeDistribution id="av1b-dist">
        <!--Route3: r-Av1 -->
        <route id="route3" edges=" 164011290 4348660#8 4348660#0 4348660#1 4348660#2
        4348660#3 " probability= "1" />
        </routeDistribution>

<!--Density at t= 600 -->
```

```
<flow id="av1b-c0-t600" color="1,1,0" type="typedist1" route="av1b-dist"  begin="600" end=
"1800" vehsPerHour="360" departLane="best" arrivalLane="0">
</flow>
<flow id="av1b-c1-t600" color="1,1,0" type="typedist1" route="av1b-dist"  begin="600" end=
"1800" vehsPerHour="360" departLane="best" arrivalLane="1">
</flow>
```

SUMO Traffic Lights definition

File <name>.net.xml (this script is only a portion of the complete file)

```
<tlLogic id="-30494" type="static" programID="0" offset="0">
    <phase duration="25" state="GGrr"/>
    <phase duration="4" state="yyrr"/>
    <phase duration="50" state="rrGG"/>
    <phase duration="4" state="rryy"/>
</tlLogic>

<tlLogic id="740856411" type="static" programID="0" offset="0">
    <phase duration="25" state="rGGG"/>
    <phase duration="4" state="ryyy"/>
    <phase duration="50" state="Grrr"/>
    <phase duration="4" state="yrrr"/>
</tlLogic>
```

Published papers

F. Granda et al., "Characterization of Radio Propagation Channel in Urban Vehicle to Infrastructure Environments to support WSNs," in Proceedings of the 3rd Int. Electron. Conf. Sens. Appl., 2016, vol. 3, pp. 2–7.

L. Azpilicueta et al., "Optimization and Design of Wireless Systems for the Implementation of Context Aware Scenarios in Railway Passenger Vehicles," IEEE Trans. Intell. Transp. Syst., vol. 18, no. 10, 2017.

F. Granda et al., "Spatial Characterization of Radio Propagation Channel in Urban Vehicle-to-Infrastructure Environments to Support WSNs Deployment," Sensors (Switzerland), vol. 17, no. 6, p. 1313, 2017.

F. Granda et al., "Deterministic Propagation Modeling for Intelligent Vehicle Communication in Smart Cities," Proceedings, vol. 18, no. 7, p. 28, 2018.

F. Granda, et al., "Deterministic propagation modeling for intelligent vehicle communication in smart cities," Sensors (Switzerland), vol. 18, no. 7, 2018.

F. Granda, et al., "Integration of Wireless Sensor Networks in Intelligent Transportation Systems within Smart City Context.", IEEE International Symposium on Antennas and Propagation and USNC-URSI Radio Science, 2018, Boston, Massachusetts.

F. Granda et al., "3D ray launching simulation of urban vehicle to infrastructure radio propagation links," in XIII Congreso de Ciencia y Tecnología ESPE., 2018, vol. 13,num 1, pp. 2–7.

Curriculum Vitae

Fausto Lenin Granda Gutiérrez was born in Loja, Ecuador, on November 26th, 1976. He earned the Electrical and Electronic Engineering degree from the Universidad de las Fuerzas Armadas ESPE, Sangolquí Campus in November 2001. He was accepted in the Doctoral program in Information Technologies and Electronics in August 2014.

This document was typed in using Microsoft Word by Fausto Lenin Granda Gutiérrez